Coastal and Hydraulics Laboratory

ERDC/CHL TR-19-14

US Army Corps of Engineers®
Engineer Research and Development Center

ERDC
ENGINEER RESEARCH & DEVELOPMENT CENTER

Probabilistic Flood Hazard Assessment Framework Development: Extreme Rainfall Analysis

Brian E. Skahill and Joseph Kanney

August 2019

ERDC/CHL TR-19-14
August 2019

Probabilistic Flood Hazard Assessment Framework Development: Extreme Rainfall Analysis

Brian E. Skahill

Coastal and Hydraulics Laboratory
U.S. Army Engineer Research and Development Center
3909 Halls Ferry Road
Vicksburg, MS 39180-6199

Joseph Kanney

U.S. Nuclear Regulatory Commission
Office of Nuclear Regulatory Research
11555 Rockville Pike
Rockville, MD 20852-2738, Mail Stop TWFN-10A12

Final report

Prepared for U.S. Nuclear Regulatory Commission
11555 Rockville Pike, Rockville, MD 20852-2738

Under U.S. Nuclear Regulatory Commission NRC Agreement Number NRC-HQ-60-14-I-0022, "Probabilistic Flood Hazard Assessment Framework Development"

Abstract

This report introduces a framework for probabilistic flood hazard assessment (PFHA) whose basis leverages recent advances in the science of spatial extremes. The framework basis includes a latent variable model (LVM) or a max-stable process application wherein for either case model inference is likelihood based. The framework is flexible in that it can leverage robust approaches to quantify model uncertainty while also supporting the capacity to readily combine additional relevant data types; for example, historical and/or paleoflood data for flood frequency analyses. This report profiles applications of Bayesian inference for flood hazard curve development for at-site and spatial LVM analyses. Pointwise spatial model development using an LVM or a max-stable process requires the parameters of the model characterizing the pointwise extremes to vary spatially as a function of gridded covariate data relevant to the hydrometeorological extreme under consideration. Recent advances in mathematical regularization facilitate spatial pointwise model reduction. The PFHA framework accommodates the multiple model parameterizations encapsulated within a given LVM or max-stable process deployment by generalizing model choice using information criteria.

Contents

Figures and Tables

Figures

Tables

Preface

This study was conducted for the U.S. Nuclear Regulatory Commission, Office of Nuclear Regulatory Research, under U.S. Nuclear Regulatory Commission NRC Agreement Number NRC-HQ-60-14-I-0022, “Probabilistic Flood Hazard Assessment Framework Development.” The technical monitor was Dr. Joseph Kanney.

The work was performed by the Hydrologic Systems Branch of the Flood and Storm Protection Division, U.S. Army Engineer Research and Development Center – Coastal and Hydraulics Laboratory (ERDC-CHL). At the time of publication of this report, Dr. Hwai-Ping Cheng was Branch Chief; Dr. Cary Talbot was Division Chief; and Dr. Julie Rosati was the Technical Director for Flood Risk Management. The Deputy Director of ERDC-CHL was Mr. Jeffrey R. Eckstein, and the Director was Dr. Ty V. Wamsley.

COL Ivan P. Beckman was the Commander of ERDC, and Dr. David W. Pittman was the Director.

1 Introduction

1.1 Background

The United States Nuclear Regulatory Commission (NRC) is currently developing a risk-informed analytical approach for flood hazards and design standards at new nuclear facilities and significance determination tools for evaluating inspection findings related to flood protection at operating facilities. It is part of the NRC Probabilistic Flood Hazard Assessment (PFHA) research plan whose aim is to build upon recent advances in deterministic, probabilistic, and statistical modeling of extreme precipitation events to develop regulatory tools and guidance for NRC staff with regard to PFHA for nuclear facilities. The tools and guidance developed will support and enhance the NRC capacity to perform thorough and efficient reviews of license applications and license amendment requests. They will also support risk-informed significance determination of inspection findings, unusual events and other oversight activities.

1.2 Objective

The NRC PFHA research plan emphasizes the need for probabilistic treatment of flood hazard phenomena wherein application of such an approach would provide quantitative estimates of conservatism (in terms of probability or frequency of exceedance) and thus contribute to the risk-informed assessment of flooding hazards. For inland nuclear facility sites (i.e., non-coastal sites), a PFHA must be able to incorporate probabilistic models for a variety of processes (e.g., precipitation, runoff, stream flow, operation of water control structures), allow for characterization and quantification of aleatory and epistemic sources of uncertainty, and facilitate propagation of uncertainties and sensitivity analysis. A PFHA for inland flooding must be able to accommodate models for various types of event scenarios: for example, (1) local intense precipitation, (2) larger-scale rainfall via convective or synoptic processes, and (3) cool-season synoptic processes. Moreover, the PFHA framework should be capable of modeling spatial and temporal correlation between and within precipitation events.

1.3 Approach

This report presents and demonstrates an ongoing technology-transfer focused applied research activity directed at the development of a conceptual, mathematical, and logical framework for the probabilistic modeling of extreme rainfall. Recent advances in extreme rainfall analysis are its basis, wherein by "extreme" the focus, in part, is directed to the presentation and application of methods with mathematical foundations that credibly support extrapolation rather than heuristic approaches that persist in engineering practice but that have not been shown to necessarily conform with the fundamentals of extreme value theory (EVT). This report primarily presents and demonstrates relevant applications of the Bayesian inference methodology that formally supports probabilistic analysis to yield point-based estimates of extreme rainfall for a given duration. Included in this report are several case study applications that demonstrate individual component parts of a general framework developed not only for the analysis of extreme precipitation but also other extreme hydrometeorological data. It is acknowledged that for some readers the adopted individual case study approach that is presented in this report may not be convincing, or lack cohesion; however, from a pedagogical perspective it might be easier to attempt to digest and understand individual component pieces rather than application of the complex whole simultaneously. The regional extreme rainfall analysis case study presented later in this report profiles an application of Bayesian inference to develop pointwise return-level maps of extreme rainfall. Precipitation and other PFHA relevant hydrometeorological data occur naturally as spatial processes; hence, formal spatial analysis of extremes methods is required. This section also includes additional related analysis methodology and discussion of spatial methods whose application fully conforms with the extremal paradigm and furthermore, how either of these approaches, or their adaptions, can be employed within the proposed general framework for probabilistic flood hazard analysis.

2 Background

The ability to estimate the depth, duration, and frequency of extreme rainfall is an essential component of flood hazard assessment. Extreme rainfall directly affects the infrastructure and residents of its impact area while also having an indirect economic effect. However, extreme rainfall analysis is difficult not only due to incomplete process understanding but also because there is a paucity of extreme data to support empirical model construction. As a result, extreme value models are based on formal mathematical limit arguments (Gumbel 1958; Fisher and Tippett 1928; Gnedenko 1943). These models based on asymptotic argument are the basis to credibly extrapolate from observed to unobserved levels. A succinct review of salient features of EVT is included in Appendix A.

A flood hazard assessment may likely benefit from or require a regional rather than simply an at-site analysis. Extremal models are also used while inferring the spatial process of hydrometeorological (e.g., rainfall) extremes by simultaneously considering a finite set of monitoring station observations in a region of interest. This partial realization of the spatial process is then used to predict extreme values at other locations throughout the region. The PFHA framework for regional analysis enables this broad interpolation, despite the existence of only a finite set of surface network observation locations, by specifying an associated structured dependence (Banerjee et al. 2015; Ribatet 2013).

The standard sequential approach to modeling extremes involves data analysis, extremal model selection, inference, and prediction. Its application may be iterative by virtue of inference and a possible model selection process. For example, pointwise trend surface model development may involve the evaluation of multiple models of varying complexity while considering process-relevant available covariate data. Models commonly used in engineering practice for the analysis of rainfall extremes include the Kappa (Hosking 1988; Hosking and Wallis 1997; Parida 1999), exponential (Guo and Adams 1998), Weibull (Schoof et al. 2010), gamma (Şen and Eljadid 1999), Gumbel (Hershfield 1962; Miller et al. 1973), generalized extreme value (GEV) (Schaefer 1990; Hosking and Wallis 1997; Overeem et al. 2008) and log-Pearson type III (Phien and Jivajirajan 1983) distributions. Awadallah and Younan (2012) grouped the point-frequency distributions (models) widely used for the analysis of rainfall extremes in hydrology into three categories, which include Fréchet

(EV2), Halphen IB, Log-Pearson three, Inverse Gamma, Halphen type A, Halphen type B, Gumbel (EV1), Pearson type III, Gamma, and exponential distributions. Appendix B includes some commentary about distributions beyond those from EVT that have been documented to model extreme rainfall. The noted existence of multiple models for extreme rainfall analysis is a source of epistemic uncertainty. In an attempt to account for this source of uncertainty, the PFHA framework proposed in this report presents in Appendix C some available methods by which to generalize the problem of model selection.

The Bayesian inference methodology is heavily profiled in this report for several reasons. First, it is a formal means by which to account for and compute both aleatory and epistemic sources of uncertainty (Banerjee et al. 2015; Economou et al. 2014; Dyrrdal et al. 2015; Cooley et al. 2007; Cooley and Sain 2010; Soltyk et al. 2014; Steinschneider and Lall 2015). Second, the approach coherently and flexibly combines different data types such that there is a maximal use of all available complementary data sources relevant to the analysis of extreme rainfall (Coles and Tawn 1996; Coles and Pericchi 2003; Smith 2005; Cheng and AghaKouchak 2014; Katz et al. 2002; Eckersten 2016; Winter 2011; Economou et al. 2014; Dyrrdal et al. 2015; Cooley et al. 2007; Cooley and Sain 2010; Soltyk et al. 2014; Steinschneider and Lall 2015). Third, it is applicable for both at-site and regional extreme rainfall analyses (Coles et al. 2003; Economou et al. 2014; Dyrrdal et al. 2015; Cooley et al. 2007; Cooley and Sain 2010; Soltyk et al. 2014; Steinschneider and Lall 2015; Reich and Shaby 2012). Fourth, it permits the inclusion of covariate information in the extreme value model parameters (Cheng and AghaKouchak 2014; Katz et al. 2002; Eckersten 2016; Winter 2011; Economou et al. 2014; Dyrrdal et al. 2015; Cooley et al. 2007; Cooley and Sain 2010; Soltyk et al. 2014; Steinschneider and Lall 2015); hence, for example, it can readily support treatments of non-stationarity. Last, it supports the capacity to compute the posterior distribution for a future prediction based on the observed data (Coles 2001; Renard et al. 2015).

While there exist many different approaches to estimate the parameters of a statistical model selected for the analysis of extreme rainfall data, the Bayesian inference methodology is primarily profiled in this report for PFHA framework application for several reasons. First, Bayesian-based modeling fully supports the capacity to make formal probabilistic statements about related quantities of interest, including, among possible others, the extremal model parameters and extreme rainfall quantile levels. Related, its model uncertainty estimates are consistent with everyday interpretations. In addition, the Bayesian methodology is flexible in that it readily supports combining data of different types to make maximal use of all available relevant information in an analysis of rainfall extremes. For example, information derived from expert elicitation can be combined with the observed data record in an extreme rainfall analysis. The Bayesian inference methodology can also accommodate modeling treatments of non-stationarity. Furthermore, a Bayesian hierarchical modeling framework can support regional extreme rainfall analysis (Cooley et al. 2007). Moreover, Bayesian inference can support the application of Bayesian model averaging (BMA) to generalize the problem of model selection. Banjeree et al. (2015) and Congdon (2010) both underscored the relevancy of Bayesian estimation and inference to handle the types of data and problems tackled by modern scientific research. In summary, the Bayesian approach is a coherent, flexible, and revisable framework for probability-based extreme rainfall analysis.

With the Bayesian inference methodology, the focus is on updating knowledge about a model's unknowns, θ (e.g., the selected extremal model parameters, on the basis of observations y, with revised knowledge expressed in the posterior density, $p(\theta|y)$. The sample of observations y provides new information about the unknowns while the prior density $p(\theta)$ of the unknowns represents formulated beliefs about θ before observing or analyzing the data y. The benefits of using a prior distribution informed by outside information about the process itself are likely to be great in an analysis of extreme rainfall, where by definition the data are often scarce. Additional details regarding Bayesian inference are provided in Appendix D.

Direct sampling of the posterior density $p(\theta|y)$ of the unknowns is not feasible because the integral in Equation D.1 is too difficult to evaluate analytically or to compute numerically for all but a small class of problems. Markov Chain Monte Carlo (MCMC) methods, which sample from $p(\theta|y)$ without necessarily knowing its analytic form, have popularized the use of Bayesian techniques. MCMC simulation is a technique to estimate the posterior density $p(\theta|y)$ of the unknowns: for example, the GEV distribution parameters in an analysis of annual rainfall maxima. The idea behind MCMC simulation is that while one wants to compute a posterior density, $p(\theta|y)$, there is the understanding that such an endeavor may be impracticable. Additionally, simply being able to generate a large random sample from the posterior density would be equally sufficient as knowing its exact form. Hence, the problem then becomes one of effectively and efficiently generating a large number of random draws from $p(\theta|y)$. An efficient means to this end is to construct a Markov chain, a stochastic process of values that unfold in time, with the following properties: (1) the state space (set of possible values) for the Markov chain is the same as that for p; (2) the Markov chain is easy to simulate from; and (3) the Markov chain's equilibrium distribution is the desired posterior density $p(\theta|y)$. A Markov chain with the above-mentioned properties can be constructed by choosing a symmetric proposal distribution and employing the Metropolis acceptance probability (Metropolis et al. 1953) to accept or reject candidate points. By constructing such a Markov chain, one can then simply run it to equilibrium (and this period is often referred to as the sampler *burn-in* period) and subsequently sample from its stationary distribution. Quantitative convergence diagnostics such as the Gelman and Rubin (1992) quantitative measure are commonly employed to assist with diagnosis of MCMC sampler convergence. A key element of an MCMC sampler is the proposal distribution, which generates the candidate jumps for consideration as part of the Markov Chain directed random walk of the posterior. For a given problem, there are many possible acceptable proposal distributions. However, its specific choice can dramatically impact the overall efficiency of the sampler, to the target equilibrium distribution. Proposal distributions that generate either small or large jumps yield low acceptance rates and slow convergence. The primary goal is to choose a proposal distribution that is easy to sample from, generates unbiased moves, and which results in optimal mixing of the chains. The interested reader is directed to Gelman et al. (2004), Banerjee et al. (2015), and Renard et al. (2015), and references cited therein, for more information regarding technical details and implementation issues related to the theory and application of Bayesian inference and MCMC. Appendix D includes some additional details regarding application of MCMC.

An attractive methodological approach for regional extreme rainfall analysis is Bayesian Hierarchical Modeling (BHM). With BHMs, sometimes referred to as latent variable models (LVMs) (Davison et al. 2012), the product of the data likelihood and the prior in Equation D.1 is modified to account for the introduction of latent variables that define one or more latent process layers intermediate between the observed data and the priors. BHM employs MCMC for simultaneous model optimization and inference and distributes EVT model parameters in space using covariate information pertaining to geographical and climatological factors that influence regional rainfall extremes (Wikle et al. 1998; Davison et al. 2012; Ribatet et al. 2012; Banerjee et al. 2015). One or more of the extremal model parameters may also be indexed in time to support the development of a spatiotemporal BHM (Wikle et al. 2001; Kwon et al. 2008; Sang and Gelfand 2008; Ghosh and Mallick 2011; Economou et al. 2014; Steinschneider and Lall 2015). The advantages of BHM-based analysis of hydrometeorological extremes, in contrast with regional frequency analysis (RFA), are that BHM does not require the decomposition of the study region into homogeneous sub-regions (Cooley et al. 2007), it includes the spatial components of the data, it is robust in the treatment of uncertainty (Cooley et al. 2007; Banerjee et al. 2015), and it can be easily adapted to accommodate treatments of non-stationarity (Banerjee et al. 2015; Cheng et al. 2014; Economou et al. 2014). Additionally, the Bayesian framework permits one to combine additional data types into the analysis (e.g., information derived via elicitation and climate indices [Coles and Tawn 1996; Kwon et al. 2008; Economou et al. 2014; Steinschneider and Lall 2015]). Appendix E includes a succinct mathematical summary of BHM for the spatial analysis of extremes.

While spatial or spatiotemporal BHM is attractive for the multiple reasons previously mentioned, it assumes conditional independence among the extremes and often treats residual dependence using a zero mean Gaussian process, which does not fully conform with the extremal paradigm (Davison and Gholamrezaee 2012; Cooley et al. 2012). Just as is the case for the univariate analysis of extremes, the spatial analysis of hydrometeorological extremes must also have a solid mathematical foundation to support any extrapolation necessary beyond the observed tail of the data. Their applications must be flexible and efficient but not violate EVT. In particular, the marginal distributions must be appropriately modeled while also accounting for the observed dependence among the extreme data (Davison and Gholamrezaee 2012). By applying spatial analysis of extremes that fully adhere to EVT, not only can traditional predictive pointwise return-level maps be produced, but in contrast with other approaches, additional more complex assessments of risk can also be evaluated. For example, the joint spatial modeling of observations (e.g., precipitation, snow water equivalent [SWE], snowmelt rate, or temperature), denoted for generality by $\Upsilon(x)$, over a basin $\mathcal{B}$, supports the capacity to compute an integral such as

$$\Pr\left\{\int_{\mathcal{B}} \Upsilon(x)dx > z_{crit}\right\} \tag{1}$$

where z_{crit} denotes a critical quantity greater than zero (Dey and Yan [2016] and references cited within). With the application of formal spatial analysis of extremes using max-stable processes, based on fitting a defined composite likelihood, marginal distributions, while fixed and defined by the GEV model, can flexibly and efficiently be modeled leveraging readily available and relevant spatial and temporal covariate data, with model selection supported using information criteria (Varin and Vidoni 2005; Takeuchi 1976). Spatial extreme (max-stable) models can subsequently be fit that combine the flexibly modeled marginals while simultaneously accounting for the observed dependence among the extremes. Pointwise return-level maps can subsequently readily be developed, and moreover, more complex spatial assessments of risk can also be computed (e.g., as is expressed in Equation 1). While Reich and Shaby (2012) did develop and demonstrate a max-stable process model for the spatial analysis of extremes approach using Bayesian inference, a limitation of their method is that it only considers one of a handful of available models to account for the dependence among the extreme data. Several recent studies have profiled the use of max-stable process models for the spatial analysis of hydrometeorological extremes (Smith 1990; Davison and Gholamrezaee 2012; Davison et al. 2012; Olinda et al. 2014; Nicolet et al. 2015; Sebille et al. 2016). These studies, and references cited within, also summarize mathematical details of max-stable processes. This report also includes a case study that applies max-stable process models (Ribatet 2013) for the spatial analysis of extreme rainfall using the R package SpatialExtremes (Ribatet 2017). The following section of this report includes comments for consideration regarding the application of spatial or spatiotemporal BHM and also max-stable process models for PFHA analyses of hydrometeorological extremes.

3 Framework

The proposed general PFHA framework adopts key components of the flood frequency hydrology concept (Merz and Blöschl 2008a,b). Merz and Blöschl (2008a,b) proposed the concept of flood frequency hydrology, which emphasizes the importance of combining local flood data with additional types of temporal, spatial, and causal information using hydrologic reasoning to perform a flood frequency analysis at a site of interest. Temporal expansion involves the collection and consideration of information on flood behavior before or after the period of record of measured discharge. It accommodates short records that are not completely representative of a system's flood behavior. Flood marks on buildings and paleoflood information are two types of temporal information expansion data. Spatial information expansion involves trading space for time by using flood information from neighboring systems, viz., a regional flood frequency analysis methodology such as the index flood method (Dalrymple 1960), to improve upon the flood frequency analysis at the site of interest. Introducing hydrologic understanding of local flood production factors is the goal of causal information expansion.

With flood frequency hydrology, in estimating flood frequencies, the intent is to extract the maximum amount of information from all available complementary data sources and to combine the additional data types (i.e., temporal, spatial, causal) using hydrologic reasoning. Merz and Blöschl (2008a,b) underscore that a key element of the combination process is to account for the uncertainty of the various pieces of information. Whereas Merz and Blöschl (2008a,b) relied upon heuristic hydrologic reasoning to combine the different data types, Viglione et al. (2013) approached the flood frequency hydrology concept within a Bayesian analysis framework.

The general PFHA framework proposed herein adopts key ideas and terminology from the flood frequency hydrology concept. In particular, it also employs causal, spatial, and temporal information expansion data in attempts to leverage all available and relevant complementary data for an analysis of hydrometeorological extremes. It can be viewed as a two-step process as is shown in Figure 1. The foundation for the first step is of course solid statistical data analysis to ensure proper extremal model selection and likelihood function formulation. The first step involves combining causal, spatial, and temporal information expansion data. The first step is iterated K times using K distinct applicable models selected for the analysis of extremes. The second and final step averages the K models.

It is recommended that the vehicle for PFHA framework application either be adaption of a selected BHM or a max-stable process model based upon an initial assessment of (in)dependence among the extreme data. If it is determined to be reasonable to assume independence among the extremes, then one could proceed with applying a BHM, adapted, if and as necessary, to accommodate for the inclusion of any available temporal information expansion data. For example, in a flood frequency analysis application context, the spatial BHM likelihood (i.e., Equation E.5) could be readily adapted to flexibly combine location-specific historical/paleoflood data with the pooled systematic data record. Instead, if the application involves extreme rainfall or snow water equivalent data, then selection of a spatiotemporal BHM may be more appropriate to potentially leverage climate index data that could be interpreted as temporal information expansion data to combine with the pooled systematic record. With BHM application, process understanding (i.e., causal information expansion data, can be included either via elicitation and/or by also combining into the analysis extreme data derived using a simulation model calibrated, most likely, using a subset of the available pooled systematic record). For example, cool season process flood hazard assessments might capitalize upon extending limited station specific SWE records using a calibrated model and forcing data that exists outside of the station's SWE data period of record. The process layer modeling and its related covariate data could also be viewed as a means by which to incorporate process understanding (i.e., causal information) into the PFHA analysis. Regardless of the specific hydrometeorological extreme data considered, with application of a spatial/spatiotemporal BHM or adapted BHM, the K different models to average in attempts to generalize the problem of model selection could be one or more identified acceptable distributions, and for each given distribution a set of different process layer configurations of varying complexity.

Conversely, if it is not reasonable to assume independence among the extreme data, hence, problematic to employ a spatial/spatiotemporal BHM designed with a likelihood assuming conditional independence, or it is simply preferred to employ a spatial extremes methodology that fully conforms with EVT wherein any hazard curve extrapolation rests on solid mathematical ground, then it is recommended to use max-stable process models for PFHA analyses. With application of max-stable process models, it is conjectured that the likelihood (Ribatet 2013) can also be adapted, much as was the case with BHM samplers constructed assuming conditional independence, to potentially accommodate the inclusion of historical/paleoflood data in a flood frequency application context. Max-stable process model applications permit the modeler to interject into the analysis a degree of process understanding through inclusion of spatial and temporal covariate data, and these data can be interpreted as causal and/or possibly also temporal information expansion data. Also, as with BHMs, when using max-stable process models for PFHA analysis, process understanding could also involve the inclusion of simulated extreme data from a model calibrated using the available pooled systematic record. It is emphasized that the PFHA framework proposed herein leverages, rather than solely relies upon, any additional extreme data to be gained from a process-based simulation model for flood hazard curve characterization primarily due to the potentially problematic nature of such an approach, by itself, to fully leverage all relevant and available complementary data. By contrast, the PFHA framework approach proposed herein does readily combine all of the available complementary data identified as relevant to characterize the flood hazard curve. Moreover, and quite important, max-stable spatial process model applications solidly rest on EVT for credible flood hazard curve extrapolation. Generalization of model selection can be accounted for through consideration of one or more max-stable models and for each selected max-stable model, different trend surface configurations for defining the marginal distributions.

Several case studies now follow. The first four case study demonstrations focus on the foundational issue of data analysis and, related, model selection and likelihood formulation while also profiling the merits of Bayesian inference and covering basic issues pertaining to the practical application of MCMC for univariate extreme rainfall analysis. The fifth demonstration profiles the value of using informed priors in a Bayesian analysis of extreme rainfall. The sixth demonstration is a simple example that profiles the capacity of Bayesian inference to readily support an at-site non-stationary extreme rainfall analysis. It is readily acknowledged that the first five demonstrations are simple at-site analyses, but the intent in each case is to clearly demonstrate specific individual merits of Bayesian inference for PFHA analyses. The seventh and eighth demonstrations profile application of BHM and max-stable process models, in particular, instance applications of the proposed framework, for the spatial analysis of extreme rainfall, respectively. The final demonstration profiles an application of multi-model averaging as a means by which to generalize the problem of model selection. The case studies that follow mostly use readily available and documented R software packages (R Core Team 2013) that exist in the public domain and which support clear, technically sound, consistent, complete, and efficient PFHA analyses of varying complexities. It is emphasized that their application herein is not an endorsement or recommendation. There is no recommendation that one would need to evaluate any particular R software package regarding its suitability for use for any specific application.

Figure 1. PFHA framework for extreme rainfall analysis. (Trenberth, Kevin, and National Center for Atmospheric Research Staff [eds.]). Last modified 02 February 2016. "The Climate Data Guide: Nino SST Indices (Nino 1+2, 3, 3.4, 4; ONI and TNI. " Retrieved from https://climatedataguide.ucasr.edu/climate-data/nino-sst-indices-nino -12-3-34-4-oni-and-tni.)

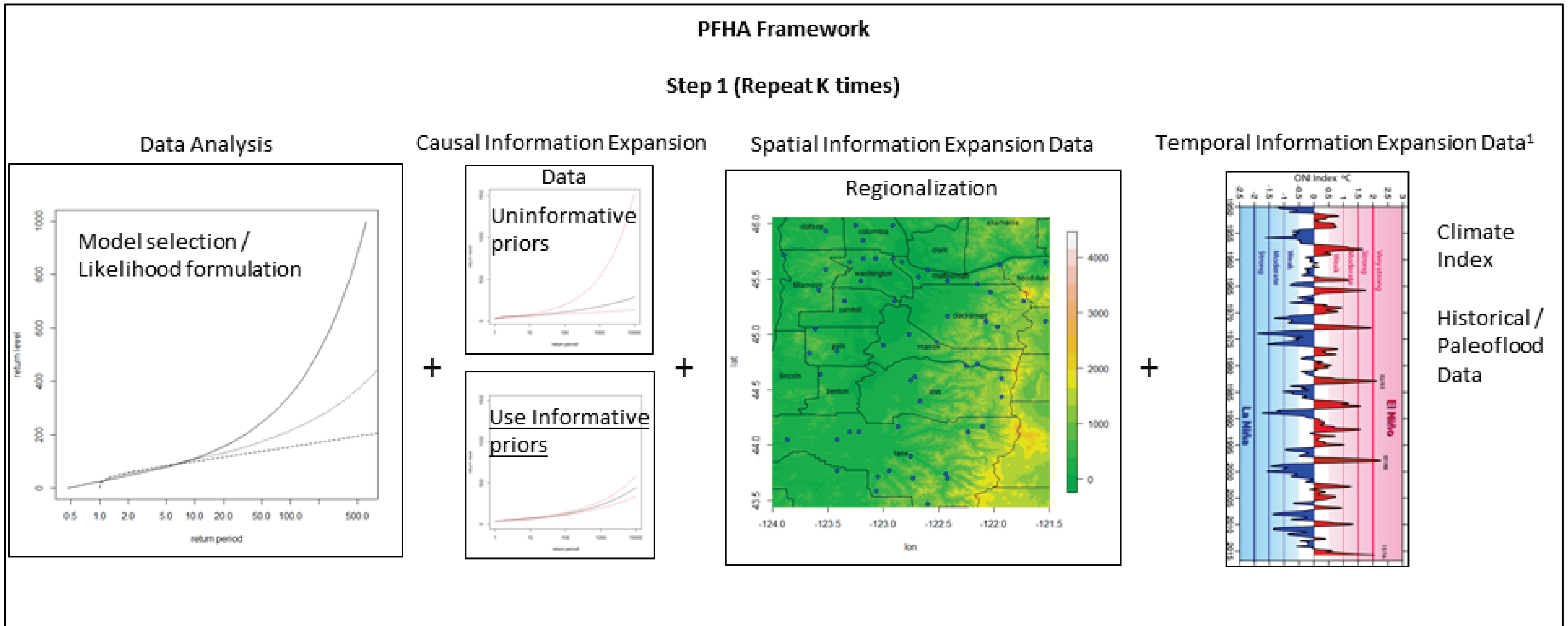

Step 2 Apply a multi-model averaging technique

For example

Bayesian Model Averaging

$$p(\Delta \mid M_1, \ldots, M_k) = \sum_{k=1}^{K} w_k g_k(\Delta \mid M_k)$$

or

Information Criterion Averaging

$$\beta_k = \frac{\exp\left(-\frac{1}{2} I_k\right)}{\sum_{k=1}^{K} \exp\left(-\frac{1}{2} I_k\right)}$$

3.1 Station specific analysis

3.1.1 Systematic data only

3.1.1.1 Block maxima data

This case study revisits simple but important at-site extreme rainfall analyses that were originally presented by Coles et al. (2003). This first demonstration primarily focuses on application of Bayesian estimation using a relatively unique and interesting annual maxima rainfall dataset to infer models from EVT. Principal topics of emphasis, beyond some demonstration of basic issues related to the practical application of MCMC using readily available R software packages, are extremal model selection and inference methodology. With Bayesian estimation and inference, as indicated in Equation D.3, the two main elements to describe include the likelihood and the prior distribution. For this data scenario, the likelihood is as indicated in Equation D.2. For example, if the GEV or Gumbel model is selected, then the density in Equation D.2 is given by $f = G'$ where G is as defined in Equation A.1 or A.4, respectively. The prior distribution on the parameters is commonly specified using arbitrary distributions with a large variance, viz., uninformative distributions, to reflect prior beliefs that are often rather vague relative to the information in the likelihood. Following successful completion of an MCMC simulation, empirical estimates of posterior densities for given quantile levels are easily computed using the MCMC sampler post burn-in monitoring period draws, together with use of either Equation A.3 or A.5 depending upon whether the GEV or Gumbel model is chosen. Related, return level plots are easily generated from the posterior draws as well by simultaneously evaluating multiple return periods, also using either Equation A.3 or A.5 depending upon the selected EVT model. Moreover, the predictive return levels for a future annual maximum observation can also be computed using Equation D.8.

<u>Case study demonstration – annual maxima rainfall data from the Maiquetia international airport station</u>

Heavy rainfall from the storm of 14–16 December 1999 caused catastrophic landslides and flooding along a 40-kilometer coastal strip north of Caracas in the northern coastal state of Vargas, Venezuela. More than 8,000 homes and 700 apartment buildings were destroyed in Vargas, displacing up to 75,000 people. Public services such as roads, telephone, electricity, and water and sewage systems were severely disrupted, and in some places completely disappeared. Total economic losses are estimated at $1.79 billion U.S. dollars (Salcedo 2000). Early estimates suggested that between 5,000 and 50,000 people may have perished (Brandes 2000; Sancio and Barríos 2000; Salcedo 2000; USAID 2000), the figure of 30,000 is now generally cited as the approximate number of fatalities (USAID 2000), which amounts to approximately 10% of the local population. Many people were buried or carried out to sea by the debris flows and flooding, and only approximately 1,000 bodies were recovered. Widespread looting and sacking forced the military to implement martial law. The volume of debris-flow deposits and the large boulders that the flows transported qualified the 1999 event amongst the largest historical rainfall-induced debris flows documented worldwide (Wieczorek et al. 2001). The annual maxima rainfall data for the Maiquetia international airport, originally analyzed by Coles et al. (2003), were requested and received from the second and third authors of the study (Drs. Pericchi and Sisson). The annual maxima data are shown in Figure 2.

Figure 2. Annual maxima daily rainfall values recorded in Maiquetia, Venezuela.

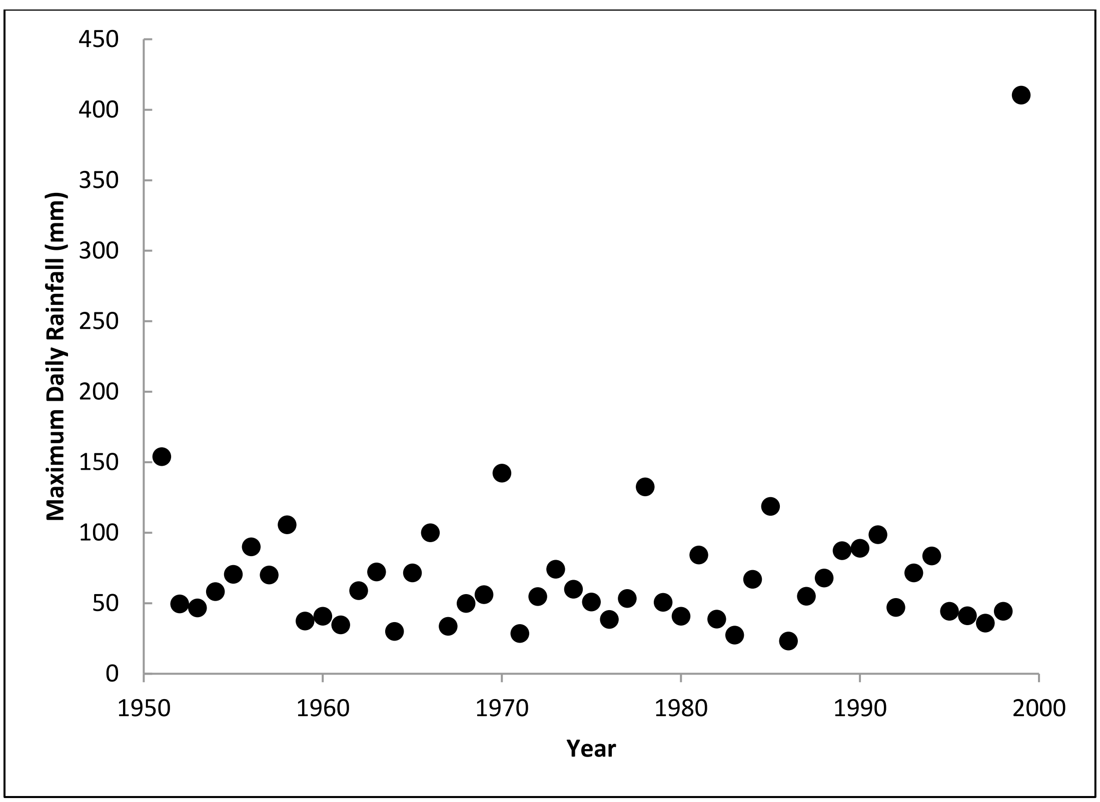

The R software (R Core Team 2013) and its evdbayes (Stephenson and Ribatet 2014), extRemes (Gilleland and Katz 2011), and coda (Plummer et al. 2006) packages, all in the public domain, are used to demonstrate application of Bayesian estimation and inference using the Maiquetia international airport station annual rainfall maxima dataset. The evdbayes and extRemes R packages include MCMC samplers to support application of the Bayesian inference methodology. As originally profiled by Coles et al. (2003), model selection involves consideration of the GEV distribution and also the simplified Gumbel model. As observed in Figure 2, the annual maxima dataset is punctuated at the end of its record with the 1999 event. It is of interest to examine how well an event the magnitude of the 1999 event could have been anticipated statistically prior to its occurrence.

The MCMC sampler as implemented in the evdbayes R package was employed to infer GEV model parameters using the annual rainfall maxima from the Maiquetia international airport station excluding the 1999 datum. In particular, the following sequence of R commands resulted in the plots shown in Figure 3 (a), (b), and (c), respectively.

```
mcmcA<-
posterior(1000000,init=c(5,1,.1),prior=pn,lh=”gev”,data=vam_pre99[,2],psd=c(.02,.1,.1))
mcmcA_coda<-as.mcmc(mcmcA)
plot(mcmcA_coda)

mcmcB<-
posterior(1000000,init=c(5,1,.1),prior=pn,lh=”gev”,data=vam_pre99[,2],psd=c(.1,.1,.1))
mcmcB_coda<-as.mcmc(mcmcB)
plot(mcmcB_coda)

mcmcC<-
posterior(1000000,init=c(5,1,.1),prior=pn,lh=”gev”,data=vam_pre99[,2],psd=c(.5,.1,.1))
mcmcC_coda<-as.mcmc(mcmcC)
plot(mcmcC_coda)
```

Figure 3. Trace and density plots of the GEV model parameters for three distinct MCMC simulations using the pre-1999 annual rainfall maxima from the Maiquetia international airport station and the MCMC sampler as implemented in the R software package evdbayes.

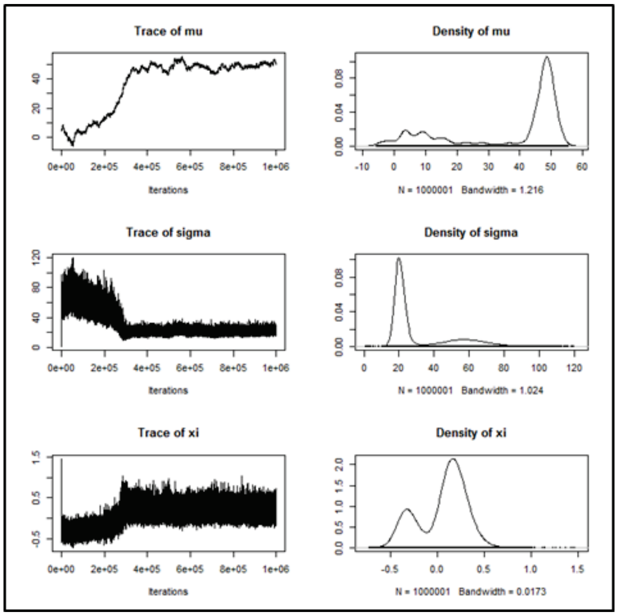

(a)

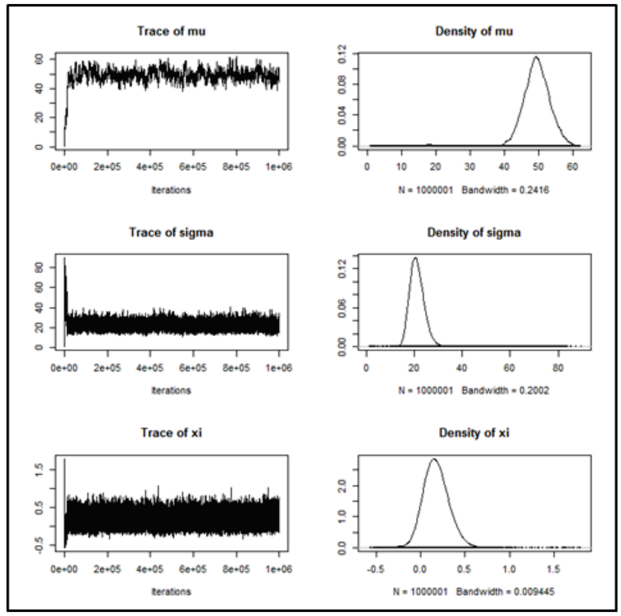

(b)

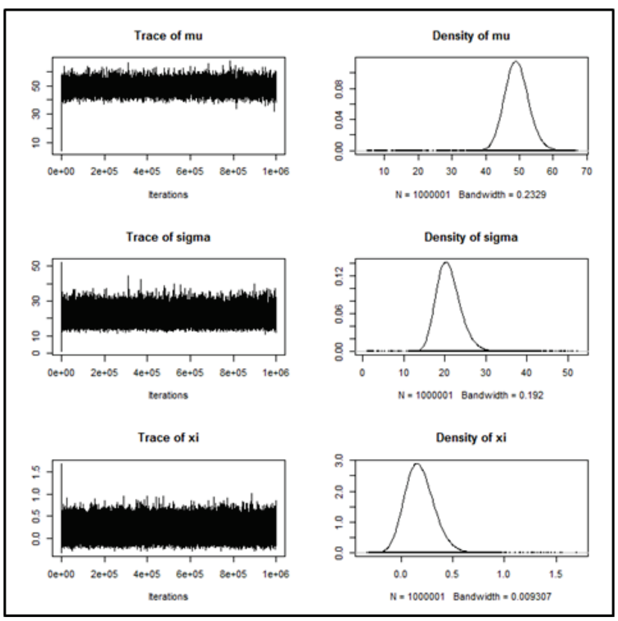

(c)

The active reader is directed to the R documentation for a complete summary description of the evdbayes package posterior function call (Stephenson and Ribatet 2014) including input specifications to follow for its application. However, briefly, the sequence of inputs provided to the posterior function calls listed directly above include the total number of iterations to perform, the initial values, the prior, the likelihood, the annual block maxima rainfall data excluding the 1999 datum, and a vector containing the standard deviations for the MCMC sampler proposal distributions. The prior was defined by the marginal distributions $\mu \sim N(0, 10^4)$, $\sigma \sim LN(0, 10^4)$, and $\xi \sim N(0, 10^2)$. The specified high variances reflect the absence of prior beliefs regarding the extremal model parameters (Stephenson and Ribatet 2014). Despite the trace plots in Figure 3 (c) indicating highly efficient convergence for the given sampler configuration, the first 200,000 iterations are arbitrarily discarded as transient burn-in samples using the first in the sequence of specified R commands listed directly below. The final summary R command listed directly below results in a reporting of posterior estimates for the GEV model parameters as shown in Figure 4, which are in close agreement with the values originally reported by Coles et al. (2003) when using Bayesian inference with the pre-1999 annual block maxima extreme rainfall dataset from the Maiquetia international airport station. As can be verified upon brief examination of the sequence of R commands that resulted in Figure 3 (a), (b), and (c), respectively, the only difference among the three MCMC simulations was the standard deviation specified for the proposal distribution for the location parameter of the GEV distribution. Clearly, the MCMC sampler as implemented in the R software package evdbayes does require tuning of the proposal distribution input parameters for optimal performance, wherein by optimal it is meant efficient characterization of the posterior, which is better achieved when the sampled values exhibit lower serial correlation.

```
mcmcCarb<-mcmcC[200001:1000000,]
mcmcCarb_coda<-as.mcmc(mcmcCarb)
summary(mcmcCarb_coda)
```

Figure 4. Summary of posterior estimates for the GEV model parameters using the pre-1999 annual rainfall maxima from the Maiquetia international airport station and the MCMC sampler as implemented in the R software package evdbayes.

```
Iterations = 1:8e+05
Thinning interval = 1
Number of chains = 1
Sample size per chain = 8e+05

1. Empirical mean and standard deviation for each variable,
   plus standard error of the mean:

         Mean     SD  Naive SE Time-series SE
mu    49.2178 3.5039 0.0039174      0.0592907
sigma 20.9975 2.9339 0.0032802      0.0253755
xi     0.1818 0.1396 0.0001561      0.0008262

2. Quantiles for each variable:

          2.5%      25%     50%     75%  97.5%
mu    42.68739 46.80774 49.0996 51.4877 56.475
sigma 15.96565 18.93778 20.7495 22.7879 27.453
xi    -0.06734  0.08386  0.1732  0.2707  0.478
```

While the MCMC sampler as implemented in the R package evdbayes is a single chain sampler, it can be run multiple times with the same configuration but with different initial points, at nominal compute cost, and the results from the multiple simulations can be combined to further assess sampler convergence beyond an inspection of the trace plots from any one given simulation. For example, the R commands listed directly below execute three separate MCMC simulations, all configured in the same manner with the exception of initialization, using the sampler as implemented in the R software package evdbayes, to infer GEV model parameters using the pre-1999 annual maxima dataset from Venezuela. After each respective simulation is complete, trace and density plots are generated using the plot command. The trace and density plots for the final 1.5 million iterations (the first 500,000 were arbitrarily discarded as transient burn-in samples) are shown in Figure 5. The three simulations, upon completion, are combined into a list to support computation of the Gelman and Rubin (GR) quantitative convergence diagnostic (Cowles and Carlin 1996) using commands contained in the R software package coda. Figure 6 is a plot of the GR statistic as a function of MCMC simulation iteration for each of the GEV model parameters. The R software coda package documentation states that values for the GR statistic substantially above 1 indicate lack of convergence. Conventional guidance suggests GR values to be less than approximately 1.1 (Gelman et al. 2004). However, sole reliance upon the GR quantitative diagnostic to assess sampler burn-in is not advised as it can misdiagnose convergence (Gelman et al. 2004). The plots of the GR statistic shown in Figure 6 clearly indicate lack of convergence. The trace plots of the chains for the location parameter shown in Figure 5 corroborate this assessment. The serial correlation present in the trace plots for the GEV location parameter in Figure 5 suggest tuning its related proposal distribution in attempts to improve sampler performance. Highly useful additional measures and capabilities exist within the R software package coda not only to assist with convergence diagnosis but also overall MCMC sampler performance.

```
mcmcA1<-
posterior(2000000,init=c(5,1,.1),prior=pn,lh=”gev”,data=vam_pre99[,2],psd=c(.02,.1,.1))
mcmcA1_coda<-as.mcmc(mcmcA1)
plot(mcmcA1_coda)

mcmcA2<-
posterior(2000000,init=c(25,5,.5),prior=pn,lh=”gev”,data=vam_pre99[,2],psd=c(.02,.1,.1))
mcmcA2_coda<-as.mcmc(mcmcA2)
plot(mcmcA2_coda)

mcmcA3<-
posterior(2000000,init=c(30,50,.2),prior=pn,lh=”gev”,data=vam_pre99[,2],psd=c(.02,.1,.1))
mcmcA3_coda<-as.mcmc(mcmcA3)
plot(mcmcA3_coda)

mcmc_coda_list<-mcmc.list(mcmcA1_coda,mcmcA2_coda,mcmcA3_coda)
gelman.plot(mcmc_coda_list)
```

Figure 5. Trace and density plots of the GEV model parameters resulting from three MCMC simulations configured in the same manner using the pre-1999 annual rainfall maxima from the Maiquetia international airport station and the MCMC sampler as implemented in the R software package evdbayes.

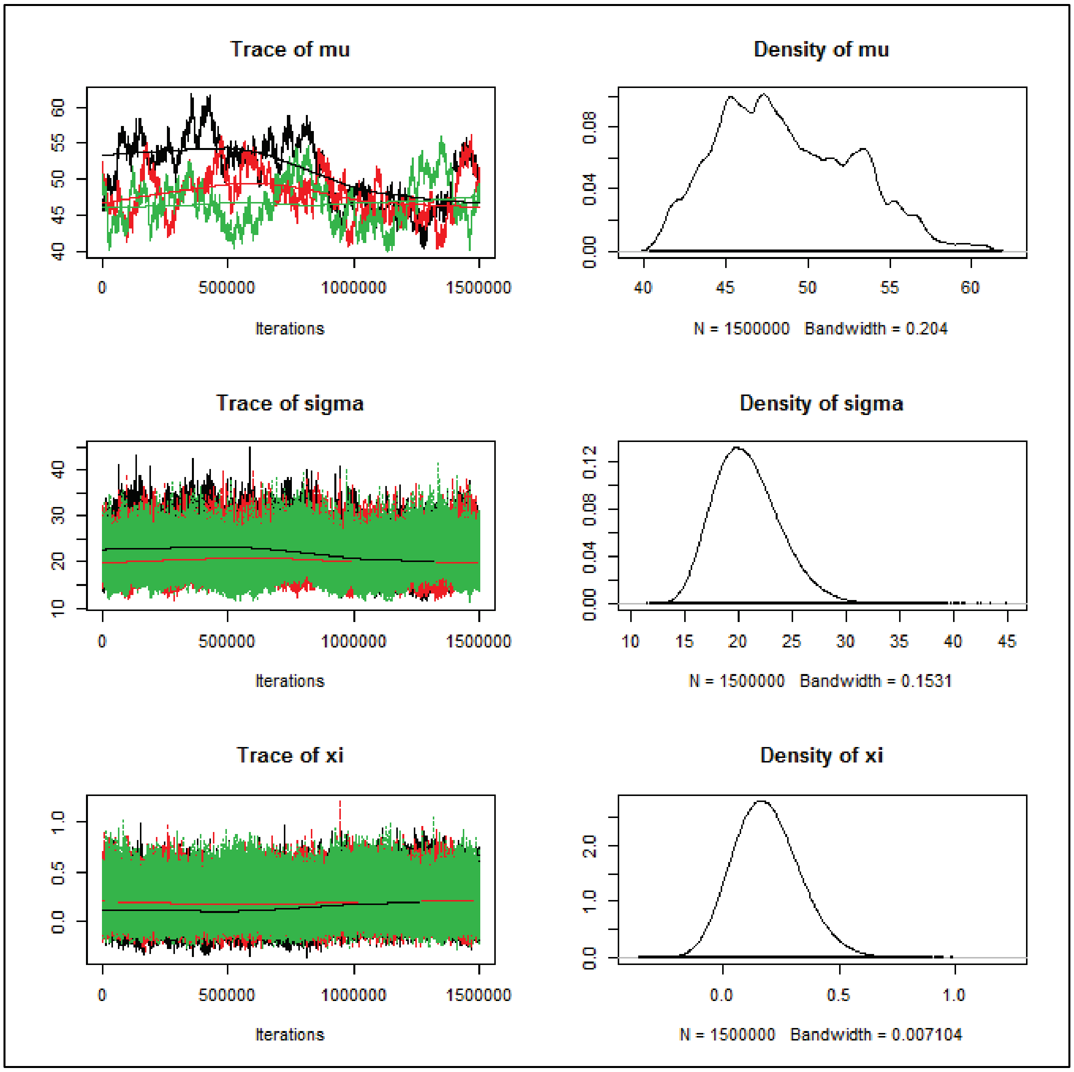

Figure 6. Plot of the Gelman and Rubin quantitative convergence diagnostic as a function of simulation iteration using the results from the three MCMC simulations profiled in Figure 5.

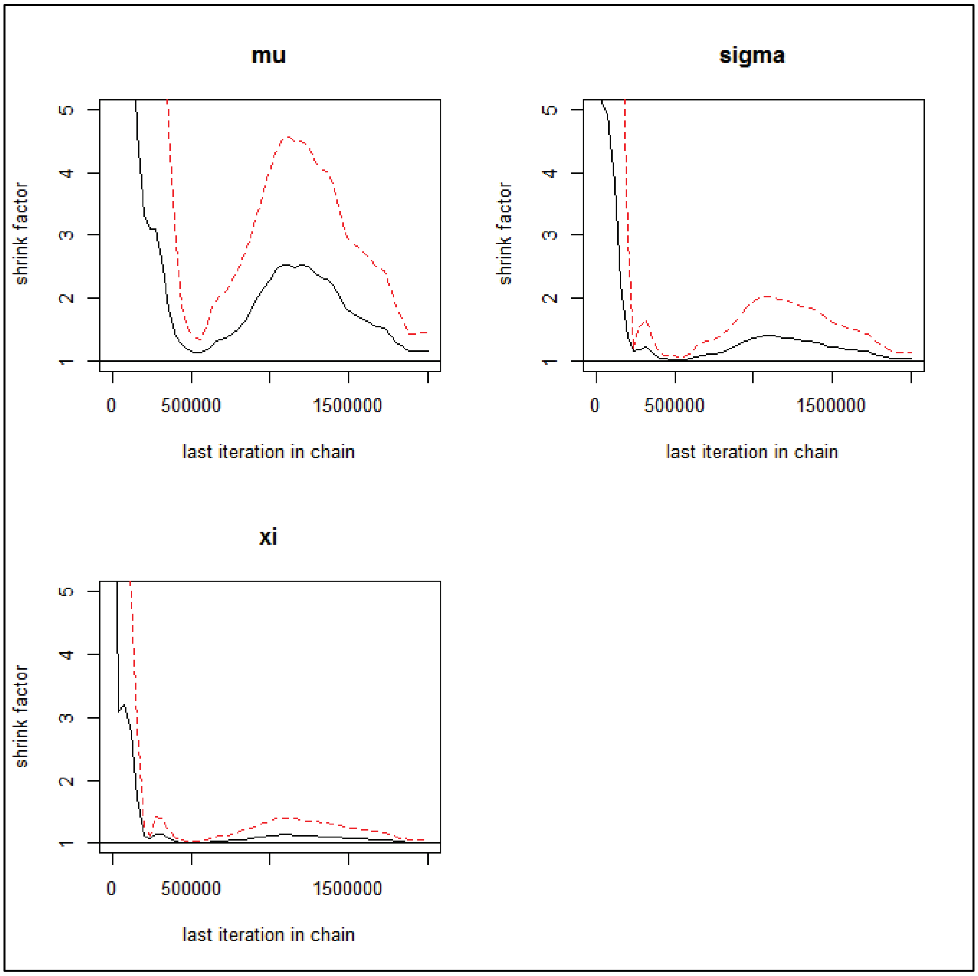

Functionalities existing within the R software package evdbayes were applied, using the monitoring period draws associated with the MCMC simulation whose results were previously presented in Figure 4 (and also in Figure 3 (c) for the entire MCMC simulation), to generate return level plots and also posterior densities for the 10-, 100-, and 1000-year quantile levels as shown in Figures 7 and 8, respectively. The densities shown in Figure 8 could be viewed as vertical slices of the return level plots shown in Figure 7 at the noted quantile levels. Emphasis is on the asymmetry of the uncertainties shown in Figures 7 and 8, which are different than traditional frequentist confidence intervals that invoke normal distribution assumptions for uncertainty. The R commands that were employed to generate the plots shown in Figure 7 and Figure 8 are provided directly below. It is readily acknowledged that critical infrastructure applications would likely focus on quantile levels greater than 1000 years. This introductory example profiles some practical aspects of Bayesian estimation and inference for a simple at-site analysis, in this case when working with a block maxima extreme rainfall dataset. This specific example including the demonstration results as shown should not be misinterpreted as a/the recommended approach for critical infrastructure applications.

```
rl.pst(mcmcCarb,lh="gev",xlim=c(1.001,100),ylim=c(0,400))
rl.pst(mcmcCarb,lh="gev",xlim=c(100,1000),ylim=c(100,1000))

poq<-mc.quant(mcmcCarb,p=c(.9,.99,.999),lh="gev")
plot(density(poq[,1), xlim=c(50,200),ylim = c(0,.05))
plot(density(poq[,2]), xlim=c(0,600),ylim = c(0,.01))
plot(density(poq[,3]), xlim=c(0,2000),ylim = c(0,.01))
```

Figure 7. Return level plots resulting from analysis of the post burn-in draws generated from application of the MCMC sampler as implemented in the evdbayes R package that was employed to infer GEV model parameters using the annual rainfall maxima from the Maiquetia international airport station excluding the 1999 datum. The red dashed lines are the computed 5th and 95th percentile values. The solid black line is the estimated median.

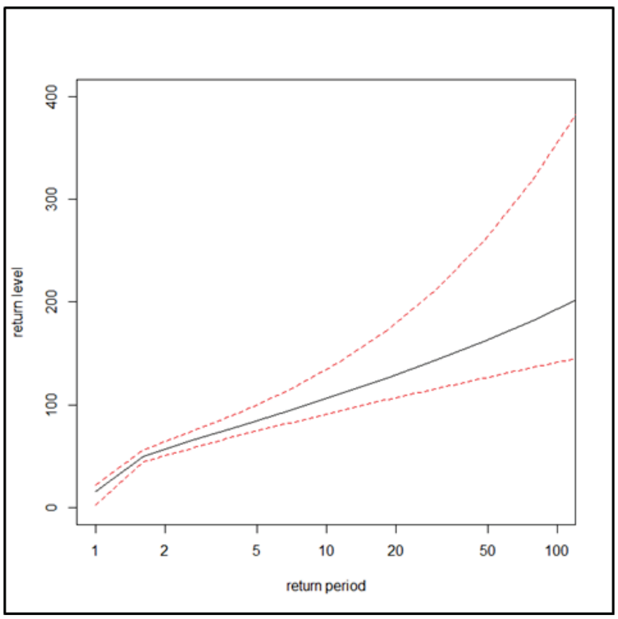

(a)

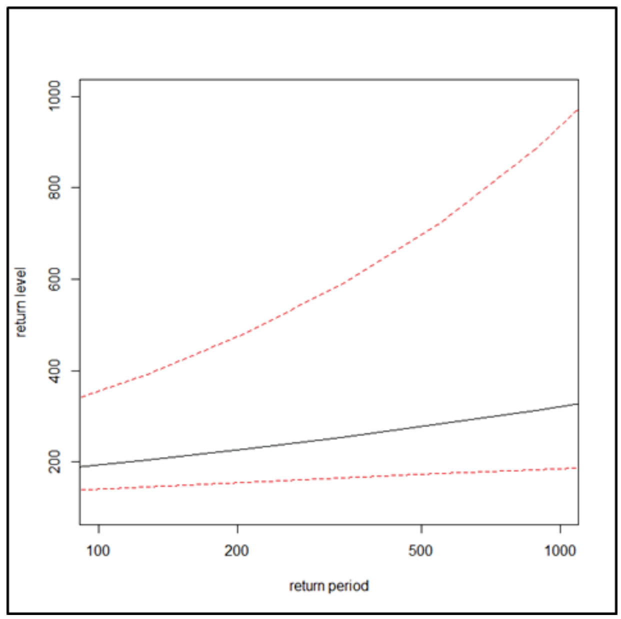

(b)

Figure 8. Posterior densities for quantile levels associated with the (a) 10-, (b) 100-, and (c) 1000-year return periods that result from analysis of the post burn-in draws generated from application of the MCMC sampler as implemented in the evdbayes R package that was employed to infer GEV model parameters using the annual rainfall maxima from the Maiquetia international airport station excluding the 1999 datum.

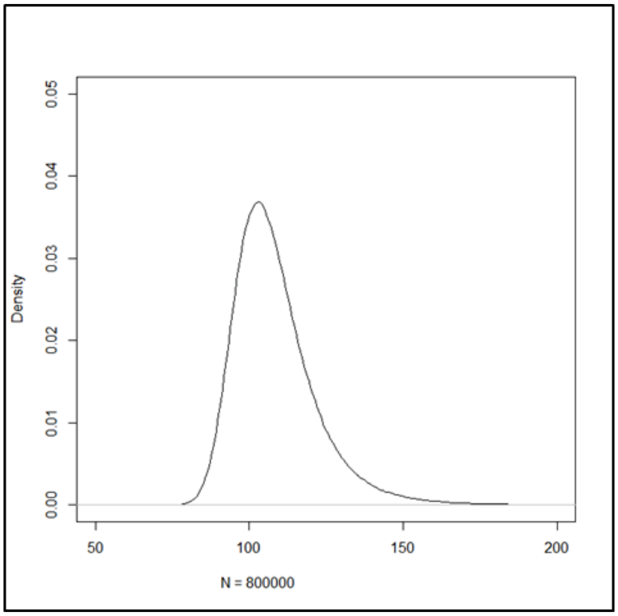

(a)

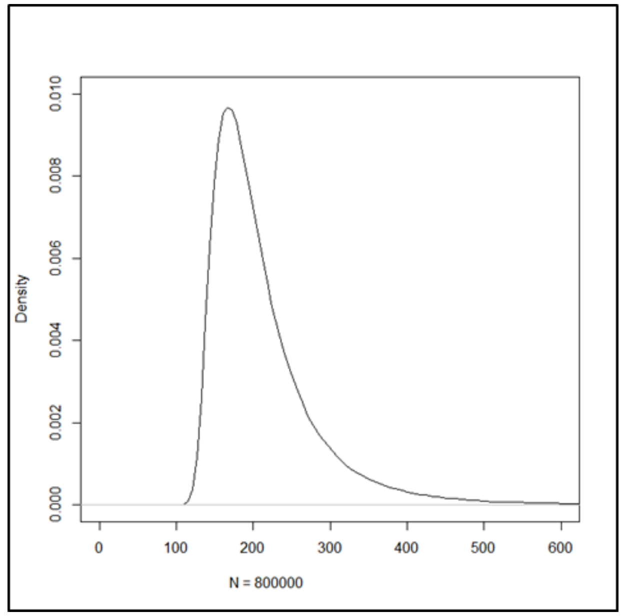

(b)

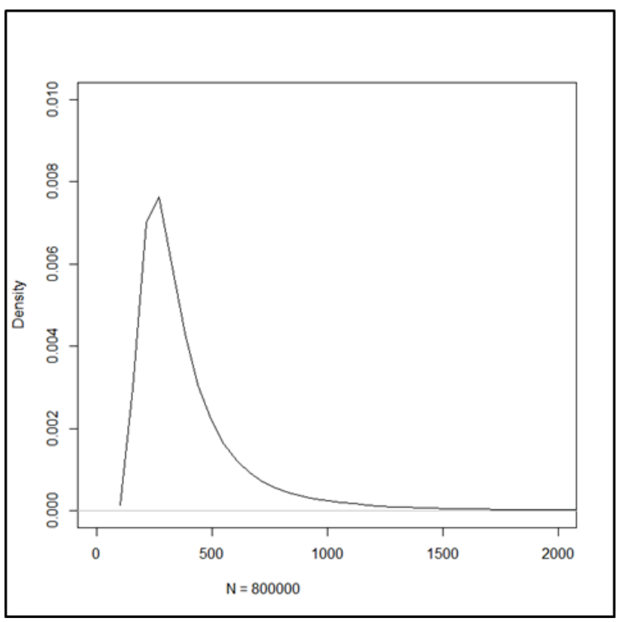

(c)

Posterior predictive return level plots were computed using the same R software package evdbayes MCMC simulation monitoring period draws that were also used to generate Figures 7 and 8. The predictive return level plots shown in Figure 9 were generated using Equation D.9 with $L = 1$. The specific R commands employed are provided below. Examining Figure 9 (b), the predictive return period estimate for the 1999 event (410.4 millimeters [mm]) is approximately 668 years, which is in close agreement with the value of 660 years originally reported by Coles et al. (2003). The R software packages evdbayes and coda were also used with the full annual maxima dataset including the 1999 datum, and in this case, the posterior predictive return period estimate for the 1999 event (410.4 mm) is approximately 162 years, which is also in close agreement with the value of 177 originally reported by Coles et al. (2003).

```
rl.pred(mcmcCarb,lh="gev",period=1,qlim=c(0,500))
rl.pred(mcmcCarb,lh="gev",period=1,qlim=c(400,420))
```

Figure 9. Posterior predictive return level plots for the GEV model of the Venezuelan annual maximum daily rainfall excluding the 1999 datum.

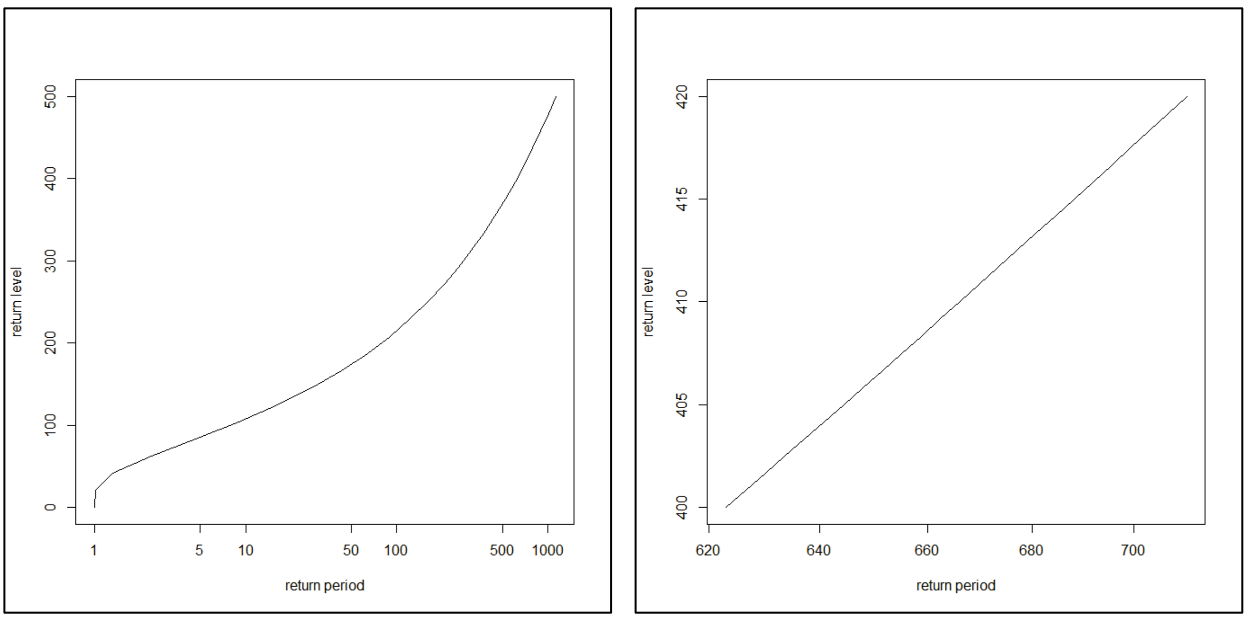

(a) (b)

While the R software package evdbayes does not explicitly support specification of the Gumbel model with its posterior function, it does seem possible to *effectively* apply the Gumbel model through user specification of the prior, proposal distribution standard deviations, and sampler initialization. The prior was updated only for the shape parameter, with its marginal distribution now given by $\xi \sim N(0, 10^{-10})$. Figures 10, 11, and 12 were obtained with the R commands provided below. The summary model parameter posterior estimates provided in Figure 11 and also the predictive return levels encapsulated in Figure 12 are in close agreement with their respective values that were originally reported by Coles et al. (2003) using the pre-1999 annual maxima dataset from Venezuela. The predictive return period estimate for the 1999 event (410.4 mm) is approximately 2,360,000 years. A similar Bayesian analysis using the R software packages evdbayes and coda with the full Venezuelan annual maxima dataset yields model parameter posterior estimates in close agreement with those originally provided in Coles and Pericchi (2003) rather than those provided in Coles et al. (2003) and a predictive return period estimate for the 1999 event (410.4 mm) of approximately 177,000 years, which is comparable with the value of 233,000 originally reported by Coles et al. (2003). The Gumbel model is of course not recommended for extreme rainfall analysis (Koutsoyiannis 2004a). Moreover, this specific application is not recommended and was performed simply for demonstration purposes in attempts to further focus on the issues of model selection and inference methodology with the noted Venezuelan block maxima dataset while revisiting analyses originally performed and reported upon by Coles et al. (2003) and Coles and Pericchi (2003).

```
mcmcG<-posterior(2000000, init=c(5,1,0.0000000000001), lh="gev",
data=vam_pre99[,2], psd=c(1,.1,.000000000000000001), prior=pn2)
mcmcGarb<-mcmcG[500001:2000000,]
mcmcGarb_coda<-as.mcmc(mcmcGarb)
plot(mcmcGarb_coda)
summary(mcmcGarb_coda)
rl.pred(mcmcGarb,lh="gev",period=1,qlim=c(0,500))
rl.pred(mcmcGarb,lh="gev",period=1,qlim=c(400,420))
```

Figure 10. Trace and density plots of the GEV model location and scale parameters for an MCMC simulation using the pre-1999 annual rainfall maxima from the Maiquetia international airport station and the MCMC sampler as implemented in the R software package evdbayes, configured in attempts to effectively apply the simplified Gumbel model.

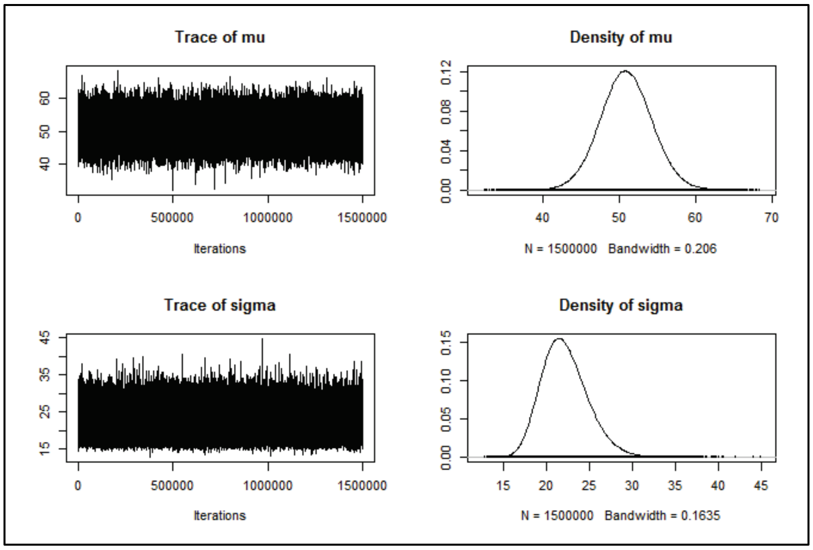

Figure 11. Summary of posterior estimates for the GEV model parameters using the pre-1999 annual rainfall maxima from the Maiquetia international airport station and the MCMC sampler as implemented in the R software package evdbayes and configured in attempts to effectively apply the simplified Gumbel model.

```
Iterations = 1:1500000
Thinning interval = 1
Number of chains = 1
Sample size per chain = 1500000

1. Empirical mean and standard deviation for each variable,
   plus standard error of the mean:

            Mean        SD  Naive SE Time-series SE
mu     5.084e+01 3.369e+00 2.750e-03       0.020666
sigma  2.214e+01 2.694e+00 2.199e-03       0.008616
xi     1.000e-13 3.732e-16 3.047e-19       0.000000

2. Quantiles for each variable:

            2.5%       25%       50%       75%     97.5%
mu     4.429e+01 4.859e+01 5.081e+01 5.307e+01 5.753e+01
sigma  1.753e+01 2.024e+01 2.191e+01 2.379e+01 2.805e+01
xi     9.922e-14 9.981e-14 1.001e-13 1.003e-13 1.006e-13
```

Figure 12. Posterior predictive return level plots for the GEV model of the Venezuelan annual maximum daily rainfall excluding the 1999 datum using the R software package evdbayes configured in attempts to effectively apply the simplified Gumbel model.

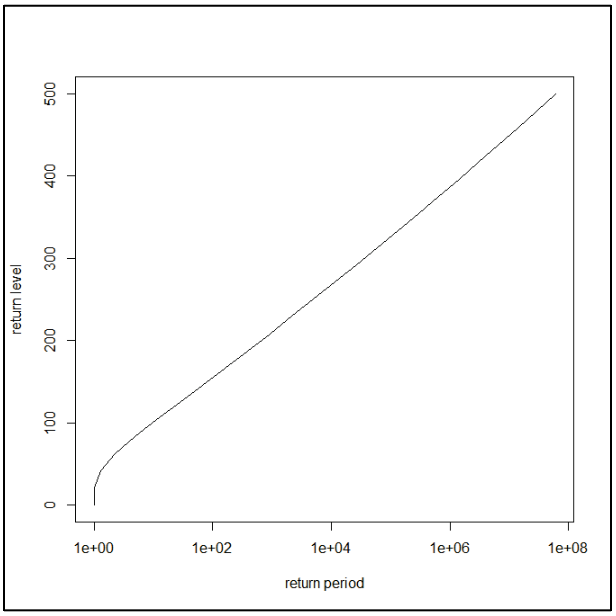

(a)

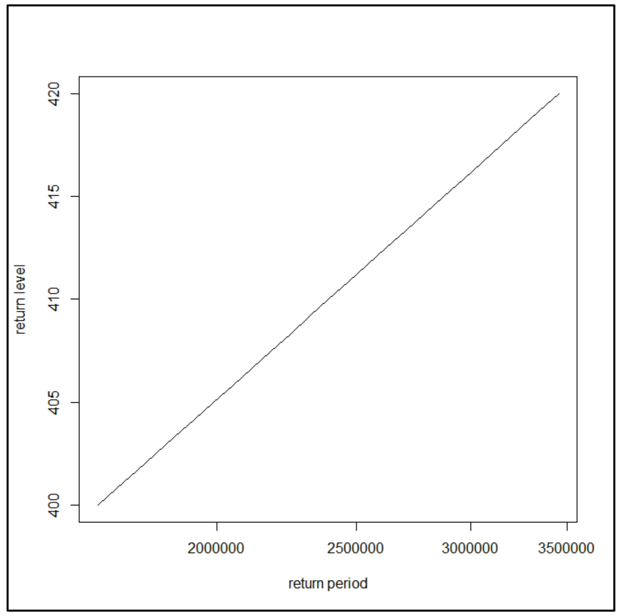

(b)

The MCMC sampler as implemented in the R software package extRemes was also applied using the Venezuelan annual maximum daily rainfall excluding the 1999 datum. Priors were defined in the same manner as they were previously specified when the MCMC sampler as implemented in the evdbayes R software package was used to infer the GEV model parameters, viz., $\mu \sim N(0, 10^4)$, $\sigma \sim LN(0, 10^4)$, and $\xi \sim N(0, 10^2)$. The default random walk proposal distribution was employed together with associated standard deviation values user specified to be equal in value to (0.5,0.1,0.1) for each respective GEV model parameter (i.e., (μ, σ, ξ)). While the trace and density plots and also plots of the GR statistic (shown in Figures 13 and 14, respectively) derived by applying the single chain sampler as implemented in the extRemes package multiple times indicated sampler convergence with each application, the computed posterior summaries for the inferred GEV model parameters did not agree with the values originally reported by Coles et al. (2003) (see Figure 15 and compare with Figure 4 above and/or Table 1 in Coles et al. [2003]). Computed GEV model parameter posterior standard deviations are consistently larger than their comparable values previously reported in Figure 4, obtained using the MCMC sampler as implemented in the evdbayes R software package. Possibly, additional simulation is required with the extRemes package MCMC sampler to explore in more detail the sensitivity of specified proposal distribution standard deviations. However, as a matter of interest, the predictive posterior return level (computed using the evdbayes package function “rl.pred”) of 410.4 mm for $L = 1$ and based on the extRemes package MCMC sampler monitoring period draws derived using the pre-1999 annual maxima was estimated to be 409 years.

Figure 13. Trace and density plots of the GEV model parameters for an MCMC simulation using the pre-1999 annual rainfall maxima from the Maiquetia international airport station and the MCMC sampler as implemented in the R software package extRemes.

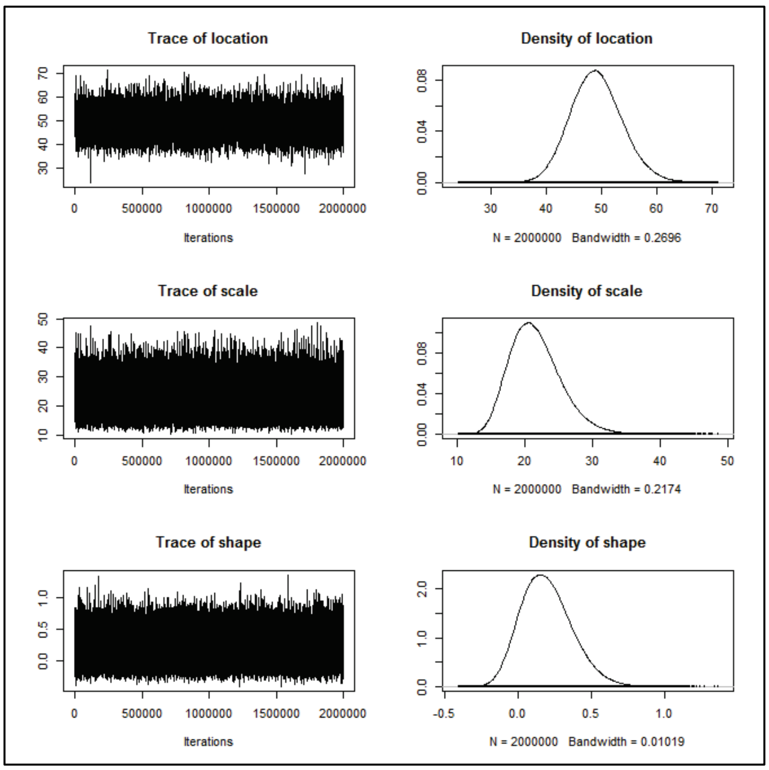

Figure 14. Plot of the Gelman and Rubin quantitative convergence diagnostic as a function of simulation iteration using the results from the two MCMC simulations performed using the R software package extRemes.

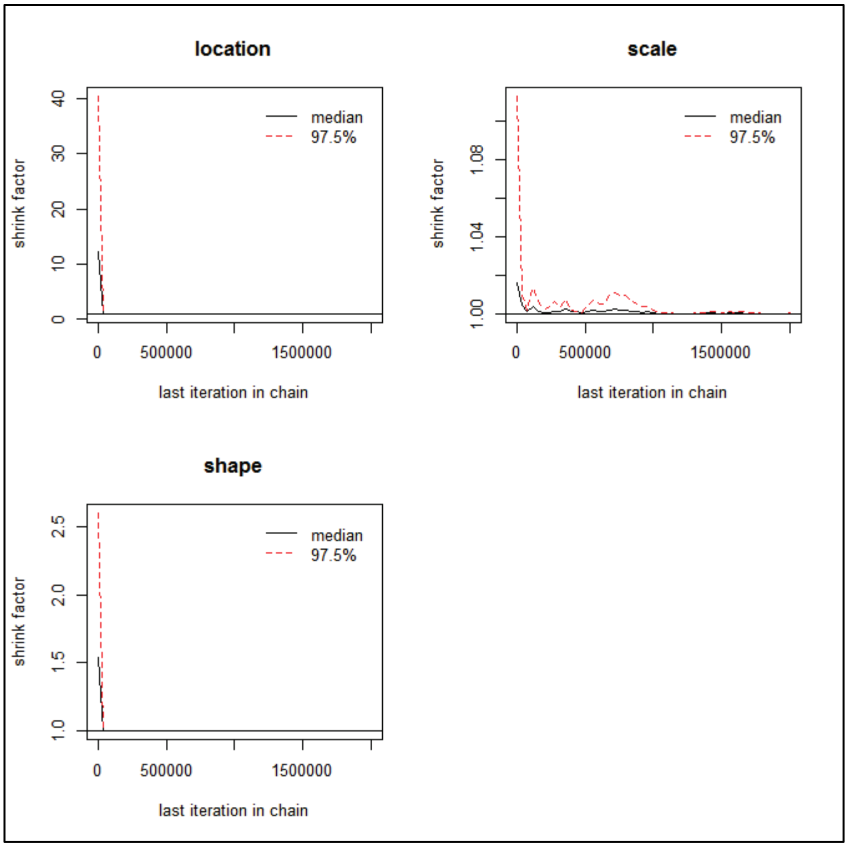

Figure 15. Summary of posterior estimates for the GEV model parameters using the pre-1999 annual rainfall maxima from the Maiquetia international airport station and the MCMC sampler as implemented in the R software package extRemes.

```
Iterations = 1:1e+06
Thinning interval = 1
Number of chains = 1
Sample size per chain = 1e+06

1. Empirical mean and standard deviation for each variable,
   plus standard error of the mean:

            Mean    SD Naive SE Time-series SE
location 49.0980 4.648 0.004648        0.09689
scale    21.5600 3.807 0.003807        0.03377
shape     0.1941 0.175 0.000175        0.00107

2. Quantiles for each variable:

            2.5%      25%     50%     75%   97.5%
location 40.5959 45.85144 48.8772 52.0837 58.9005
scale    15.2467 18.83923 21.1771 23.8566 30.0857
shape    -0.1081  0.06914  0.1808  0.3051  0.5702
```

The R software packages ismev, evd, and extRemes possess functionalities to employ maximum likelihood estimation (MLE) to estimate extremal model parameters, and the active reader is directed to their respective documentation for additional related information (Stephenson 2002; Stephensen 2016). Use of the MLE functionalities encapsulated in these R software packages did yield GEV and Gumbel model parameter and return level estimates in close agreement with the values originally reported by Coles and al. (2003) for the Venezuelan annual maximum daily rainfall, with and without consideration of the 1999 datum. For example, the return level estimates of 410.4 mm for these models, obtained using the R software package evd, were approximately 4440/310 and 18,300,000/756,000 years when the 1999 datum was excluded/included while using the GEV and Gumbel models, respectively.

This demonstration has revisited analyses originally performed and reported upon by Coles et al. (2003) and Coles and Pericchi (2003) using the Venezuelan annual maxima rainfall dataset while applying the Bayesian inference methodology by using and profiling various related capacities of readily available cited software for the analysis of extremes. The revisited analysis and its related results are particularly notable in that model selection criteria would support choosing the Gumbel rather than the GEV model when excluding the 1999 datum (Laio et al. 2008). The results further suggest, as was originally underscored by Coles et al. (2003), that not only model selection but also inference methodology matters in an extreme rainfall analysis.

3.1.1.2 Threshold exceedance model

This second example further focuses on the topics of model selection and inference methodology, now leveraging available daily rainfall data for the Maiquetia international airport rather than its annual maxima dataset, which was the basis for the first example demonstration. For this data scenario, the likelihood is as indicated in Equation D.2. For the Generalized Pareto Distribution (GPD) model, the density in Equation D.2 is given by $f = H'$ where H is as defined in Equation A.6. As with the treatment of block maxima data, the prior distribution on the parameters is commonly specified as uninformative, and among possible others following successful completion of a simulation, the MCMC sampler post burn-in monitoring period draws are used to compute posterior densities, return level plots, and posterior predictive distributions for future observations.

Case study demonstration – Daily rainfall data from the Maiquetia international airport station

The daily rainfall data for the Maiquetia international airport, originally analyzed by Coles et al. (2003), were also requested and received from Drs. Pericchi and Sisson. The 14,184 daily rainfall data, which cover the period 1 January 1961 to 31 December 1999 minus February 1996 and January 1998, are shown in Figure 16. The availability of this dataset in addition to the annual maxima permits further examination as to how well an event the magnitude of the 1999 event could have been anticipated statistically prior to its occurrence.

Figure 16. Daily rainfall values recorded in Maiquetia, Venezuela, for calendar years 1961-1999, inclusive.

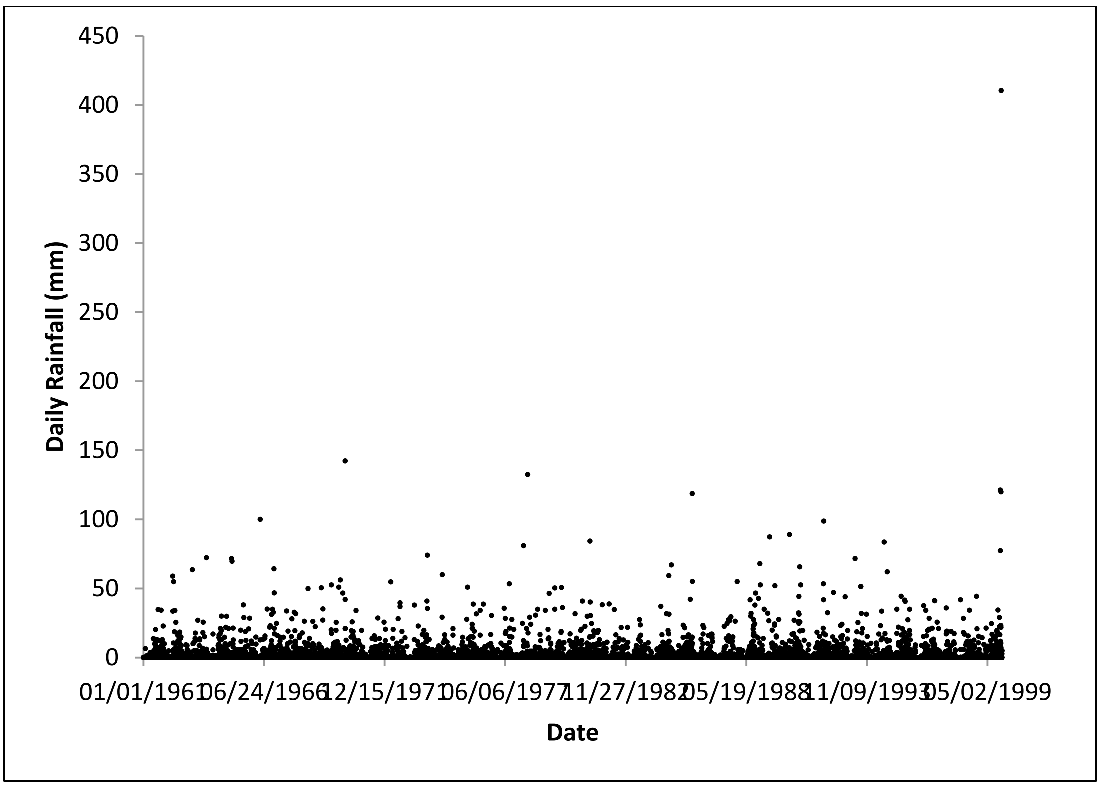

The R software packages ismev, evd, and extRemes have the capacity to generate a mean residual life plot to facilitate threshold selection. The extRemes package contains a function to facilitate declustering data above a given threshold. The evd and extRemes packages have the capacity to estimate the extremal index. Moreover, these three packages readily support application of MLE with the GPD model. MLE estimates for the GPD model parameters and their related return level estimates, obtained with and without consideration of the 1999 daily data and applying respective functionalities in each of these three R packages, agreed well with the values originally reported by Coles et al. (2003). The extRemes package estimates a return level of approximately 769/252 years for the 1999 event value of 410.4 mm following MLE estimation of the GPD model parameters without and with consideration of the 1999 daily data. These values agree well with the corresponding estimates of 752 and 251 originally reported by Coles et al. (2003) for this model selection, inference methodology, and data scenario.

The MCMC sampler as implemented in the R software package extRemes was applied to infer the GPD model parameters using a specified threshold value of 10 for the daily dataset while including and also excluding the 1999 data. The extRemes R software package was used for this modeling analysis rather than the evdbayes package due to difficulties experienced with successful application of the MCMC sampler as implemented in the evdbayes package while using the GPD EVT model. Simulation results are shown in Figures 17 and 18 for these two MCMC simulations, which modeled the daily data in the same manner as originally reported in Coles et al. (2003). The GPD model parameter trace plots shown in Figure 17 indicate the sampler was configured well for the problem and also suggest that the sampler achieved equilibrium early in the simulation. The summary posterior estimates for the GPD model parameters, based on the entire simulation in each case, are shown in Figure 18. The posterior mean shape value of 0.2721 reported in Figure 18 (a) for the simulation that excluded the 1999 daily data is less than the shape value of 0.30 originally reported by Coles et al. (2003) for the same analysis. The subsequently computed predictive posterior return levels (for $L = 1$) of 410.4 mm were estimated to be equal to 423 and 181 years for these two simulations, which excluded and included the 1999 daily data, respectively. These noted return levels values do slightly differ with the comparable values of 260 and 116 originally reported by Coles et al. (2003) for their GPD model application using Bayesian inference and the same data and threshold value. The slight discrepancy with the reported return levels is attributed to the noted difference in the shape values. Additional MCMC simulation could, and likely should, be performed to verify that the results reported in Figures 17 and 18 that were obtained using the MCMC sampler as implemented in the R software package extRemes properly reflect estimates of the posterior distribution. Regardless, this additional exploration with the available daily data does provide further reinforcement to what was originally underscored in the first example, viz., the importance not only of inference methodology but also model/data choice in an extreme rainfall analysis.

Figure 17. Trace and density plots of the GP model parameters for MCMC simulations using the daily rainfall data from the Maiquetia international airport station (a) without and (b) with consideration of the 1999 data, a threshold of 10, and the MCMC sampler as implemented in the R software package extRemes.

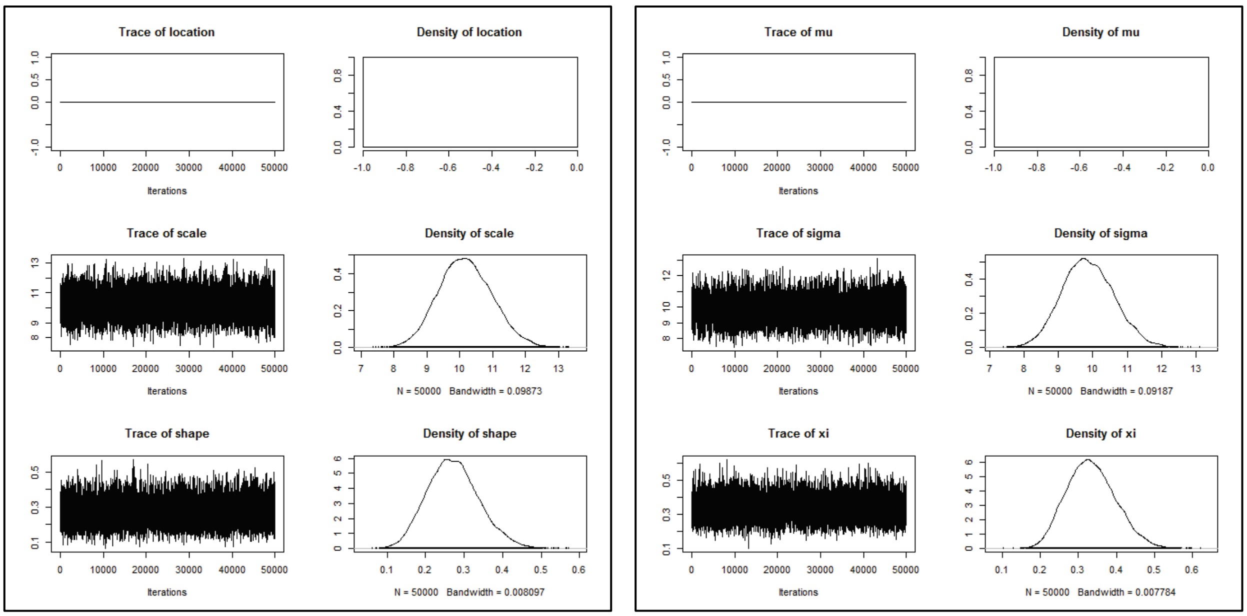

(a) (b)

Figure 18. Summary of posterior estimates for the GP model parameters using daily rainfall data from the Maiquetia international airport station (a) without and (b) with consideration of the 1999 data, a threshold of 10, and the MCMC sampler as implemented in the R software package extRemes.

	Mean	SD
location	0.0000	0.0000
scale	10.1795	0.8109
shape	0.2721	0.0665

(a)

	Mean	SD
mu	0.0000	0.00000
sigma	9.8674	0.75452
xi	0.3342	0.06393

(b)

3.1.2 Combining Different Observed Data Types

Bayesian inference is attractive in that it can flexibly support combining complementary data sources into an extreme rainfall analysis. This third example revisits work originally presented by Coles and Pericchi (2003) that demonstrates one way in which different data can be combined in an at-site analysis of extreme rainfall. As with the first two examples, this case study further analyzes the issue of data analysis, model selection, and inference methodology in an analysis of extremes.

3.1.2.1 Case study demonstration – Combine annual maxima and daily rainfall data from the Maiquetia international airport station

Coles and Pericchi (2003) observed that the annual maxima and daily rainfall datasets from the Maiquetia international airport station differed with respect to their periods of record. By considering a point process (PP) model, they exploited the fact that estimated PP model parameters correspond directly to the GEV parameters of the annual maxima distribution of the observed process and formulated a likelihood that maximally uses both of the available data sets.

The MCMC sampler as implemented in the R software package evdbayes was initially applied to infer the PP model parameters using the pre-1999 daily data, a threshold value of 10, and excluding any consideration of the annual maxima data. Simulation results are shown in Figures 19 and 20. The predictive posterior year return level (for $L = 1$) for the 1999 event from this model is 338 years. A population-based MCMC sampler (ter Braak and Vrugt 2008) was subsequently applied to infer the PP model parameters using the log likelihood defined by Coles and Pericchi (2003), which maximally uses the block maxima and threshold exceedance data from the Maiquetia international airport station, uninformative uniform priors, and while also including the annual maxima data but excluding the 1999 annual maximum and 1999 daily data. The population-based MCMC sampler (ter Braak and Vrugt 2008) was implemented and used since the MCMC samplers in the R software packages evdbayes and extRemes did not appear to readily support this case study demonstration modeling scenario. A population of size 60 was specified for the MCMC simulations. Latin hypercube sampling of the box defined by the specified lower and upper bounds for the three PP model parameters was used to initialize the population for simulation. The simulation results presented in Figure 21 and Table 1 are based on a thinned history, viz., every tenth evolution, of the approximately 500,000 specified total post burn-in monitoring period model runs. The PP model parameter posterior estimates presented in Figure 20 and Table 1 indicate that combining the daily and annual maxima datasets is of incremental value relative to simply working with the daily data itself, at least for this particular case study demonstration. This is further corroborated with a comparison of the estimated value of 287.9 for the predictive posterior 100 year return level (for $L = 1$) for the evdbayes supervised MCMC simulation that excluded the annual maxima data. This noted return level value is only slightly lower than the comparable value of 297.9 reported by Coles and Pericchi (2003), which is based on combining the pre-1999 annual maxima and daily data in the point process modeling analysis.

Figure 19. Trace and density plots of the point process model parameters for a MCMC simulation using the pre-1999 daily rainfall data from the Maiquetia international airport station, a threshold of 10, and the MCMC sampler as implemented in the R software package evdbayes.

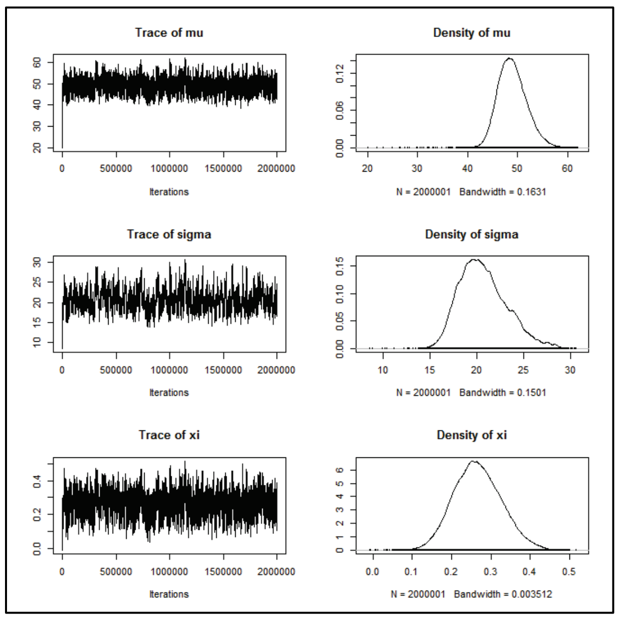

Figure 20. Summary of posterior estimates for the point process model parameters using the pre-1999 daily rainfall data from the Maiquetia international airport station, a threshold of 10, and the MCMC sampler as implemented in the R software package evdbayes.

```
Iterations = 1:1500001
Thinning interval = 1
Number of chains = 1
Sample size per chain = 1500001

1. Empirical mean and standard deviation for each variable,
   plus standard error of the mean:

         Mean      SD  Naive SE Time-series SE
mu    48.8792 2.83185 2.312e-03        0.06975
sigma 20.6216 2.61972 2.139e-03        0.19746
xi     0.2644 0.06091 4.973e-05        0.00171

2. Quantiles for each variable:

         2.5%     25%     50%     75%   97.5%
mu    43.9701 46.8669 48.6514 50.6440 55.0896
sigma 16.4250 18.7198 20.2878 22.1897 26.6047
xi     0.1526  0.2214  0.2617  0.3046  0.3909
```

Figure 21. Trace plots of the point process model parameters for a MCMC simulation using the pre-1999 daily rainfall data and pre-1999 annual maxima data from the Maiquetia international airport station, a threshold of 10, and a population-based MCMC sampler (ter Braak and Vrugt 2008).

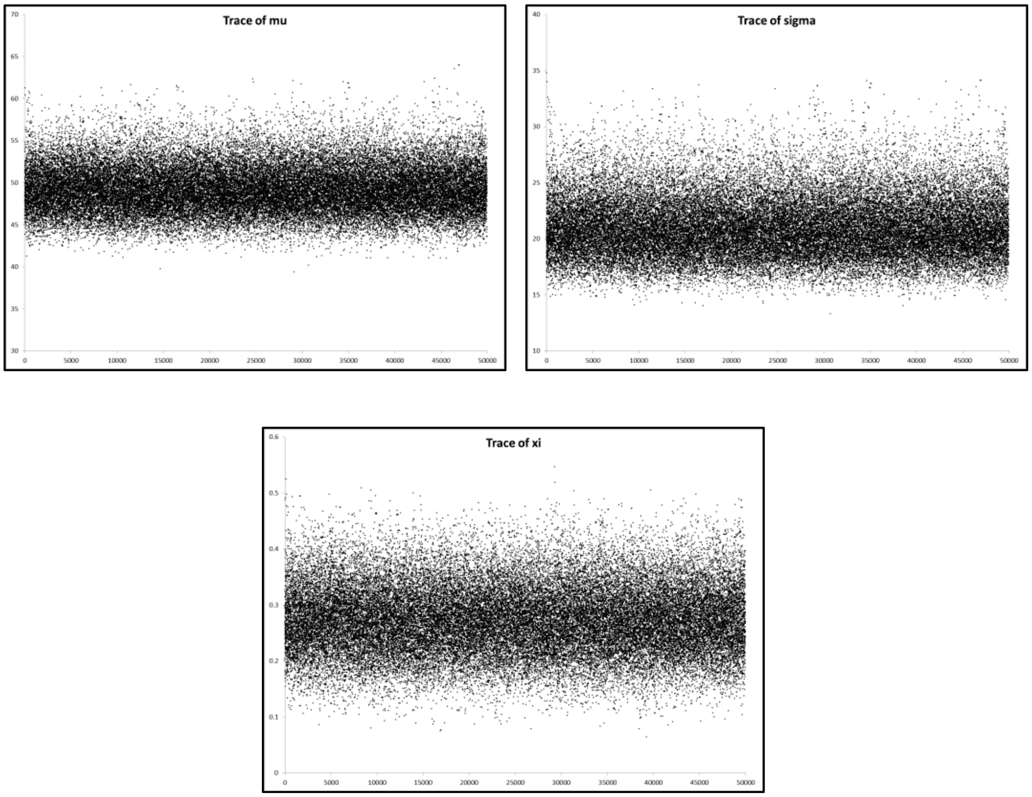

Table 1. Summary of posterior estimates for the point process model parameters using the pre-1999 daily rainfall data and pre-1999 annual maxima data from the Maiquetia international airport station, a threshold of 10, and a population-based MCMC sampler (ter Braak and Vrugt 2008).

		mu	sigma	xi	
	Mean	49.2852	21.0692	0.2740	
	SD	2.8587	2.6862	0.0615	
	2.50%	25%	50%	75%	97.50%
mu	44.2679	47.2823	49.0774	51.0741	55.4512
sigma	16.6817	19.1572	20.7546	22.6634	27.2204
xi	0.1612	0.2311	0.2715	0.3139	0.4016

3.1.3 Seasonality

In this fourth example, the focus is on applying physical rainfall process understanding into the analysis of the daily data from the previous two examples and subsequent model inference and prediction.

3.1.3.1 Case study demonstration – A seasonal model of daily rainfall data from the Maiquetia international airport station

Coles and Pericchi (2003) developed a model that divided the year into two seasons based on previously documented summaries that the rainfall climatology in Venezuela exhibits a two-season cycle with events determined by cold fronts in the winter and tropical storms in the summer, respectively. Their changepoint model considered two seasons, viz., $\mathrm{I}_1 = [1, k_1 - 1] \cup [k_2, 366]$ and $\mathrm{I}_2 = [k_1, k_2 - 1]$, where the two seasons are indexed by the day of the year and k_1 and k_2 are changepoint parameters introduced to account for uncertainty regarding the timing of the seasonal changes. Their likelihood formulation involved distinct point process model parameterizations for I_1 and I_2. The two changepoint parameters were also included as part of the model inference using uninformative uniform priors ($k_1 \sim \mathrm{U}[50{,}250]$ and $k_2 \sim \mathrm{U}[200{,}366]$) and the constraint that $k_1 < k_2$. Coles and Pericchi (2003) underscored the capacity of the Bayesian inference methodology to accommodate this variable changepoint modeling analysis. With its application, regardless of whether the 1999 daily data from the Maiquetia International Airport Station were included or excluded in the analysis, Coles and Pericchi (2003) indicated that mid-November to April best defined the winter period and the remainder of the year the summer period.

The R software package evdbayes was used to infer point process model parameters for a 167-day long winter period mid-November to April using the daily data, excluding 1999, from the Maiquetia international airport station and a threshold of ten. The winter dataset consisted of 157 daily exceedances. The subsequently computed predictive posterior return level (for $L = 1$) of 410.4 mm was estimated to be equal to 133 years for this simulation, which excluded 1999 daily data. This value agrees well with the estimate of 131 years originally reported by Coles et al. (2003) for their related seasonal GPD modeling analysis. This case study demonstration clearly underscores the importance and impact of data analysis in the analysis of extreme rainfall.

The first four examples have revisited at-site extreme rainfall analyses originally profiled by Coles et al. (2003) and Coles and Pericchi (2003), primarily using R software packages that are in the public domain. In particular, there was a re-examination of the available block maxima and threshold exceedance rainfall data for the Maiquetia international airport station individually and in combination, and for the daily data also seasonally while primarily using Bayesian inference but also by comparing with results obtained using MLE. Table 2 summarizes results from the noted analyses, presenting return period estimates for the 1999 event (410.4 mm) from EVT models obtained using either Bayesian inference or MLE without and also with consideration of the 1999 data. The results in Table 2 clearly underscore the importance of data analysis, model selection, and inference methodology in an analysis of extremes. The seasonal PP model inferred using the pre-1999 daily data assigns an anticipatory non-negligible probability to the catastrophic 1999 event.

Table 2. Return period estimates for the 1999 extreme rainfall event (410.4 mm) at the Maiquetia international airport station.

		Return Period of 410.4 mm	
Inference Method	Model	1999 Datum Excluded	1999 Datum Included
MLE	Gumbel	18,300,000	756,000
	GEV	4,440	310
Bayes	Gumbel	2,360,000	177,000
	GEV	668	162
	PP (daily)	338	
	Seasonal PP	133	

3.1.4 Expert elicitation

This simple at-site case study example is included to profile the potential value of prior information. Coles and Tawn (1996) underscored the importance of injecting expert knowledge, independent of the available systematic record, into the analysis of extremes. They analyzed a 54-year series of daily rainfall totals and combined that dataset, within a Bayesian framework, with supplemental information obtained by way of expert elicitation. Coles and Tawn (1996) elicited the expert information in terms of extreme quantiles rather than distribution parameters, noting that extreme quantiles is a scale on which the expert has familiarity. Coles and Tawn (1996) elicited prior information in terms of three distinct ordered return levels (i.e., $q_{p_1} < q_{p_2} < q_{p_3}$ for $p_1 > p_2 > p_3$) but worked with their differences (i.e., $\tilde{q}_1 = q_{p_1}$, $\tilde{q}_2 = q_{p_2} - q_{p_1}$, $\tilde{q}_3 = q_{p_3} - q_{p_2}$) to ensure the correct ordering of quantiles. The $\tilde{q}_i$, $i = 1,2,3$, were specified by gamma distributions

$$\tilde{q}_i \sim \Gamma(\lambda_i, \nu_i) \tag{2}$$

whose parameters were determined by way of the expert elicitation. The joint prior for the q_{p_i} is given by

$$p(q_{p_1}, q_{p_2}, q_{p_3}) \propto q_{p_1}^{\lambda_1 - 1} \exp(-\nu_1 q_{p_1}) \prod_{i=2}^{3} (q_{p_i} - q_{p_{i-1}})^{\lambda_i - 1} \exp\left(-\nu_i (q_{p_i} - q_{p_{i-1}})\right) \tag{3}$$

on $q_{p_1} \leq q_{p_2} \leq q_{p_3}$. Substituting the quantile expression in Equation A.3 into Equation 3 and multiplying by the Jacobian of the transformation $(q_{p_1}, q_{p_2}, q_{p_3}) \rightarrow (\mu, \sigma, \xi)$ (Smith 2005) leads directly to an expression for the prior in terms of the GEV model parameters. Multiplication by the likelihood then gives the posterior. This expert elicitation framework is implemented in the R software package evdbayes to support at-site block maxima and/or point process threshold exceedance modeling analysis of extremes. Smith (2005) further examined this approach of prior elicitation in a multivariate Bayesian analysis of extreme rainfall. Morris et al. (2014) recently profiled a web-based tool for eliciting probability distributions from experts.

The previously mentioned expert elicitation framework was applied using a relatively short record of annual maxima rainfall data for the city of Oxford located in the United Kingdom (see Figure 22 (a)). In this simple example, there was the use of return level information previously elicited from an expert regarding extreme rainfall for Oxford (Fawcett 2013) to obtain prior distribution estimates for the 10-, 100-, and 1000-year return levels, defined as $q_{10} \sim \Gamma(126{,}2)$, $q_{100} \sim \Gamma(200{,}2)$, and $q_{1000} \sim \Gamma(250{,}1.5)$, and which are plotted in Figure 22 (b). Return level plots obtained from GEV models inferred using Bayesian inference with uninformative and the previously mentioned informative priors are shown in Figure 22 (c) and (d), respectively. By using the informative prior distributions obtained via expert elicitation, one can better leverage the full capability of the Bayesian inference methodology. It is clear to see the value of including such prior information in terms of vastly increasing the precision of return level estimates in this example, which involves a simple at-site analysis with a short period of record. Further note that sensitivity analyses can easily be performed to evaluate the worth of the elicited data by considering different parameterizations for the $\tilde{q}_i$.

Figure 22. (a) 35 years of annual maxima rainfall data for the city of Oxford in the UK; (b) prior distributions for the 10-, 100-, and 1000-year return levels informed via elicitation; (c) and (d) extreme rainfall return levels, including uncertainty, for Oxford computed using Bayesian inference with uninformative and informative priors, respectively.

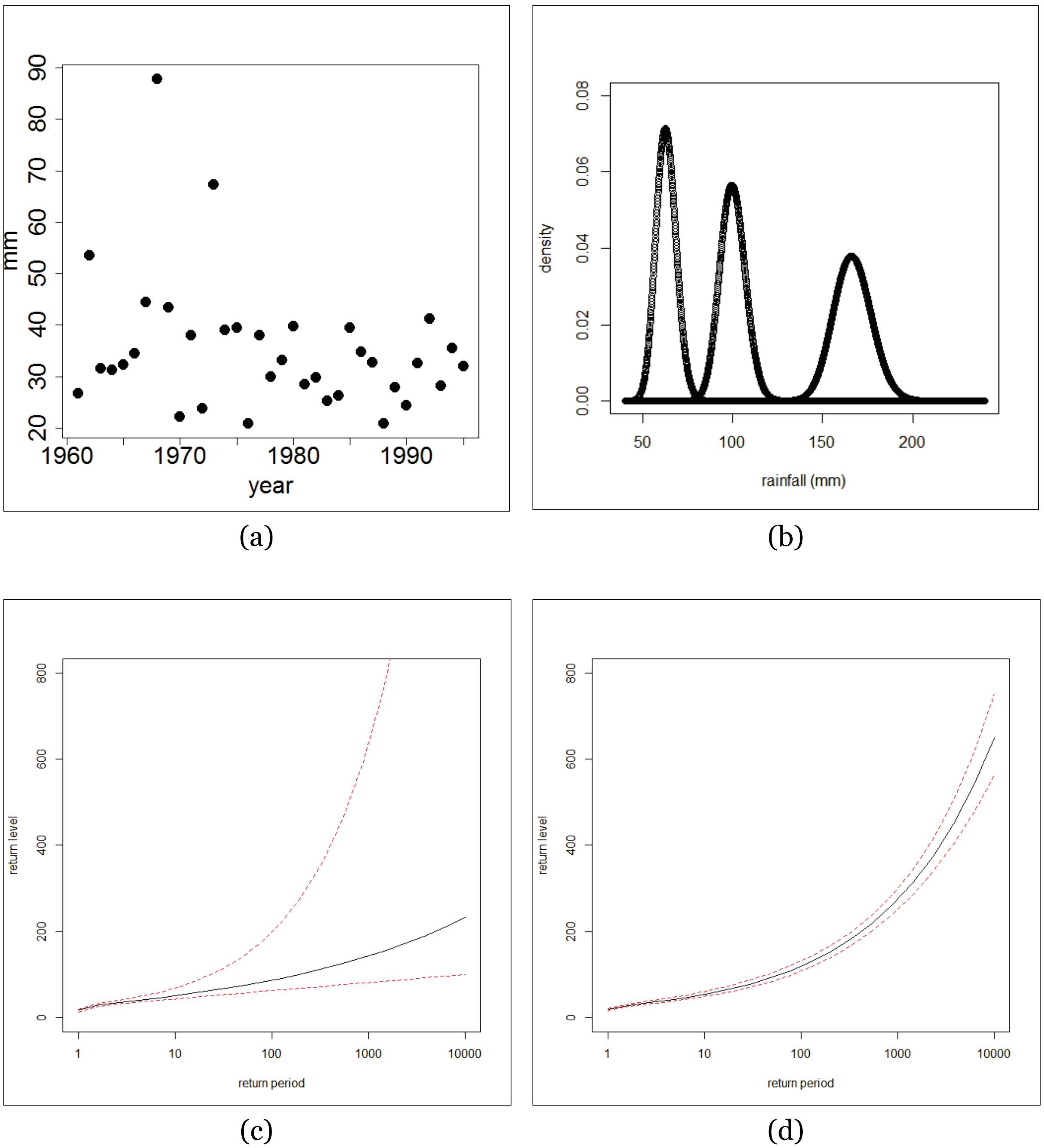

3.1.5 Non-stationary climate condition

Coles (2001), Katz et al. (2002), and AghaKouchak et al. (2013), and references cited within discuss the treatment of nonstationary sequences in the analysis of extremes, which is an active and evolving area of research. Garcia-Aristizabal et al. (2015), Cheng and AghaKouchak (2014), Economou et al. (2014), Renard et al. (2013), Winter (2011), Renard and Bois (2006), and references cited within examine the treatment of non-stationarity while using Bayesian inference for the analysis of extremes. The principal approach is to assume a regression model that links the extremal model parameters with time-variant covariates (e.g., a climate index). For example, Garcia-Aristizabal et al. (2015), Cheng and AghaKouchak (2014), and Winter (2011) considered a linear trend in the GEV EVT model location parameter with their Bayesian supervised extremes analyses. Both Garcia-Aristizabal et al. (2015) and Cheng and AghaKouchak (2014) simply considered a linear model in time for the GEV model location parameter, whereas with Winter (2011), their linear trend involved use of the North Atlantic Oscillation (NAO). Renard and Bois (2010) considered a simple linear trend in the location and scale parameters in their extremes analysis using the GEV EVT model. Economou et al. (2014) considered latitude and the NAO as covariates in their spatio-temporal BHM analysis of extreme cyclones. Renard et al. (2013) underscored the attraction of the Bayesian inference methodology in terms of its adaptability to support the analysis of nonstationary sequences. The R software packages evdbayes does provide some functionality for the treatment of a non-stationary analysis of local extremes using Bayesian inference. The R software package SpatialExtremes (Ribatet 2017) supports treatments of non-stationarity, primarily through the inclusion of time variant covariate data.

3.1.5.1 Case study demonstration - White Sands National Monument rainfall station Intensity-Duration-Frequency (IDF) curve development

The purpose of this case study is to demonstrate a very simple treatment of non-stationarity while using the flexible Bayesian inference methodology for an analysis of extreme rainfall. It is readily acknowledged that treatments of non-stationarity likely of more relevance to extreme rainfall analyses within the PFHA framework would rather involve the use of climate indices as covariate information as has been profiled by Economou et al. (2014) and Winter (2011), for example.

The Bayesian supervised IDF curve development analysis for the White Sands National Monument rainfall station originally profiled by Cheng and AghaKouchak (2014) is independently revisited, albeit by applying a different MCMC sampler (ter Braak and Vrugt 2008), to further focus on a comparison of Bayesian-inferred IDF curves under stationary and nonstationary conditions. As with Cheng and AghaKouchak (2014), non-stationarity is treated by defining the GEV location parameter to vary linearly in time, t:

$$\mu = \mu(t) = \mu_1 t + \mu_0. \tag{4}$$

This specific temporal treatment of the GEV location parameter is but one of many possible time variable approaches one could apply for IDF curve development using Bayesian MCMC. The linear in-time treatment of the GEV location parameter is employed primarily for the purposes of demonstration. In so doing, an additional random variable is introduced such that there are now four random variables, viz., μ_1, μ_0, σ, and ξ, to simultaneously optimize and infer using MCMC. The quantiles are computed from the post burn-in random draws as described in Cheng and AghaKouchak (2014). In particular, for each given post burn-in random draw, the 95th percentile value for the location parameter, obtained by applying Equation 4 (i.e., 95th percentile of $\mu(t = 1)$,..., $\mu(t = 100)$), is used to compute its related quantile value for a specified value of p. The entire set of x_p computed from the post burn-in draws characterize its posterior distribution.

Annual rainfall maxima series associated with the National Oceanic Atmospheric Administration (NOAA) Atlas 14 update for the White Sands National Monument rainfall station located in the state of New Mexico (latitude: 32.7817; longitude: 106.1747; elevation: 1217.7 m) for the 52-year period 1949–2000 were collected using the NOAA National Weather Service Hydrometeorological Design Studies Center Precipitation Frequency Data Server for eight specific durations (1 hour [hr], 2 hr, 3 hr, 6 hr, 12 hr, 24 hr, 48 hr, and 96 hr) to support Bayesian supervised IDF curve development analysis under stationary and nonstationary conditions. With the intent to illustrate the potential negative impacts of ignoring non-stationarity at a site that has been assessed otherwise based on application of the Mann-Kendall trend test (Cheng and AghaKouchak 2014), 16 distinct MCMC simulations were performed to develop IDF curves under stationary and nonstationary conditions using the annual rainfall maxima for the noted eight durations for the White Sands National Monument rainfall station. As previously mentioned, an adaptive population-based MCMC sampler (ter Braak and Vrugt 2008) was employed to infer the joint posterior for the GEV distribution parameters. All 16 MCMC simulations specified a population size to evolve equal in value to five times the dimensionality of the estimation problem. Latin hypercube sampling was used to initialize the population. The size of the initial history of past simulated states to draw upon to generate jump proposals was specified to be equal in value to one hundred times the dimensionality of the estimation problem. For each simulation, an uninformed uniform prior distribution was employed as well as a likelihood function as indicated in Equation D.2 with the density in Equation D.2 given by $f = G'$ where G is as defined in Equation A.1.

For each MCMC simulation, the Gelman and Rubin (1992) quantitative convergence diagnostic was used together with visual inspection of trace plots of the chains to in aggregate assess the completion of sampler burn-in. In each case, subsequent to the weight of evidence-based assessment that sampling is occurring with stable frequency from the target distribution, a thinned history, viz., every tenth evolution of the approximately 1 million specified total post burn-in monitoring period model runs was saved and used to support IDF curve development.

Figure 23 is a result from 2 of the 16 MCMC simulations, with the remaining summarized in Tables F-1 through F-3 and Figures F-1 through F-8 located in Appendix F. Tables F-1 and F-2 list the posterior mode (PM) (i.e., the GEV model $\mathbf{p}$ which maximizes $p(\mathbf{p}|D)$) estimates computed for each of the eight previously mentioned duration-based simulations under stationary and nonstationary conditions, respectively, and in each case, the related quantile estimates calculated for five distinct return periods, viz., 2, 10, 25, 50, and 100 years. It is underscored to the reader that the nonstationary results, as mentioned above, are computed and processed for a discrete point in time. Tables F-1 and F-2 also list by duration the computed 2.5, 50, and 97.5 percentiles of the posterior predictive distribution for each of the five quantiles. These noted percentile values are the basis for Figure 23 and also Figures F-1 through F-7, which are plots of the IDF curves computed under stationary and nonstationary conditions for the White Sands National Monument station, by duration. On each IDF curve shown in Figure 23 and also Figures F-1 through B-7, the 95% credible interval, based on the respective 2.5 and 97.5 percentile values listed in Tables F-1 and F-2, is shown for each quantile. Each figure also includes plots of the predictive distributions derived from the post burn-in random draws for the 2-year and 100-year return period quantiles. Table F-3 summarizes the computed percent increase obtained when the nonstationary, PM-based quantile estimates presented in Table F-2 are compared with their counterparts listed in Table F-1, which were obtained assuming a stationary climate. Figure F-8 is a plot of the data presented in Table F-3.

A strength of the MCMC methodology for IDF curve development is the flexibility and ease with which one can readily incorporate a treatment of a nonstationary climate condition into the analysis. Cheng and AghaKouchak (2014) underscored a primary strength of the MCMC methodology for IDF curve development, viz., its capacity to formally quantify uncertainty for the computed quantiles. This capacity is clearly emphasized graphically in Figure 23 and also Figures F-1 through F-7 wherein the posterior distributions (pdfs and cdfs) for the 2-year and 100-year quantiles, under stationary and also nonstationary conditions, characterized using the post burn-in random draws, are shown for each duration. It is also emphasized in the same set of figures, with the IDF curves themselves including a display of the 95% credible interval together with the 50th percentile value at each quantile level.

Figure 23. Bayesian MCMC simulation-derived, 1 hr IDF curves for the White Sands National Monument rainfall station computed under stationary and nonstationary conditions. The 2.5, 50, and 97.5 percentile values from each respective predictive posterior distribution are shown at each quantile level. These three values are clearly identified for the stationary 10-year return period results. Their relative locations equally apply for the remaining return periods for both the stationary and nonstationary analyses not only in this figure but also Figures F-2 through F-7. Plots of the posterior predictive distributions for the 2-year and 100-year return period level quantiles are also shown.

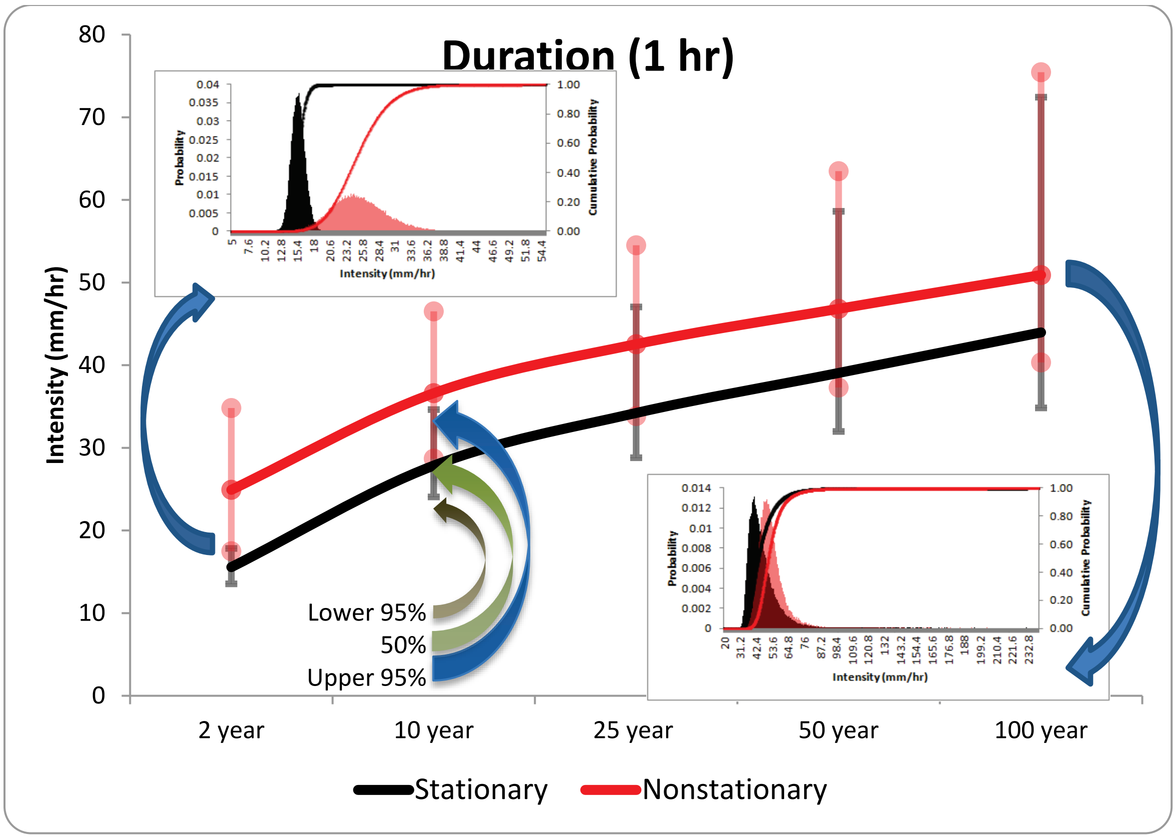

3.2 Multiple station analysis

The station-specific types of analyses profiled in the previous section could be applied on a point-by-point basis to generate, by way of interpolation, spatial maps of hydrometeorological extremes; however, such an approach is not explicitly spatial. An alternative approach for updating precipitation frequency estimates under stationary and/or nonstationary climate conditions involves using spatial modeling analysis methodologies such as spatial or spatiotemporal BHM or max-stable processes as previously mentioned in this report. These methods, or their adaptions, in fact are the basis for the PFHA framework outlined earlier in this report. For the purposes of demonstration, this section profiles applications of spatial BHM and max-stable process models for the spatial modeling of extreme daily precipitation in the Willamette River Basin, Oregon.

3.2.1 WRB summary description

The 11,478-square-mile WRB is located in northwestern Oregon, a major tributary of the Columbia River whose 187-miles-long main stem, the Willamette River, flows northward between the Coastal and Cascade Ranges. The WRB contains approximately two-thirds of Oregon's population and 20 of the 25 most populous cities in the state. The U.S. Army Corps of Engineers (USACE) Portland District operates 13 dams in the WRB. Extreme rainfall estimates are required to support risk-informed hydrologic analyses for these projects as part of the USACE Dam Safety Program. The primary operative mechanism for extreme rainfall in the WRB is winter storms that occur between October and March, which typically make up to 75%-80% of the region's annual precipitation (Redmond and Koch 1991; Lee and Risley 2002; Chang and Jung 2010). Temperature fluctuations are relatively small due to the basin's proximity to the Pacific Ocean; however, elevation plays a major role in its variability (Melack et al. 1997; Lee and Risley 2002). Elevations within the WRB range from near sea level along the Columbia River to over 10,000 feet in the Cascade Range. The orographic effect of the Cascade Range results in relatively high amounts of rainfall along the Columbia River Gorge (Daly et al. 1994). Overall, the Pacific Northwest region experiences warm, dry summers due to intensification of the Pacific subtropical high, and cool, wet winters as the polar jet stream dips southward bringing storms from the Gulf of Alaska (Mock 1996). Figure G-1 located in Appendix G depicts the Willamette River Basin, including hydrography, projects, and cities located in the basin, and also its relative location in the state of Oregon. (http://www.nwp.usace.army.mil/Locations/Willamette-Valley/)

3.2.2 Annual maxima data summary description

The time series of Annual Maxima (AM) data for the WRB was produced for the Oregon Department of Transportation by Schaefer et al. (2008), which was conducted due to the lack of a NOAA precipitation atlas update for the region (Bonnin et al. 2006). The data set is comprised of daily annual precipitation maxima for 128 stations throughout Oregon, where annual is defined as the period between January 1 and December 31 (Schaefer et al. 2008). The length of record for each location ranges from 10 to 66 years, with a combined 2,912 AM for the WRB. Stations were used that fall within the specific study region; 68 stations fall within the WRB region (Figure 24). Schaefer et al. (2008) performed quality checks on the station records for errors, incomplete records, and any anomalous precipitation amounts relative to neighboring gages. Schaefer et al. (2008) also checked the station data for stationarity and independence using a null hypothesis of zero slope and zero serial correlation, respectively; they could not reject the null hypothesis at a significance level of 0.05. Figure 25 presents a summary count by month for the occurrence of annual maxima across all of the stations located in the WRB extreme rainfall analysis study area. The pooled extreme daily rainfall data for the study area underscore the previously mentioned seasonal storm climatology for the WRB.

Figure 24. Locations of the 68 rain gages with daily AM data that were used to perform spatial analyses of extreme rainfall in the Willamette River Basin. The numeric index assigned to each station is also shown.

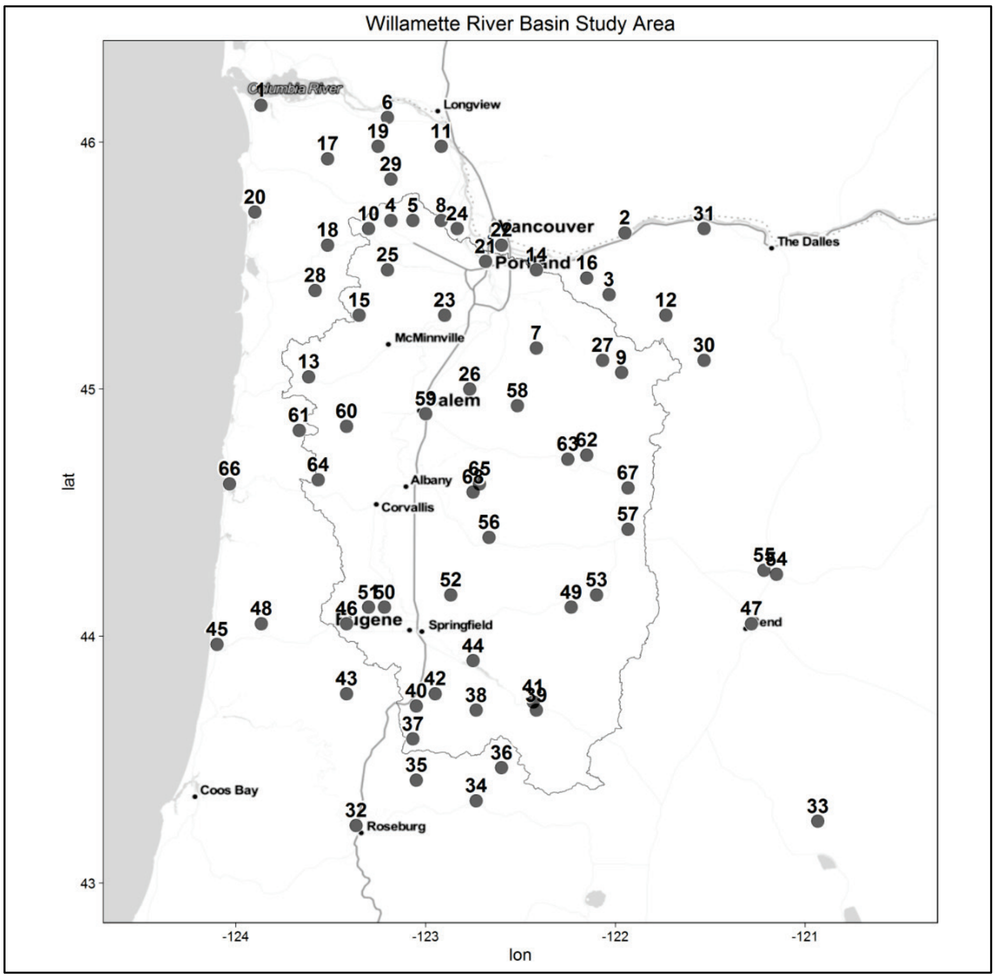

Figure 25. Summary count by month of the daily AM across all stations located in the WRB extreme rainfall analysis study region.

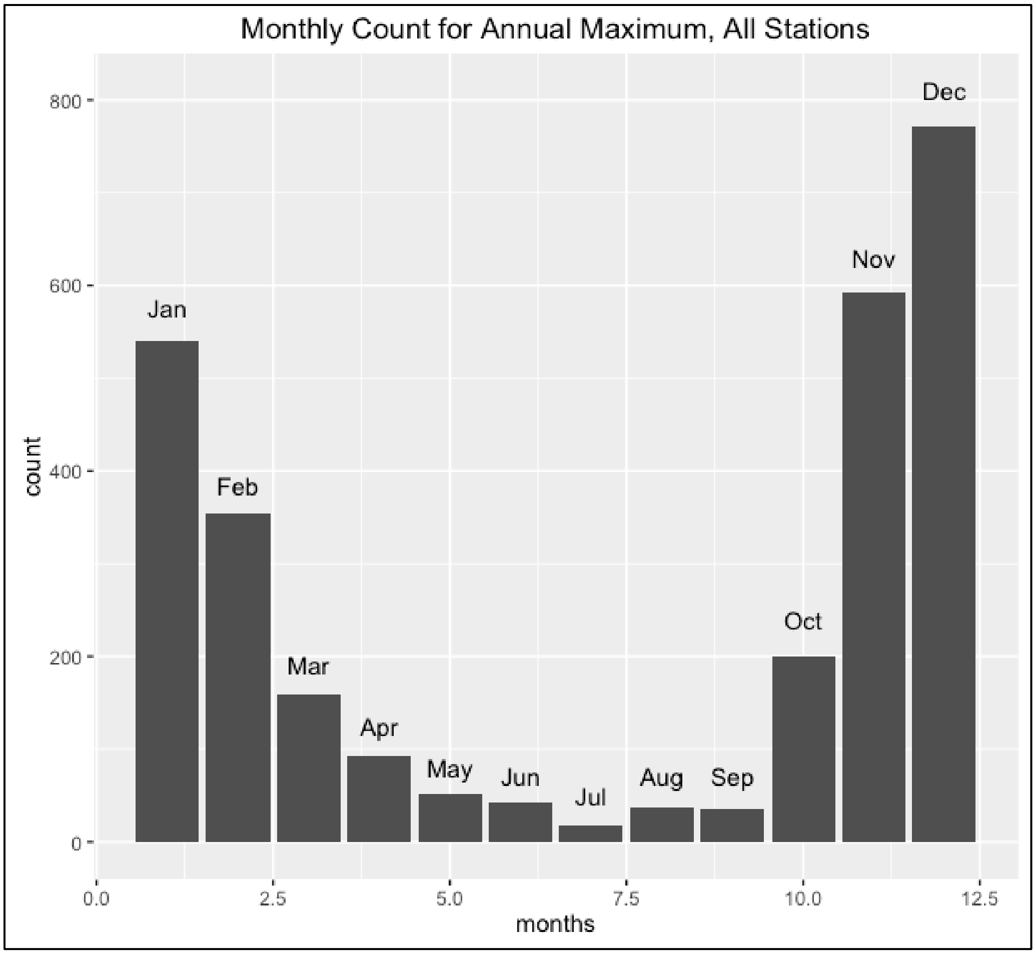

3.2.3 Covariate data

The Parameter-elevation Relationships on Independent Slopes Model (PRISM) data sets are the source of gridded covariate information to support the spatial analyses of extreme daily rainfall in the WRB, as they not only have the advantage of being extensively peer-reviewed but also a relatively fine spatial resolution across the entire conterminous United States (~ 800m). PRISM is a *knowledge-based mapping system* that uses a local linear regression function to combine point measurements with digital elevation model (DEM) grid cells and spatial data sets to produce gridded climate data sets (Daly et al. 2008; Daly et al. 2015). Interpolation of the precipitation and temperature data is performed using a DEM as the predictor grid. The PRISM long-term mean monthly data set used in this study is Norm81m, which is based on the climatology for the time period of 1981 to 2010 and has a 30-arc-second resolution. It contains monthly averages for the following elements: precipitation; temperature minimum, maximum, and mean; mean dew point temperature; and vapor pressure deficit minimum and maximum.

Temporal covariate data can also be leveraged with an application of a spatiotemporal BHM or a max-stable process model, and herein for the analysis of extreme daily rainfall in the WRB, there is an exploration in a limited manner use of the Oceanic Niño Index (ONI) data averaged over the winter period, by year.

3.2.4 Spatial Bayesian hierarchical modeling

The spatial BHM extreme rainfall analyses were performed using the R software package spatial.gev.bma (Dyrrdal et al. 2015; Lenkoski 2014). The R software package spatial.gev.bma implements an MCMC sampling methodology to estimate the spatially dependent parameters of the GEV distribution (Dyrrdal et al. 2014). Additionally, it uses BMA to assess model uncertainty related to the covariates employed (Dyrrdal et al. 2014). The spatial BHM developed by Lenkoski (2014) assumes stationarity with time (Dyrrdal et al. 2014).

The covariates employed include the x and y location for each station (longitude and latitude converted to Universal Transverse Mercator coordinates), along with the elevation, monthly and annual precipitation, mean temperature, and mean dew point temperature from the PRISM Norm81m long-term (1981-2010) mean monthly gridded data set. From the PRISM data set, there was derived the seasonal mean (November-March and April-October means) of the three climatological variables for use in the models. As is suggested by Dyrrdal et al. (2014) to improve inference, all covariates were standardized prior to model simulation. The choice of specific covariate data used for each of the models varies from simple (just x and y; model XY) to more complex (x, y, elevation, monthly precipitation (P), monthly dew point temperature (T_d), and monthly mean daily temperature (T); model XYZPT6) (Table 3).

Table 3. Model acronyms and covariates employed. (Numbered subscripts denote month (e.g., 1 for January, 12 for December). An asterisk denotes the mean across wet season months [November-March] while a superscript "c" denotes the mean across dry season months [May-April]. Annual means [January-December] are denoted with a subscript "A".)

Acronym	Model Covariates
XY	Latitude, Longitude
XYZ	Lat., Lon., Elevation
XYZPT1	Lat., Lon., Elevation, P_A
XYZPT2	Lat., Lon., Elevation, P^*, $T_d{}^*$, T^*
XYZPT3	Lat., Lon., Elevation, P_A, T_{dA}, T_A
XYZPT4	Lat., Lon., Elevation, P^*, $T_d{}^*$, T^*, P^c, $T_d{}^c$, T^c
XYZPT5	Lat., Lon., Elevation, P_1, ..., P_{12}, T_{dA}, T_A
XYZPT6	Lat., Lon., Elevation, P_1, ..., P_{12}, T_{d1}, ..., T_{d12}, T_1, ..., T_{12}

The predictive performance of each model was evaluated through application of leave-one-out cross validation (LOO-CV) and minimization of the continuous ranked probability score (CRPS) and root mean squared error (RMSE). The CRPS compares the simulated and observed cumulative distribution functions, and can be defined as

$$CRPS = \int_{-\infty}^{\infty} \left[F(z) - H(z - z_j)\right]^2 dz \quad (5)$$

where z represents the simulated values and z_j the observed values (Gneiting and Raftery 2007; Hersbach 2000). For $F(z)$, the median of the simulated GEV cumulative distributions across all iterations was used (post burn-in). $H(z)$ is the Heaviside step function where

$$H(z) = \begin{cases} 0, z < 0 \\ 1, z \geq 0 \end{cases}. \quad (6)$$

As the distributions become increasingly similar, the CRPS approaches zero (Hersbach 2000). As noted by Dyrrdal et al. (2014), a small (hundredths) change in CRPS corresponds with a substantial difference in performance. For this study, a derivation of CRPS was used, which can be written as

$$CRPS = \frac{1}{JK} \sum_{j=1}^{J} \sum_{k=1}^{K} [F(z_k) - H(z_k - z_j)]^2 \quad (7)$$

where k is the number of simulated values and j is the number of observed values.

Application of LOO-CV with the WRB extreme daily rainfall dataset involves 68 separate BHM model runs wherein for each simulation the data from an individual station is withheld, and following each simulation model predictive performance is subsequently evaluated at the hold-out data station location. It is readily acknowledged that application of LOO-CV is compute intensive and atypical for many practical application settings. LOO-CV is asymptotically equivalent with the Akaike's Information Criterion (AIC) (Stone 1977) and the Bayesian Information Criterion (BIC) (Shao 1997); hence, its application not only supports a comprehensive assessment of model performance but also model selection. The deviance information criterion was proposed by Spiegelhalter et al. (2002) to provide a criterion appropriate for BHMs, and it is straightforward to implement and by contrast with LOO-CV computationally efficient to use. It has been applied in several studies for model comparison and selection (Cooley et al. 2007; Najafi and Moradkhani 2013; Sang and Gelfand 2008; Yan and Moradkhani 2014).

<u>Spatial BHM results</u>

Following application of LOO-CV with the WRB extreme daily rainfall dataset for each BHM configuration (Table 3), the mean and median CRPS and RMSE were computed across all 68 stations as summary measures of overall model performance (Figure 26). As is indicated in Figure 26, the overall performances, regardless of chosen aggregate metric, for four of the eight spatial BHM configurations listed in Table 3, viz., XYZPT2, XYZPT4, XYZPT5, and XYZPT6, cluster closely together away from and with improved values relative to the remaining four BHM configurations considered for modeling extreme daily rainfall in the WRB. These four BHMs with improved mean overall performance scores relative to the remaining four either include seasonality or monthly rather than annual or no mean climatological covariate information in the general linear model terms which define the GEV model parameters by location.

Figure 26. Plot of mean and median CRPS and RMSE for the eight spatial BHM configurations listed in Table 3 which were considered for modeling extreme daily rainfall in the WRB.

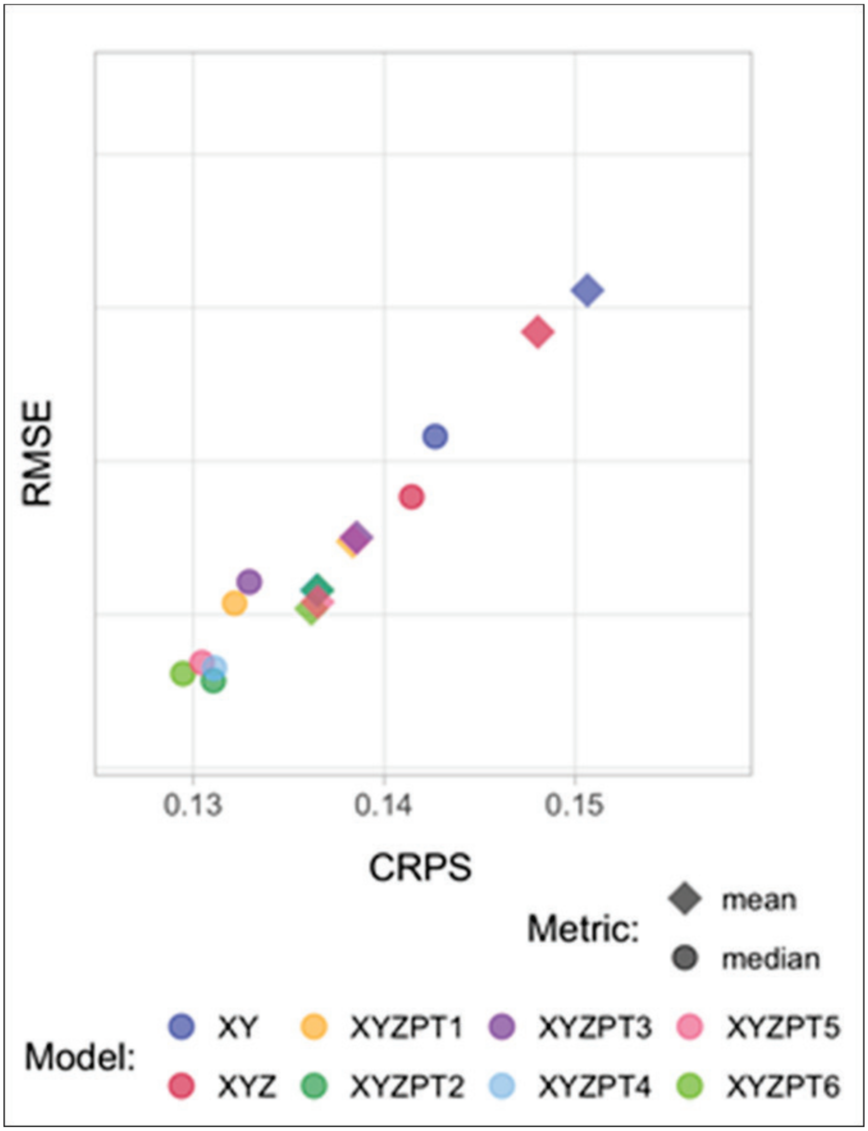

The station-specific computed CRPS values resulting from application of LOO-CV with the XYZPT2 BHM configuration listed in Table 3 are plotted in Figure 27. Similar location-specific model performance values as that shown in Figure 27 were also obtained from the other three mentioned BHM configurations with comparable overall model performance measures. The LOO-CV results shown in Figure 27 clearly demonstrate that BHM performance does vary by location. For the XYZPT2 BHM configuration, individual plots of station specific performance versus any one of the normalized model covariate data (i.e., x, y, z, P^*, T_d^*, and T^*) show little correlation. However, as mentioned previously, the methodology used here includes a BMA functionality that provides an estimate of the posterior inclusion probability (PIP) for the general linear model terms of the BHM. While most covariates have a non-negligible PIP, it is demonstrated that mean wet-season precipitation (November-March) has the greatest influence on the location parameter, μ, of the GEV distribution (Figure 28). Seasonal precipitation and temperature and also longitude (x) have the largest PIP for the inverse-scale parameter, κ (Figure 28). Elevation (z) appears to have the most influence on the shape parameter, ξ (Figure 28).

Figure 27. Location specific model performance computed based on application of LOO-CV with the XYZPT2 spatial BHM configuration listed in Table 3.

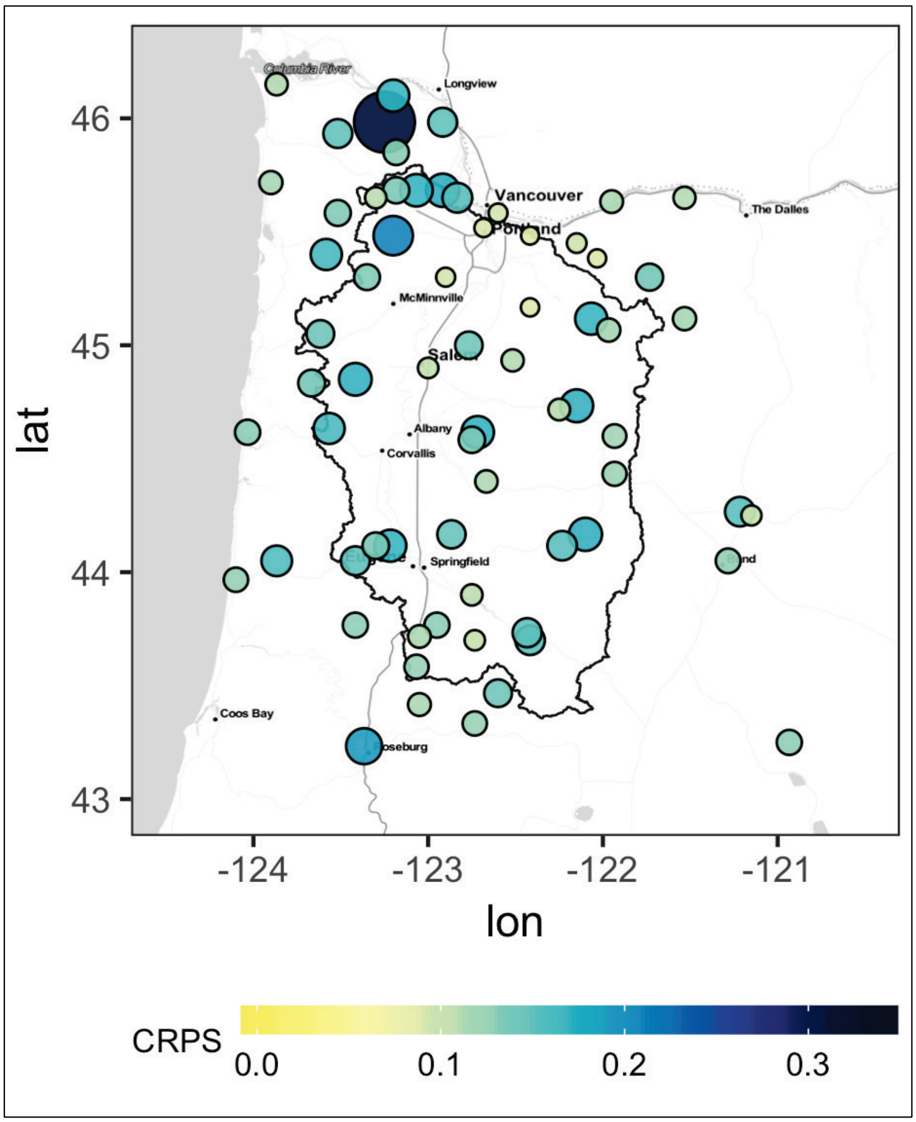

Figure 28. Posterior inclusion probability for each covariate of BHM configuration XYZPT2 listed in Table 3.

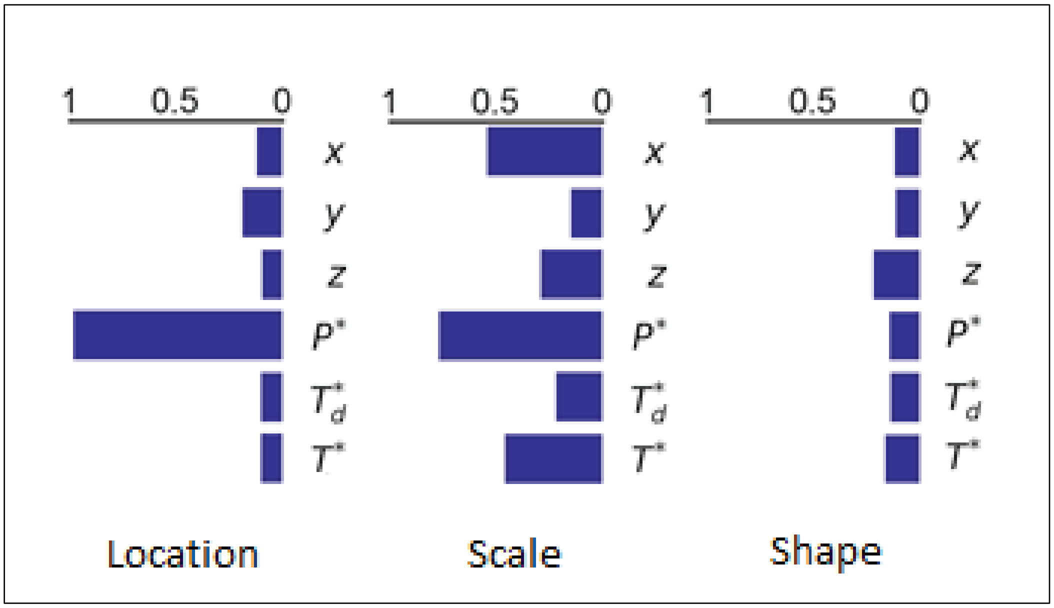

BHM predictions from configurations XYZPT2, XYZPT4, XYZPT5, and XYZPT6 at three distinct hold-out locations, viz., station numbers 25, 26, and 63 (Figure 24), that resulted in categorically "low," "average," and "high" location-specific model performances are shown in Figure 29. These plots are a means by which to visualize and qualitatively assess and also compare reported performance scores. The spatial BHM configuration XYZPT2 resulted in CRPS scores of 0.2104, 0.1415, and 0.1083 at stations 25, 26, and 63, respectively. For comparison, station number 25 yielded the second highest CRPS score value among the 68 stations with application of LOO-CV using the spatial BHM configuration XYZPT2. In addition, 5 and 41 of the 68 stations yielded better location specific CRPS scores than those reported for stations 63 and 26, respectively. Figures 30-32 are return level plots for stations 25, 26, and 63, respectively, obtained using BHM configurations XYZPT2, XYZPT4, XYZPT5, and XYZPT6 wherein for each of the four models the data from all 68 stations is used for optimization and inference. Figures 30-32 show the value of *trading space for time* for improved at-site analysis, not only in terms of reducing uncertainty as is notably evident in Figure 32 but also in influencing estimates to better align on a regional basis. The latter mentioned benefit of regionalization is particularly apparent in Figure 30 for station number 25, where by contrast the at-site analysis is based on a very short record of 10 annual maxima data points.

The spatial BHM analysis structure and a given configuration's associated gridded covariate datasets are the means by which to generate pointwise return level plots as well as spatial surfaces of other relevant parameters of interest throughout the study area. With an extreme rainfall analysis, parameters of potential interest to map, beyond return levels and their uncertainty, might include the posterior extremal model parameters and their respective linear model and random effects terms. For example, Figure 33 is a representative spatially coherent map of the distribution of pointwise extreme daily precipitation for the Willamette River Basin generated using a BHM and daily precipitation measurements from a relatively sparse network of the 68 observation stations combined with geographic and other meteorological information.

Figure 29. LOO-CV predictions from spatial BHM configurations XYZPT2, XYZPT4, XYZPT5, and XYZPT6 (Table 3) at stations with IDs 63, 26, and 25 (Figure 24).

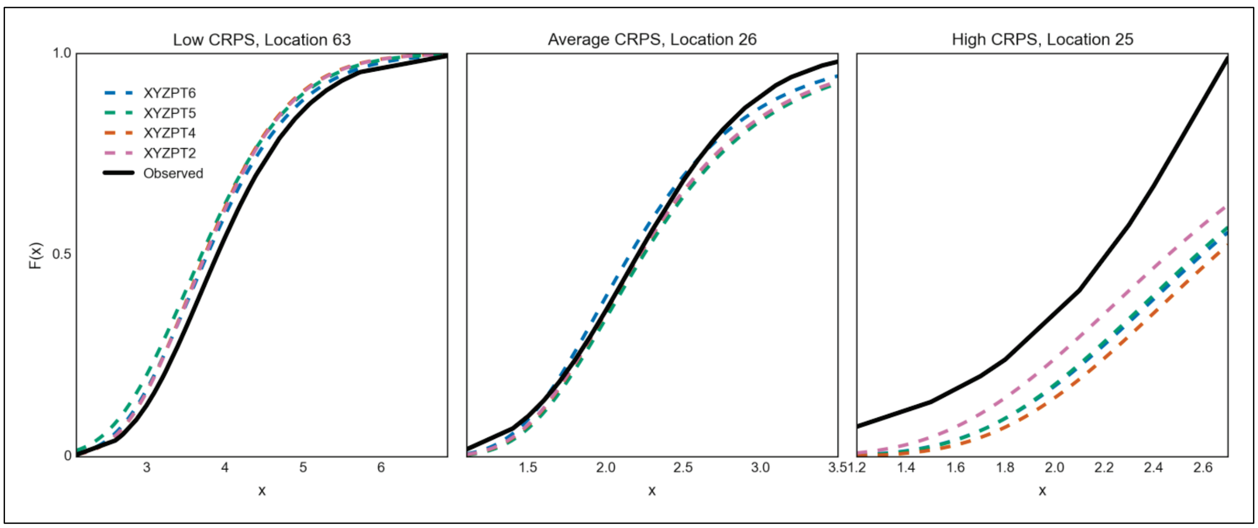

Figure 30. Return level plots, including 95% uncertainty bounds, for station 25 obtained via application of spatial BHM configurations XYZPT2, XYZPT4, XYZPT5, and XYZPT6 together with at-site analysis results obtained also using Bayesian inference. (red=at-site analysis; black/grey=BHM analysis; solid lines=median)

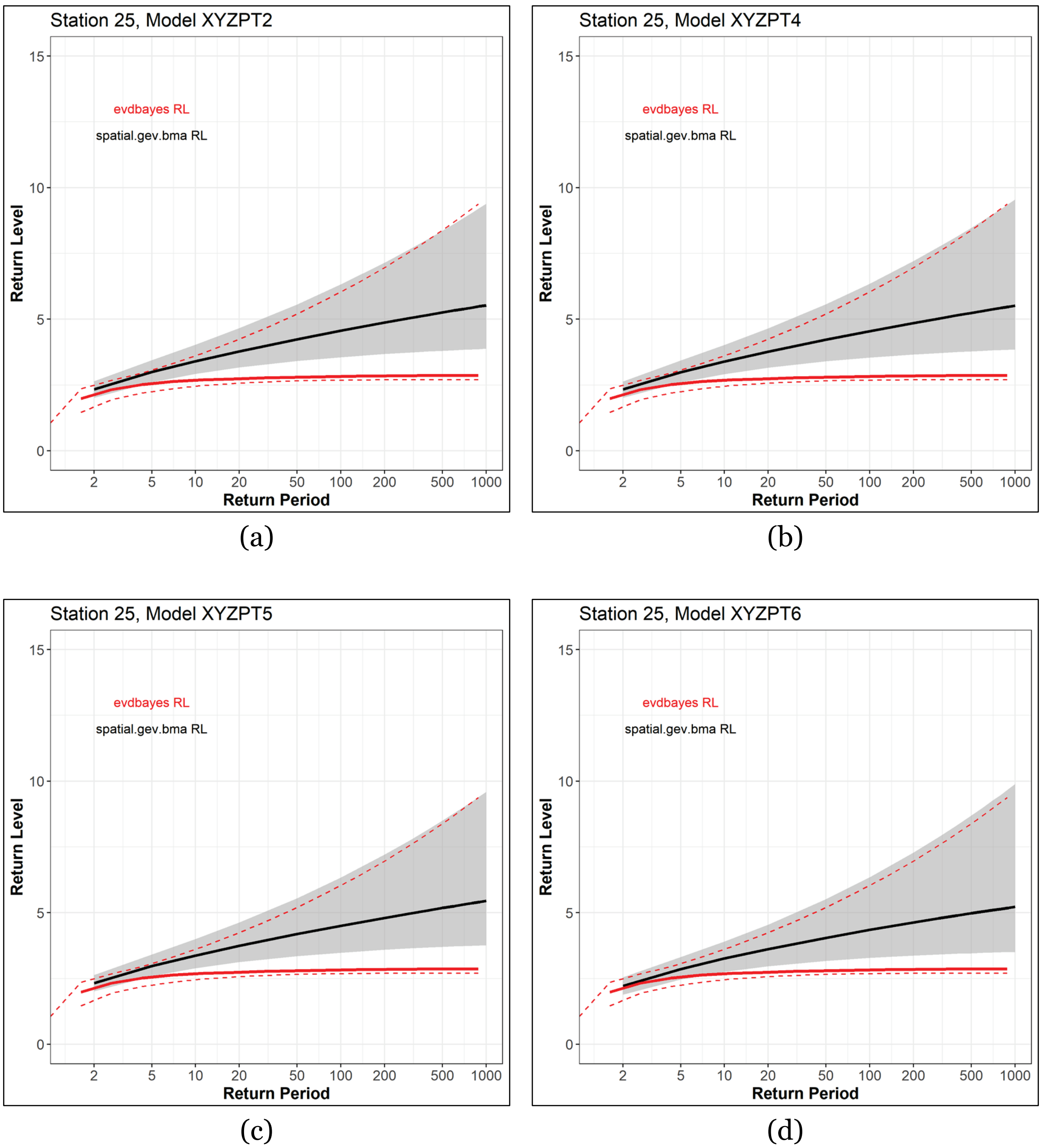

Figure 31. Return level plots, including 95% uncertainty bounds, for station 26 obtained via application of spatial BHM configurations XYZPT2, XYZPT4, XYZPT5, and XYZPT6 together with at-site analysis results obtained also using Bayesian inference. (red=at-site analysis; black/grey=bhm analysis; solid lines=median)

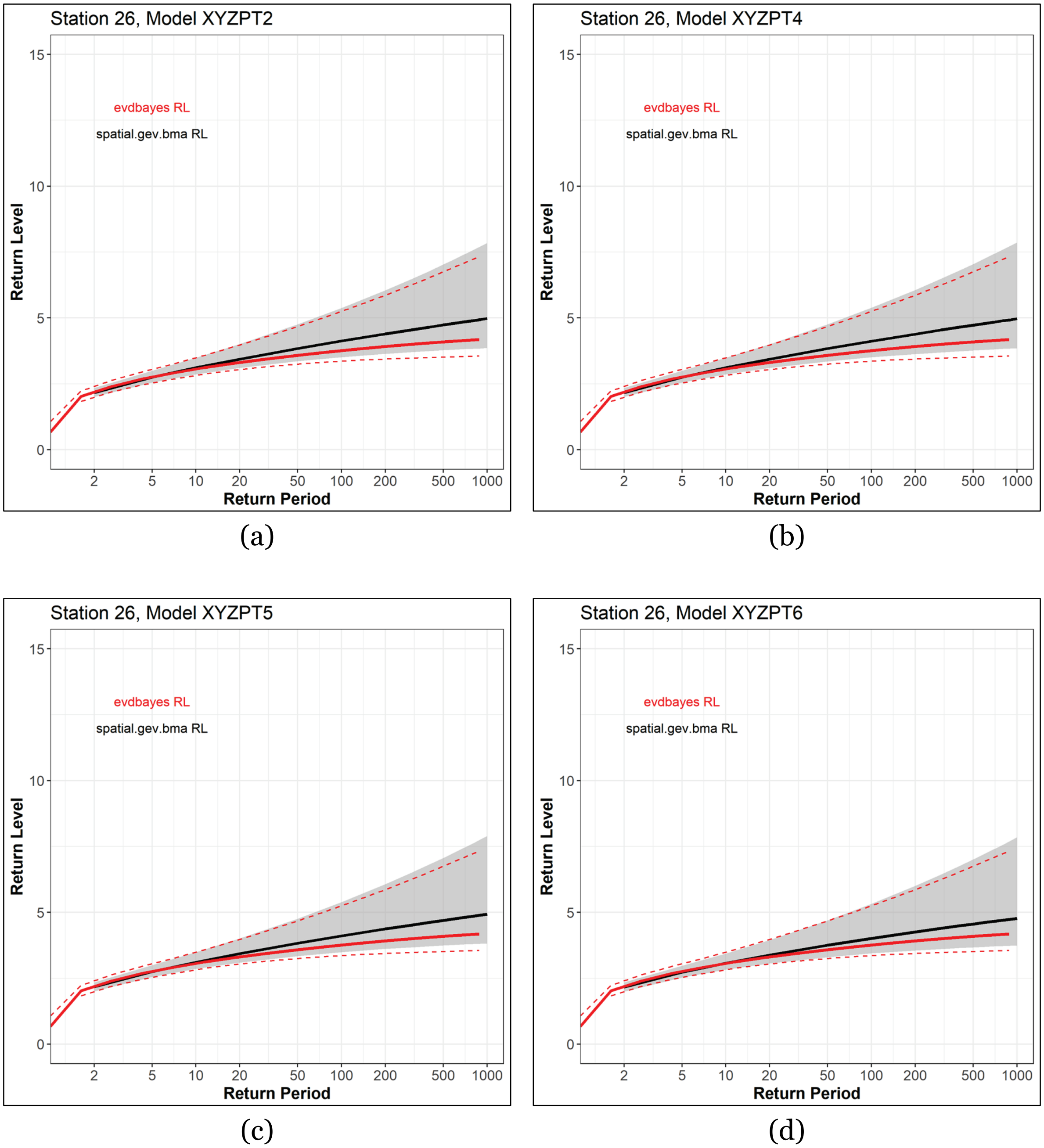

Figure 32. Return level plots, including 95% uncertainty bounds, for station 63 obtained via application of spatial BHM configurations XYZPT2, XYZPT4, XYZPT5, and XYZPT6 together with at-site analysis results obtained also using Bayesian inference. (red=at-site analysis; black/grey=bhm analysis; solid lines=median)

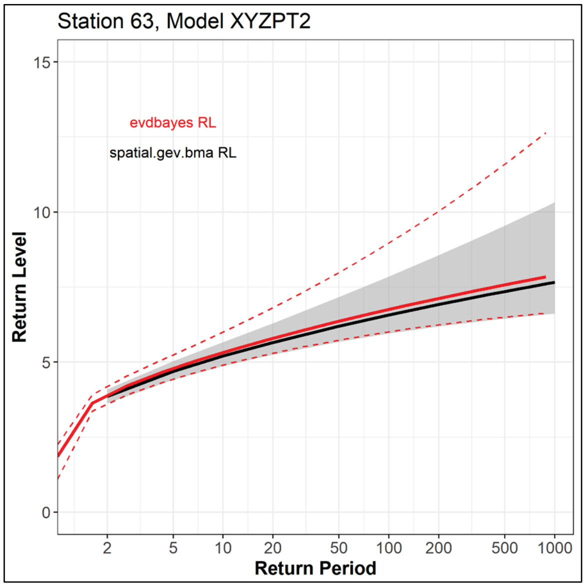

(a)

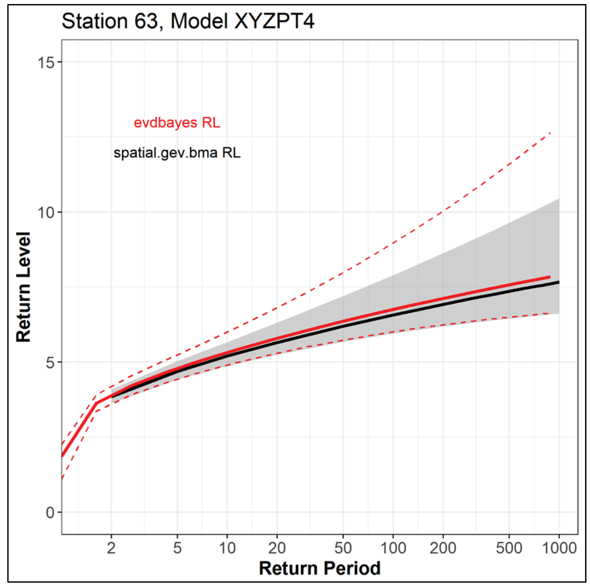

(b)

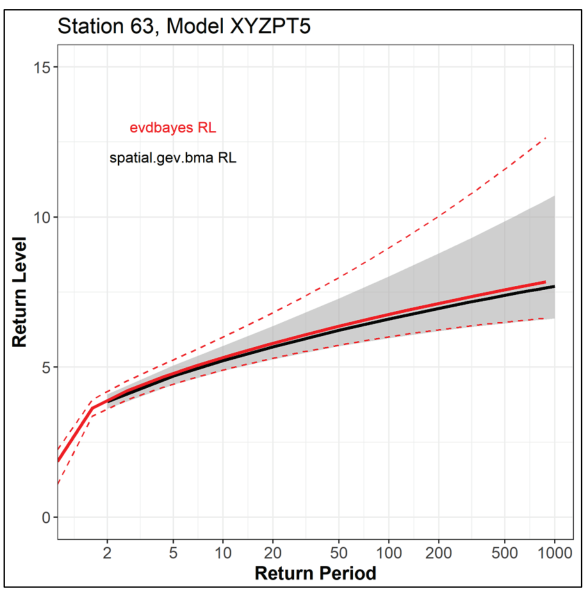

(c)

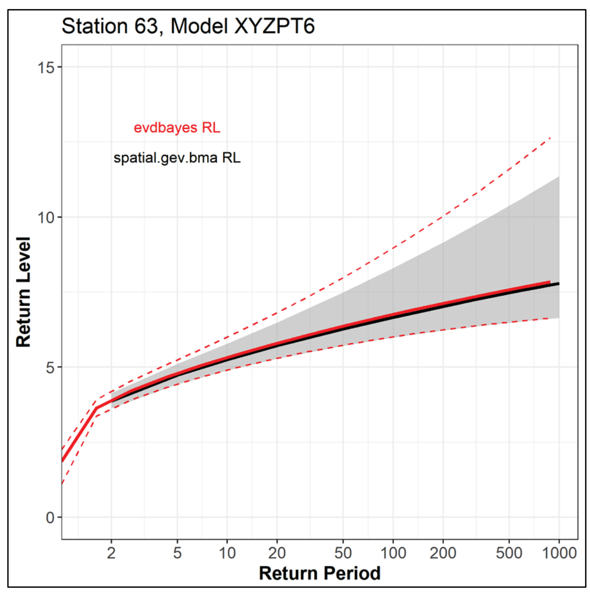

(d)

Figure 33. A representative return level map generated using a BHM configuration defined in Table 3.

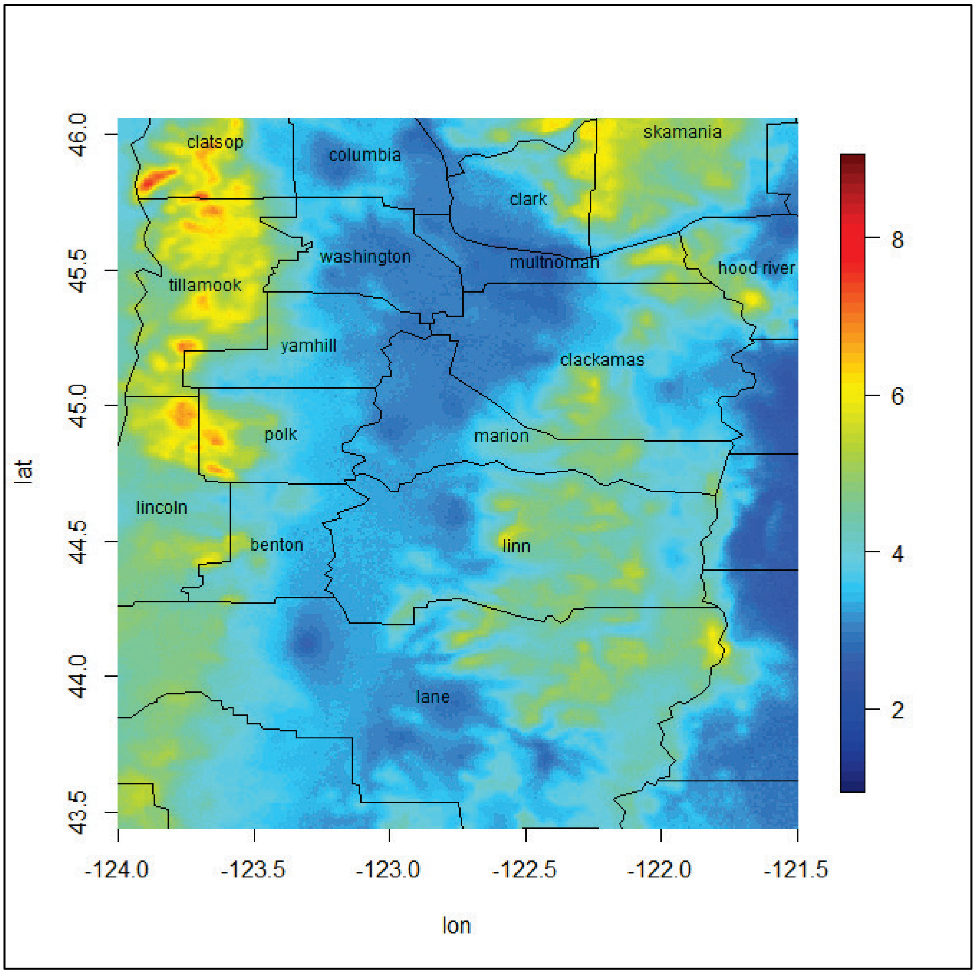

3.2.5 Max-stable process model application

While the application of spatial or spatiotemporal BHMs is highly flexible and uncertainty quantification and also prediction at unobserved sites is straightforward, as previously mentioned, their design does not fully conform with EVT, and the assumption of independence among the observed extreme data is problematic. This section briefly profiles a second base application approach of the PFHA framework proposed earlier in this report for the analysis of hydrometeorological extremes. Here, regional extreme rainfall analyses of the daily AM rainfall dataset for the WRB are performed using a max-stable process via application of capabilities encapsulated in the R software package SpatialExtremes (Ribatet 2017). Max-stable process models fully conform with EVT and account for the dependence among the extreme data. Hence, their application supports more complex risk analysis beyond the generation of pointwise return level maps. In moderate to large basins, hydrologic engineers and hydrologists use depth-area relationships to convert point rainfall depths to areal average depths for the same duration and recurrence interval since point estimates are not representative. A depth-area reduction factor (ARF) is defined as the ratio of two expectations wherein the denominator is the average of n point estimates and the numerator is the spatially averaged depth of rainfall over an area for the same duration and return period as the point rainfall. All stations used for its computation are assumed to be simultaneously experiencing rainfall over the duration of interest (Durrans et al. 2002). Svensson and Jones (2010) noted that ARFs are a function of rainfall characteristics, physical characteristics of the basin, and also the data and methods used for their computation. The empirical approaches that are commonly used to compute ARFs are data intensive and laborious. Moreover, ARFs suffer from being the same for all watersheds falling within a large region and do not provide a pattern of rainfall variation over space within the watershed (see Singh [2017] and references cited within). By contrast, estimation of integrals such as Equation 1, not only for rainfall, but also other relevant hydrometeorological variables for flood hazard assessment, and also for comparison on a regional basis for any area $\mathcal{B}$ (e.g., subwatershed), are relatively straightforward to estimate via simulation from a fitted max-stable model of spatial extremes, all the while the analysis accounting for the dependence among the data and conforming with EVT whereupon there is assurance of mathematically credible extrapolation.

A key component of modeling spatial extremes is accounting for the observed dependence among the extreme data. The extremal coefficient function, denoted by $\theta(h)$, is commonly used to measure dependence as a function of distance, h, and its lower value of 1 corresponds with complete dependence and its upper value of 2 with independence (Cooley et al. 2012). Figure 34 is a plot of the extremal coefficient function for the observed daily AM rainfall data for the WRB, which clearly exhibit moderately strong dependence for distances, h (in meters), as great as the entire length of the Willamette River. This observed dependence must be accounted for when assessing the risk of daily duration extreme rainfall in the WRB.

Following the initial assessment that dependence among the extremes cannot be ignored, a typical analysis of spatial extremes involves (a) fitting simple max-stable parametric models to the extreme data transformed to fixed unit Fréchet margins such that only the dependence is treated, (b) fitting the extreme data to simple trend surface models using spatial and possibly also temporal covariates and wherein the dependence is ignored, and (c) subsequently fitting a general max-stable process model that simultaneously models the dependence and the margins by leveraging information gleaned from the previous two steps. In each step, model selection is informed using calculated information criteria. For the case study herein, only a single max-stable parametric model is considered, viz., the Schlather process (Schlather 2002). The trend surface modeling analysis considers the eight models previously listed in Table 3 with and without inclusion of a mean winter ONI temporal covariate dataset for the years 1950-2006, inclusive.

Figure 34. Plot of the extremal coefficient function for the WRB daily AM rainfall dataset.

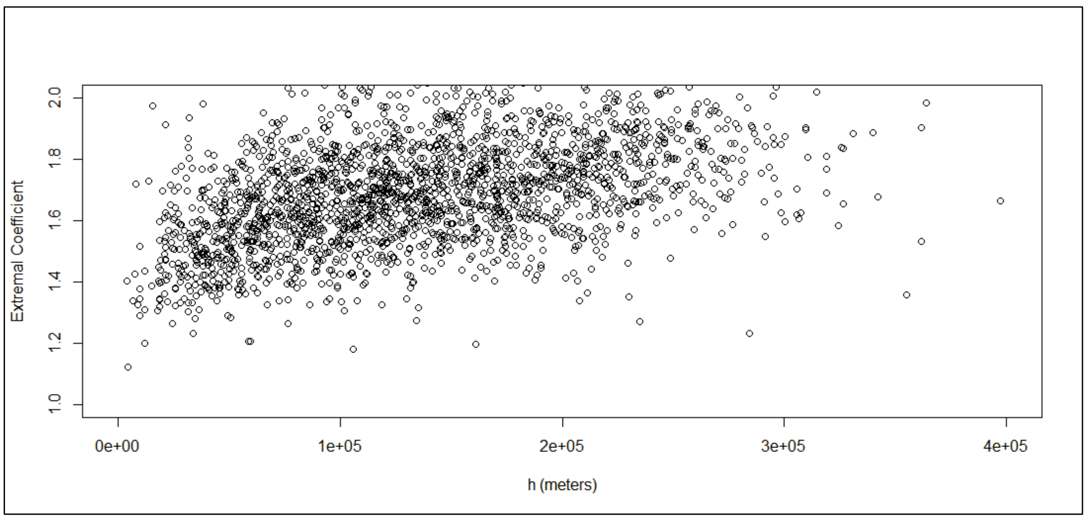

Max-stable process model results

Figure 35 is a plot of a simple max-stable Schlather process, using the Whittle-Matérn covariance model, fitted to the daily duration AM rainfall data for the WRB by maximizing the pairwise likelihood. The solid blue line is the theoretical extremal coefficient associated with the fitted model whereas the black circles are the pairwise estimates. A typical application may evaluate several max-stable process permutations with model selection based on associated information criteria; however, only the Schlather process with the Whittle-Matérn covariance model is considered herein for the purposes of demonstration. While for the Schlather process the extremal coefficient has a theoretical upper limit of 1.838 in $\mathbb{R}^2$ as $h \to \infty$ when using isotropic positive definite correlation functions, it is argued that its use for this case study is justified given the moderately strong dependence demonstrated in Figures 34 and 35 among the pairwise estimates for distances as great as the entire length of the Willamette River.

Fitting a simple max-stable process only models the spatial dependence by transforming the extreme data such that the marginals are fixed and unit Fréchet. Of course, the marginals are not unit Fréchet. The results presented in Figure 36 summarize simple and efficient trend surface modeling analysis of the marginals, leveraging previously mentioned spatial and temporal covariate information, now while assuming independence among the extreme data. As was also the case with the spatial BHM analysis of the daily AM rainfall dataset for the WRB, the XYZPT2, XYZPT4, XYZPT5, and XYZPT6 model configurations listed in Table 3 achieved lower aggregate model performance values relative to the remaining configurations that only considered spatial covariates. The results presented in Figure 36 also show that the additional use of the ONI temporal covariate data resulted in a higher information criterion value for each respective configuration listed in Table 3.

Following the trend surface analysis for modeling the marginals, five general Schlather processes were subsequently fitted, viz., the XYZPT2, XYZPT4, XYZPT5, XYZPT6, and XYXPT6 WONI configurations for the marginals, with related information criterion values for each of these five max-stable models summarized in Figure 37. After fitting a general max-stable model, it should be evaluated not only in terms of its location specific performance but also that it models well the observed dependence. While not shown, following the fitting process, the extremal coefficient was plotted to ensure that each of the five previously mentioned models captured the observed dependence among the extremes. Figure 38 contains plots of the fitted Schlather process model for the XYZPT2 configuration together with the AM data for station locations 63, 26, and 25 for which spatial BHM modeling results were presented in the previous section. Predictions from the XYZPT2 Schlather process, which obtained the highest information criterion value among the five fitted models, at each of these three locations are similar to the results obtained from the spatial BHM modeling results that were presented earlier in Figure 29. Figures 39-41 are the 10-, 100-, and 1000-year pointwise return-level maps of daily extreme rainfall that were readily generated by predicting from the fitted XYZPT2 Schlather process model using configuration specific processed PRISM gridded covariate data. Also in Figures 39-41, included simply for a quick comparison, are comparable predictions obtained from the RFA analysis performed by Schaefer et al. (2008). Figures 42-44 demonstrate the variability in pointwise return level values generated from several spatial BHM and max-stable model configurations for station locations 25, 26, and 63, respectively. One notable observation is that the XYZPT6 and XYZPT6 WONI Schlather process predictions are markedly different from the remaining three max-stable model predictions at each location. Despite these two highly complex models achieving the lowest information criterion values (see Figure 37), prior to their further application, additional evaluation is suggested (e.g., comprehensive assessments of location specific performance).

A strength of max-stable spatial process applications is their capacity to quantify complex areally based assessments of risk, via simulation, for arbitrary subareas $\mathcal{B}$ in the computational domain. For example, for extreme rainfall analyses, they can be used to compute subwatershed-specific exceedance probabilities, accounting for the dependence among the extremes and without relying upon traditional empirical ARFs. Moreover, meanwhile, and notable, the analysis framework is in compliance with EVT. Figure 45 includes four simulated independent copies of a max-stable process fitted for extreme precipitation analyses within the WRB. The contributing drainage areas associated with four dams located in the WRB are considered simply for the purpose of illustration (see Figure 46). While based on a limited number of simulations, Figure 47 presents estimation of

$$\Pr\left\{\int_{\mathcal{B}} \Upsilon(x)dx > z_{crit}\right\}, \tag{8}$$

where $\Upsilon(x)$ is the field of extreme precipitation for each of the separate drainage areas $\mathcal{B}$ as shown in Figure 46. Evaluation of integrals such as the one presented in Equation 8, readily estimated via simulation from a fitted max-stable process, is highly relevant for extreme rainfall analyses. The uncertainty associated with fitting a general max-stable process can of course be used to bound the expected areal-based return levels that are shown in Figure 47.

Figure 35. A fitted max-stable Schlather process obtained by maximizing the pairwise likelihood.

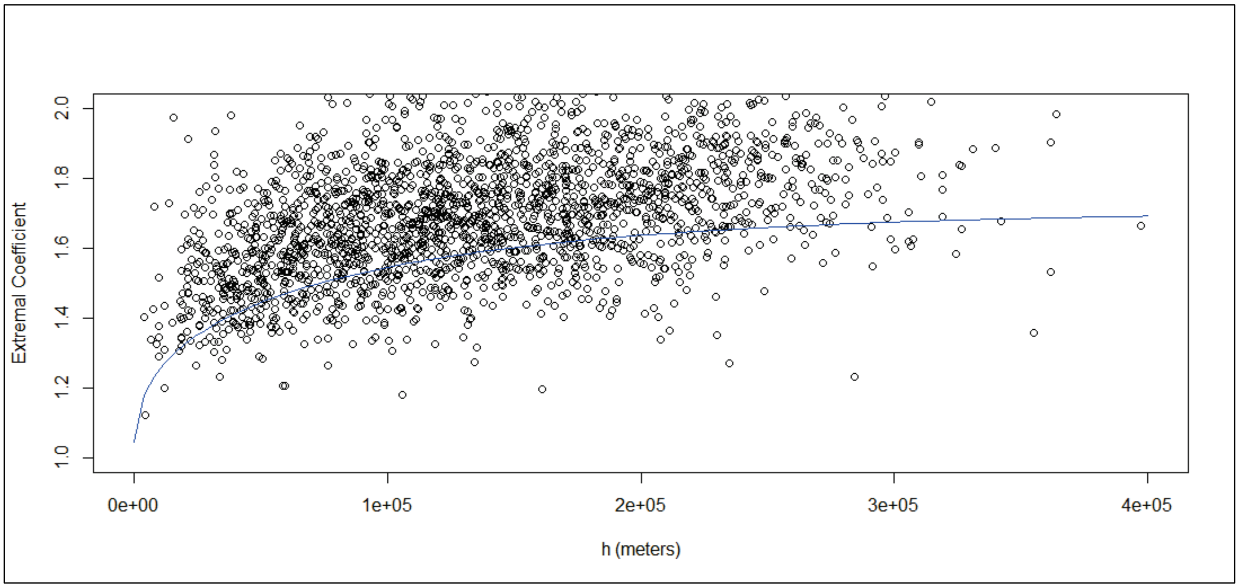

Figure 36. Information criterion values obtained from trend surface modeling analysis of the marginals.

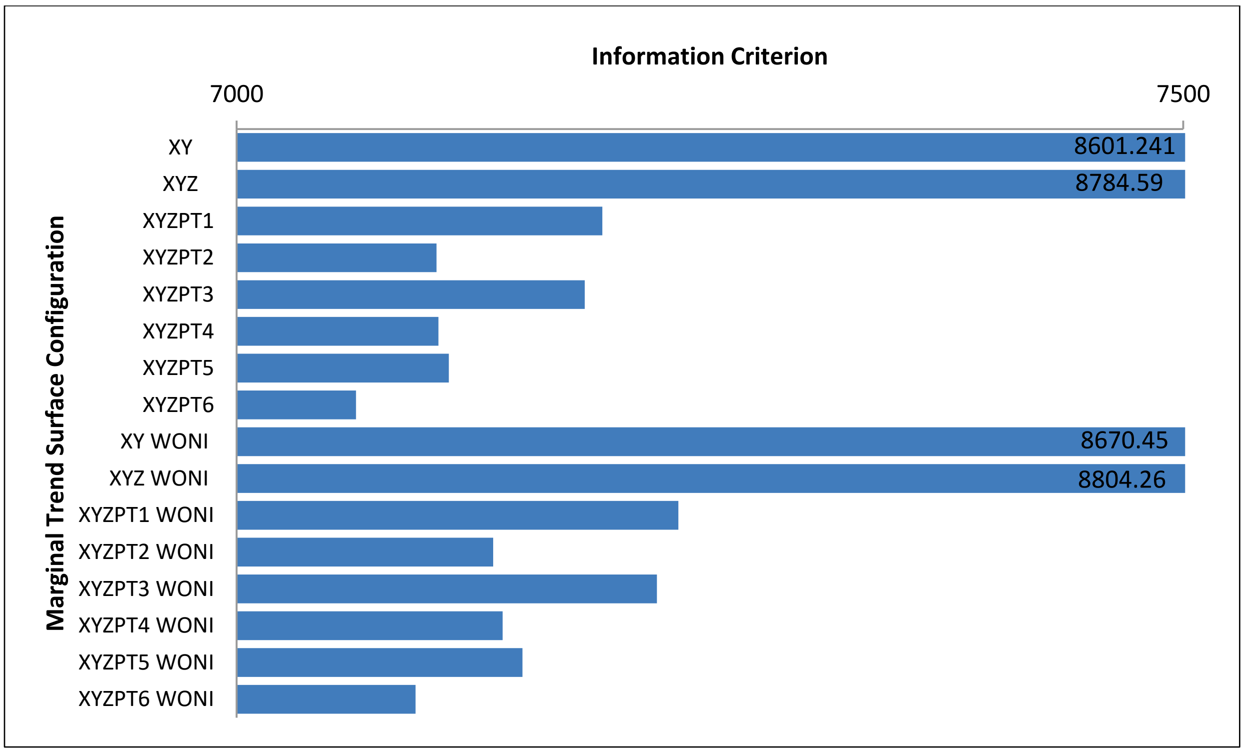

Figure 37. Information criterion values for five general Schlather processes fitted for modeling daily AM rainfall data in the WRB.

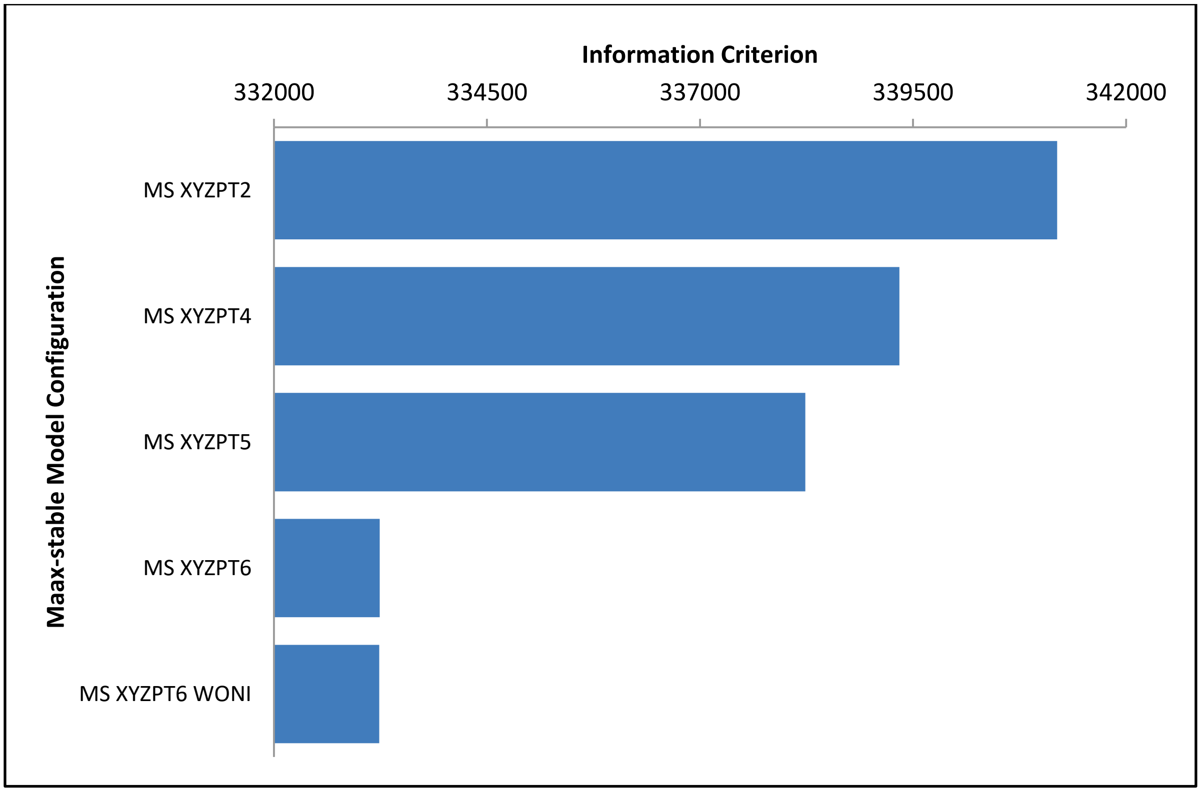

Figure 38. Plot of the MS XYZPT2 fitted Schlather model together with observations for station locations (a) 63, (b) 26, and (c) 25, respectively.

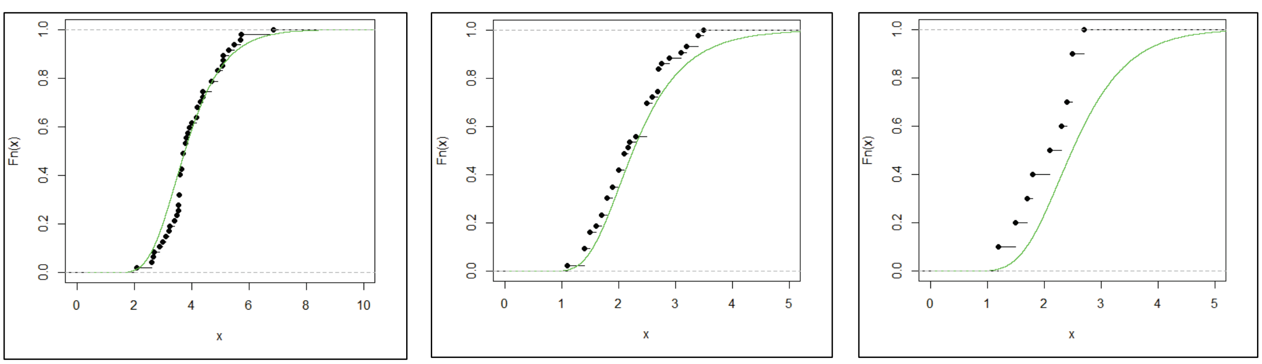

(a) (b) (c)

Figure 39. Gridded 10-year pointwise return level map predictions of daily AM rainfall (in inches) from (a) the fitted Schlather process model for the XYZPT2 configuration and (b) the RFA analysis of Schaefer et al. (2008).

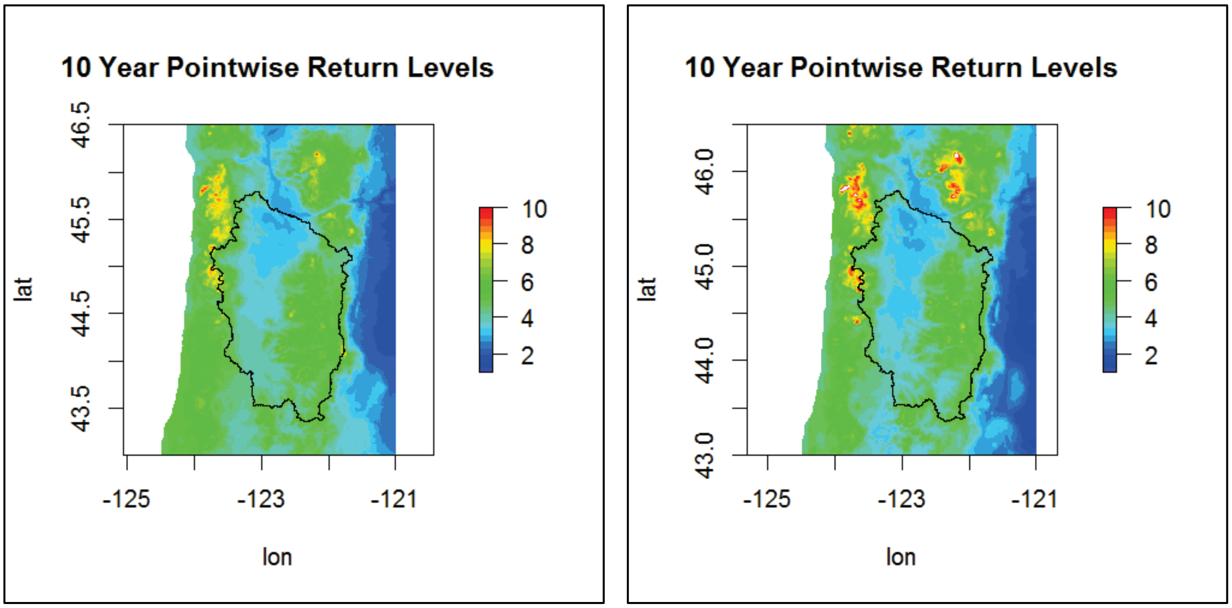

(a) (b)

Figure 40. Gridded 100-year pointwise return level map predictions of daily AM rainfall (in inches) from (a) the fitted Schlather process model for the XYZPT2 configuration and (b) the RFA analysis of Schaefer et al. (2008).

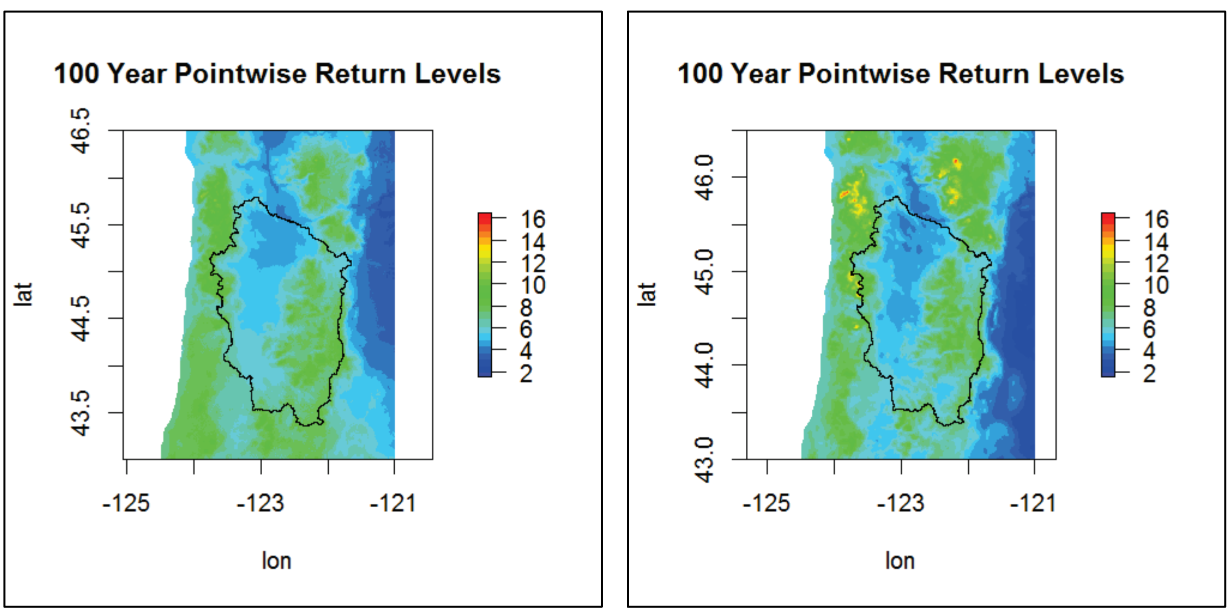

(a) (b)

Figure 41. Gridded 1000-year pointwise return level map predictions of daily AM rainfall (in inches) from (a) the fitted Schlather process model for the XYZPT2 configuration and (b) the RFA analysis of Schaefer et al. (2008).

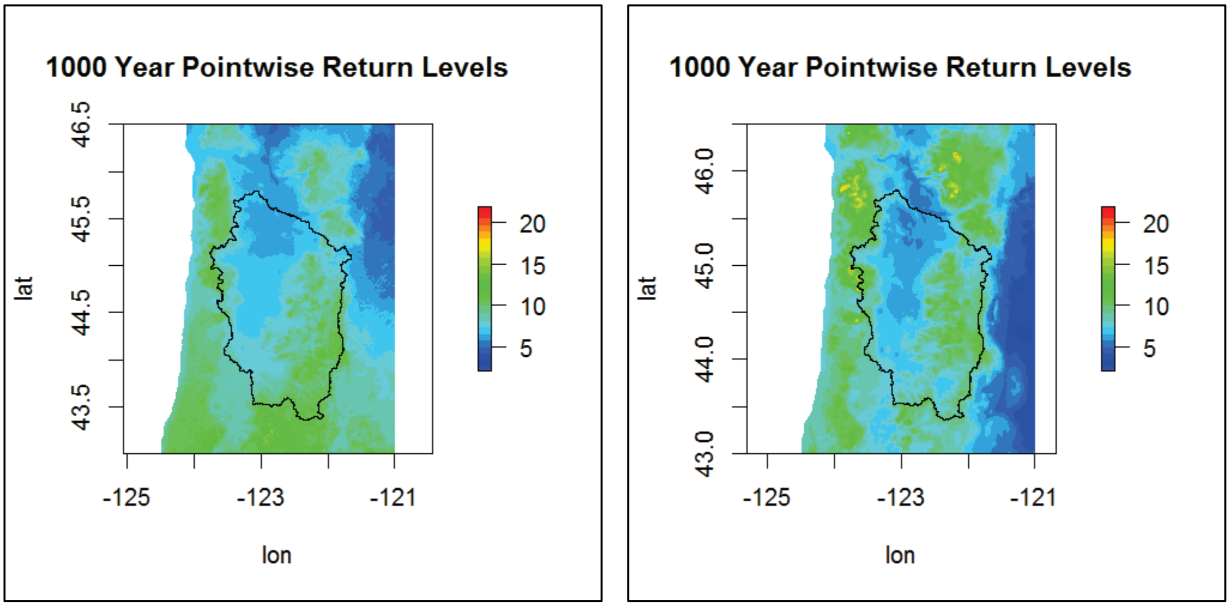

(a)

(b)

Figure 42. Return levels at station location 25 generated from several spatial BHM and Schlather max-stable process model configurations.

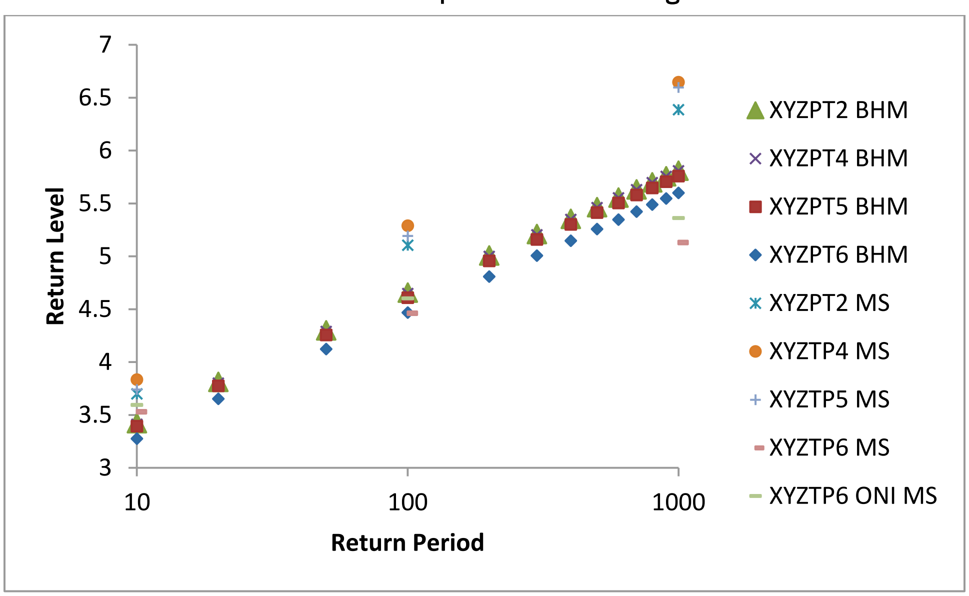

Figure 43. Return levels at station location 26 generated from several spatial BHM and Schlather max-stable process model configurations.

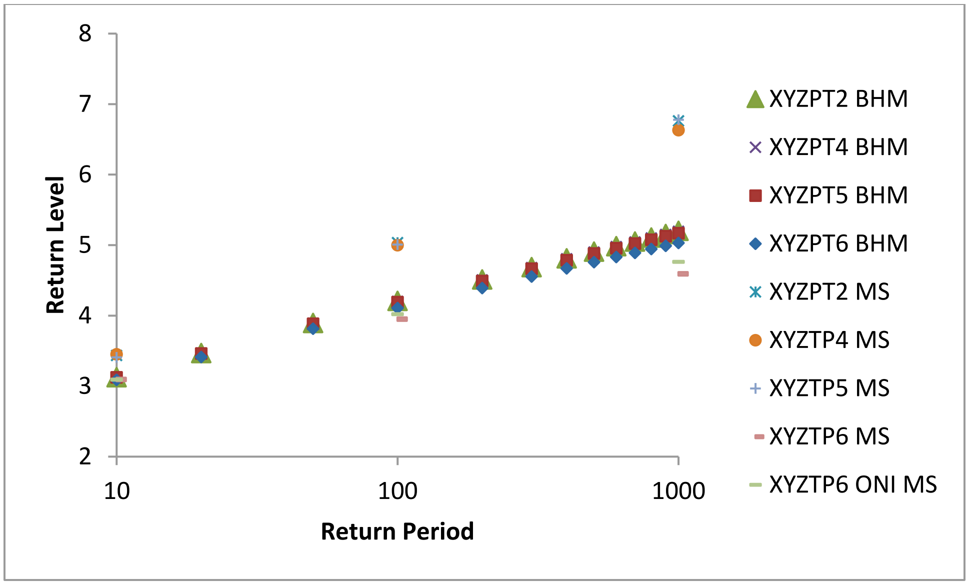

Figure 44. Return levels at station location 63 generated from several spatial BHM and Schlather max-stable process model configurations.

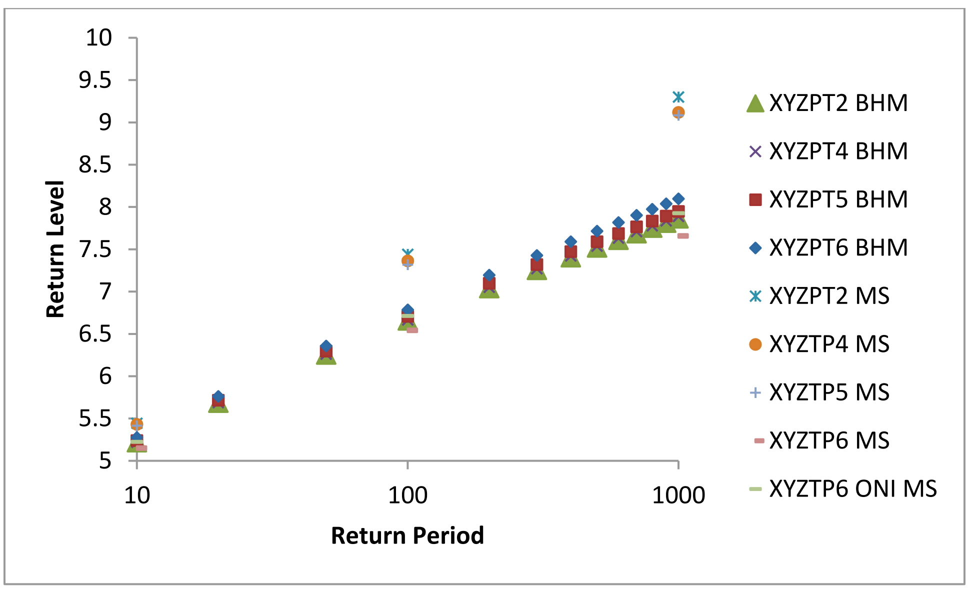

Figure 45. Simulated independent copies from a fitted max-stable process model for extreme precipitation for a 3 by 3 degree domain that contains the Willamette River Basin.

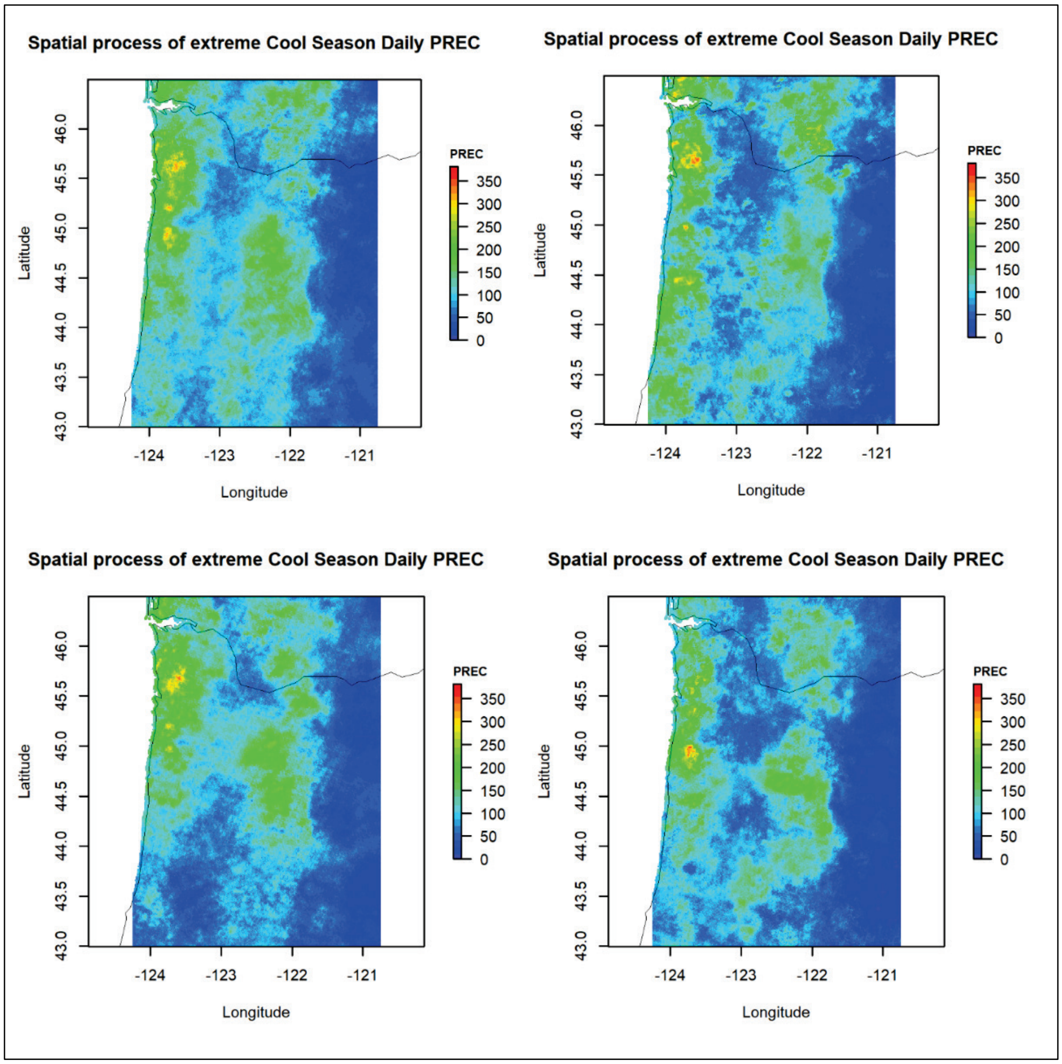

Figure 46. Four subareas $\mathcal{B}$ in the WRB defined for simulation.

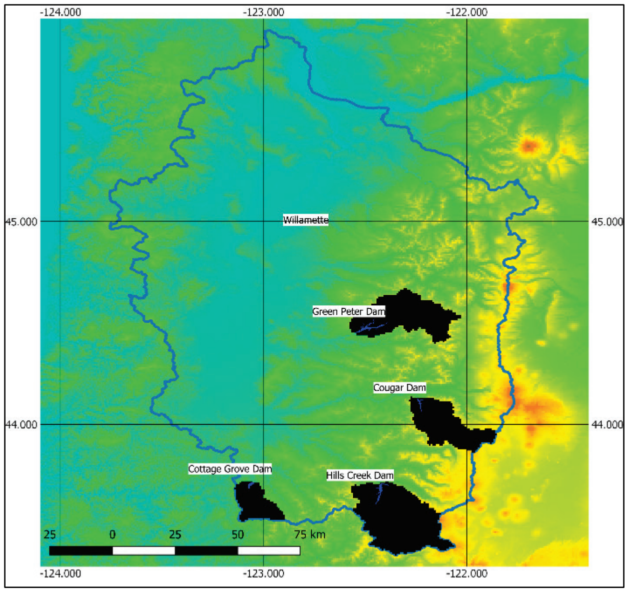

Figure 47. Estimated exceedance probability for each subarea $\mathcal{B}$ shown in Figure 46.

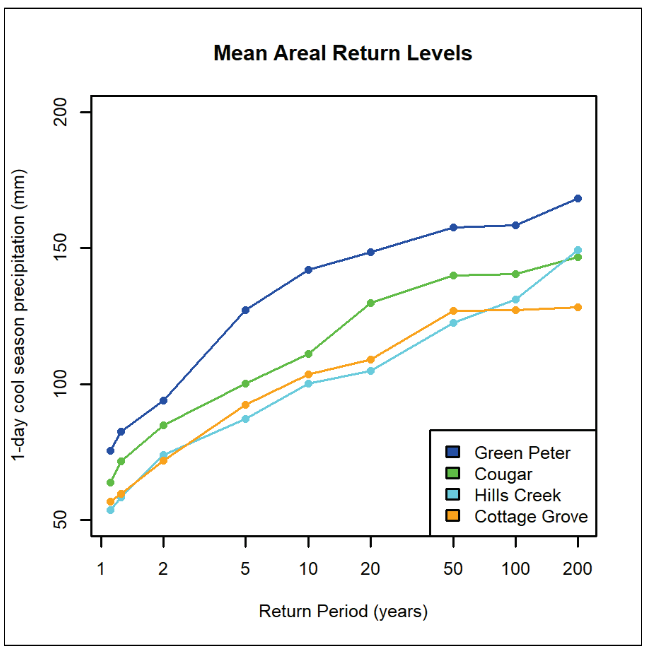

3.3 Muliti-model averaging

It is not extraordinary to expect different modelers, or modeling teams, to produce different usable models for the characterization of hazard curves. In fact, the two instance applications of the proposed PFHA framework each included results that underscore this expectation (see Figures 26, 29-32, and 42-44). With either instance application of the framework, the difference among the competing models is, of course, more apparent for larger return periods. For example, Figure 48 presents pointwise return level predictions for a 10,000-year return period from three of the fitted Schlather process configurations wherein for each model the estimate and its standard error are shown. A PFHA assessment should account for a likely range of models (e.g, including parsimonious model deployments with reduced relative uncertainty together with results from more complex models that exhibit greater relative uncertainty as is shown in Figure 48 specifically for station 59 and as was presumed, and, in fact, assessed to be the case in general for the three profiled Schlather process configurations of varying complexity based on the computed average of the pointwise predictions across all 68 locations). The development of additional figures like Figure 48 for any other station location, or any pointwise predicted location using a given configuration's covariate data, will demonstrate similar types of variability across the models. The generalization of model selection via application of a multi-model averaging technique is an important component part of the proposed PFHA framework (see Figure 1) wherein its application ensures a more complete assessment of (model structure) uncertainty for a given PFHA analysis. Also included in Figure 48 are two multi-model averages of the three Schlather process configuration's 10,000-year return period return-level predictions, viz., a simple average and an information criteria-based average. The information criterion-based average presented in Figure 48 employs the information criterion reported in Figure 36, whose values yield a strong preference to the more parsimonious XYZPT2 configuration, almost no weight to the most complex XYZPT5 model, and approximately a weight of 0.08 to the XYZPT4 model. By contrast, a weights-assignment strategy based on the information criterion reported in Figure 37 solely selects the most complex XYZPT5 model with zero weight given to the remaining two model configurations. It is argued that the former rather than the latter approach is more representative of differences across the individual configurations as the information criterion values of the latter approach (see Figure 37) are mostly associated with the assessment of spatial dependence rather than the modeling of the marginals. Areal-based exceedance probability calculations associated with multiple configurations of a given max-stable process can be weighted in a similar fashion as was shown here for pointwise return level predictions. Moreover, if more than one max-stable process parametric model is employed in the PFHA analysis, then, as mentioned earlier in the report, the model averaging would occur across the processes including each of their associated individual configurations. Figure 49 presents computed pointwise return levels for stations 25, 26, and 63 based on simply averaging the predictions from the spatial BHM configurations XYZPT2, XYZPT4, XYZPT5, and XYZPT6. As previously mentioned, if multiple distributions are used in a spatial/spatiotemporal BHM analysis, then, similar to the approach mentioned for analysis using max-stable processes, the averaging would occur across the distributions including their associated individual configurations.

Figure 48. Pointwise return level predictions at station 59 (near Salem, OR) for T=10,000 years from the fitted Schlather process configurations XYZTP2, XYZPT4, and XYZPT5 and two multi-model averages of the three models.

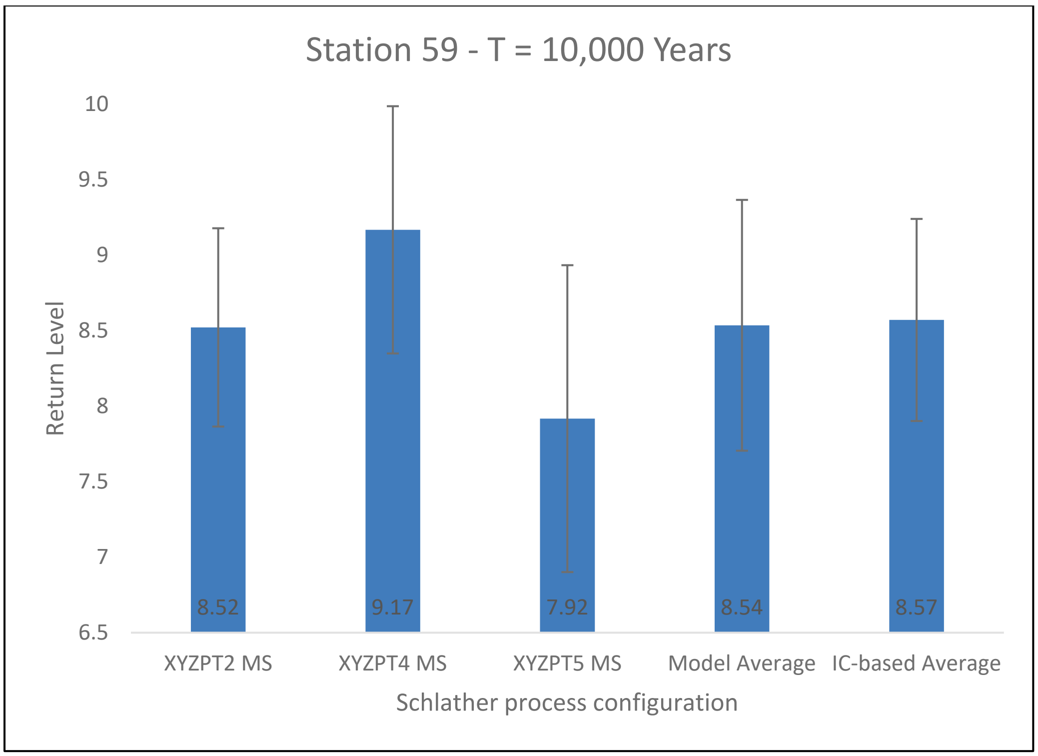

Figure 49. Simple computed average pointwise return level predictions of the XYZPT2, XYZPT4, XYZPT5, and XYZPT6 spatial BHM configurations at station locations 25, 26, and 63.

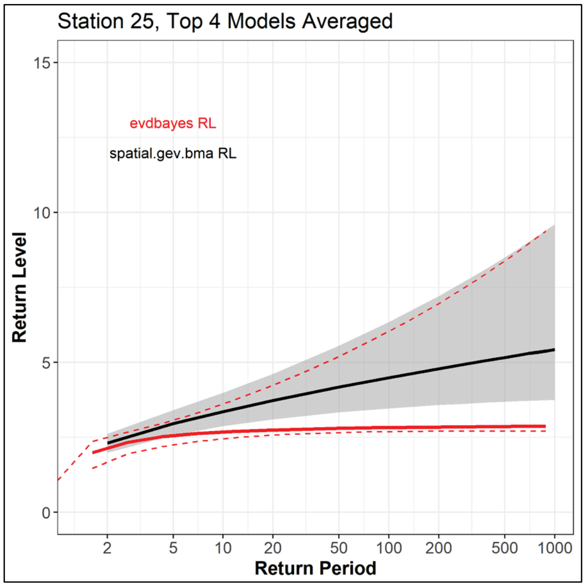

(a)

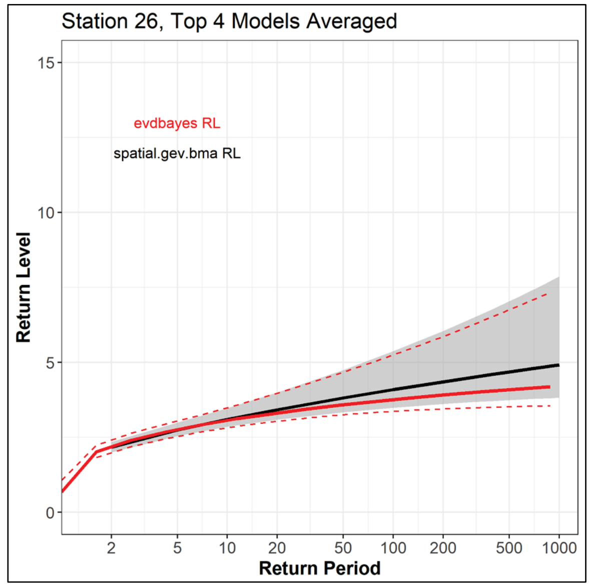

(b)

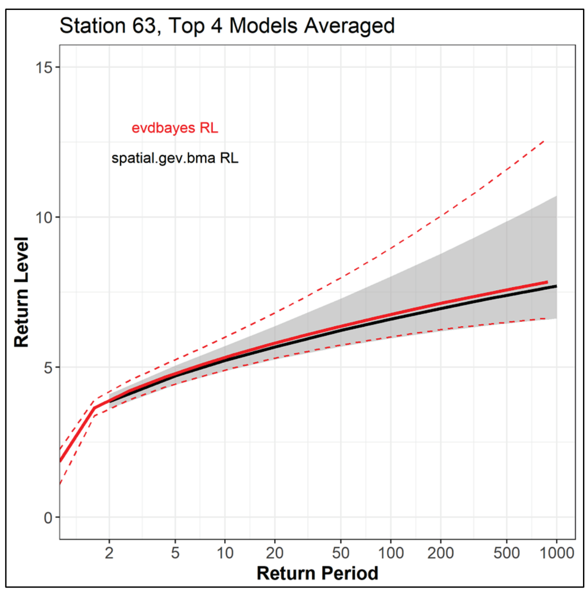

(c)

4 Discussion and Recommendations

This report proposed and demonstrated a conceptual, mathematical, and logical framework for PFHA analysis wherein while the focus is directed to the evaluation of critical infrastructure, viz., nuclear facilities, its application results in a complete flood hazard curve. The bases for the proposed framework are two distinct spatial analysis methodologies for characterizing hazard curves that each in their own right are recent advances in the modeling of extreme events. The two spatial methods were selected as the basis given that most relevant flood hazard phenomena naturally occur as spatial processes and regionalization is likely a minimum requirement toward improved accuracy and precision of estimates. Related, the two methods are each designed in a manner such that they, or their respective adaptions, can be readily applied to leverage any and all available relevant information for a given hazard analysis. The first method is spatial or spatiotemporal BHM whereas the second approach employs max-stable processes. The application of either approach involves the use of spatial and temporal covariate data to distribute extremal model parameters in space and also account for temporal trends. The spatial/spatiotemporal BHM methodology is simple and flexible and leverages the multiple merits of Bayesian inference to support probabilistic flood hazard analyses to readily develop spatially coherent pointwise return-level maps. However, its likelihood formulation assumes conditional independence among the extremes, which can be difficult to ignore for flood hazard phenomenon, and its use of a Gaussian process for the latent variable model results in a lack of conformance with EVT. The second framework approach, viz., max-stable processes, when applied, does account for the dependence among the extremes, conforms with EVT, which is highly notable as framework applications require credible extrapolation well beyond the observed record, and moreover, supports the capacity for more complex areal assessments of risk beyond the simple generation of pointwise return levels. For extreme rainfall analyses, it is particularly noteworthy that max-stable process applications can develop areal-based exceedance probabilities without having to employ empirical areal reduction factors. The proposed framework also involves a multi-model averaging step in attempts to account for the uncertainty associated with model choice.

The two separate approaches constituting the proposed PFHA framework were each applied in a limited manner to analyze extreme daily rainfall in the Willamette River Basin in the State of Oregon. However, beforehand, the individual merits of Bayesian inference, which is associated with the spatial/spatiotemporal BHM framework method, were extensively profiled by considering six simple at-site extreme rainfall analysis case studies. The first four demonstrations in aggregate clearly emphasized the importance of data analysis, model selection, and inference methodology for at-site extreme rainfall analyses. The fifth case study demonstrated the value of using informative priors when using Bayesian inference. The sixth demonstration emphasized the flexibility of the Bayesian inference methodology to accommodate treatment of non-stationarity in an analysis of extreme rainfall. The extreme rainfall analyses, which used the two distinct methods which form the basis of the proposed PFHA framework, were each limited framework applications in that neither instance was necessarily complete in combining any and all available information to improve the accuracy and precision of the estimates. For example, in the first instance application a spatiotemporal rather than spatial BHM might have been used to leverage temporal information data encapsulated in a potentially relevant climate index. In addition, causal information expansion data derived from expert elicitation to yield informative priors would have more fully leveraged the Bayesian inference methodology of the spatial BHM. Furthermore, the spatial BHM application might have also considered additional distributions beyond the GEV to support a more complete assessment of model choice. For the PFHA framework max-stable method application only a single max-stable parametric model was applied for the extreme rainfall analysis. The consideration of more than one max-stable process model, and different correlation functions associated with each selected max-stable model, would have been a more complete application of that PFHA framework methodological approach. Including causal information expansion data derived from regional rainfall modeling analysis, beyond the existing pooled systematic data record, would have, for either of the two methods, resulted in more complete applications of the PFHA framework. Last, further explorations of process understanding via the latent process modeling for the spatial BHM and the trend surface modeling of the marginals in the max-stable method could have been an additional opportunity for more complete applications of the PFHA framework. Despite these observed limitations with each of the instance applications of the proposed PFHA framework, the final two examples did profile some of the features of a framework application for each method. For an extreme rainfall analysis, either framework method can develop spatially coherent pointwise return level maps that leverage the pooled systematic record of observations, temporal covariate data, additional data developed from external analysis (e.g., modeling and/or elicitation), and process understanding as encapsulated in the latent variable/trend surface modeling. Application of the max-stable method fully conforms with EVT and also supports, via simulation, computation of areal-based exceedance probabilities, which, for extreme rainfall analyses, do not require the use of empirical ARFs. These two additional features of the max-stable PFHA method are particularly notable for characterization of hazard curves for flood phenomenon.

A flexible and efficient framework for PFHA has been proposed whose basis is application of either a spatial/spatiotemporal BHM that assumes conditional independence among the data or a formal spatial analysis of extremes approach that employs max-stable processes. PFHA framework method choice is dependent upon an initial assessment of dependence among the extreme data. If it is reasonable to assume independence, then selection of the spatial/spatiotemporal BHM method is a flexible approach that leverages all of the merits of using Bayesian inference. Moreover, it supports practical flood hazard analyses in that one can select the specific distribution(s) assumed relevant to model the data. However, if dependence cannot be ignored and/or it is desired to employ a method that fully conforms with EVT to characterize the hazard curve, then selection of max-stable modeling approach is recommended. Regardless of the chosen basis for framework application in either case, multi-model averaging can be applied in attempts to be complete in accounting for epistemic sources of uncertainty in a PFHA. Both proposed PFHA methods employ a likelihood formulation that can be readily adapted to flexibly combine location-specific historical/paleoflood data with the pooled systematic data record, and these noted adaptions of the two distinct methods are identified as opportunities for related contributions for probabilistic flood hazard assessment research and development.

References

AghaKouchak, A., D. Easterling, K. Hsu, S. Schubert, S. Sorooshian, eds. 2013. *Extremes in a Changing Climate: Detection, Analysis and Uncertainty*. New York: Springer Dordrecht. https://doi.org/10.1007/978-94-007-4479-0

Awadallah, A. G., and N. S. Younan. 2012. "Conservative Design Rainfall Distribution for Application in Arid Regions with Sparse Data." *Journal of Arid Environments* 79(0): 66-75. https://doi.org/10.1016/j.jaridenv.2011.11.032

Banerjee, S., B. P. Carlin, A. E. Gelfand. 2015. *Hierarchical Modeling and Analysis for Spatial Data, Second Edition*. Chapman & Hall/CRC Monographs on Statistics & Applied Probability, No. 35. Boca Raton, FL: CRC Press, Taylor and Francis Group. https://content.taylorfrancis.com/books/download?dac=C2009-0-07095-7&isbn=9781439819180&format=googlePreviewPdf

Bates, J. M., and C. W. J. Granger. 1969. "The Combination of Forecasts." *Operations Research Quarterly* 20(4): 451-468. https://doi.org/10.1057/jors.1969.103

Brandes, H. 2000. "The Venezuela Flash Floods and Debris Flows of 15-16 December 1999: Landslide News." *Japan Landslide Society* 13: 5-7.

Buckland, S. T., K. P. Burnham, and N. H. Augustin. 1997. "Model Selection: An Integral Part of Inference." *Biometrics* 53: 603-618. doi: 10.2307/2533961

Burnham, K. P., and D. R. Anderson. 2002. *Model Selection and Multimodel Inference: A Practical Information-Theoretic Approach*, 2nd edition. New York, Springer. http://cds.cern.ch/record/1608735/files/9780387953649_TOC.pdf

Chang, H., and I.-W. Jung. 2010. "Spatial and Temporal Changes in Runoff Caused by Climate Change in a Complex Large River Basin in Oregon." *Journal of Hydrology* 388(3-4): 186-207. https://doi.org/10.1016/j.jhydrol.2010.04.040

Cheng, L., and A. AghaKouchak. 2014. "Nonstationary Precipitation Intensity-Duration-Frequency Curves for Infrastructure Design in a Changing Climate." *Sci. Rep*. 4: 7093. https://www.nature.com/articles/srep07093.pdf

Cheng, L., A. AghaKouchak, E. Gilleland, and R. W. Katz. 2014. "Non-Stationary Extreme Value Analysis in a Changing Climate. *Clim. Change*. 127(2): 353–369. doi:10.1007/s10584-014-1254-5

Coles, S. 2001. *An Introduction to Statistical Modeling of Extreme Values*. London: Springer-Verlag. https://doi.org/10.1007/978-1-4471-3675-0

Coles, S., L. R. Pericchi, and S. Sisson. 2003. "A Fully Probabilistic Approach to Extreme Rainfall Modeling." *Journal of Hydrology* 273(1–4). 35-50. ISSN 0022-1694, http://dx.doi.org/10.1016/S0022-1694(02)00353-0

Coles, S., and L. Pericchi. 2003, Anticipating Catastrophes through Extreme Value Modelling." *Journal of the Royal Statistical Society: Series C (Applied Statistics)* 52(4): 405-416. doi: 10.1111/1467-9876.00413

Coles, S. G., and J. A. Tawn. 1996. "A Bayesian Analysis of Extreme Rainfall Data." *Journal of the Royal Statistical Society. Series C (Applied Statistics)* 45(4): 463-478. https://www.jstor.org/stable/2986068

Congdon, P. D. 2010. *Applied Bayesian Hierarchical Methods*. Boca Raton, FL: Chapman and Hall/CRC. https://content.taylorfrancis.com/books/download?dac=C2009-0-13814-5&isbn=9781584887218&format=googlePreviewPdf

Cooley D., D. Nychka, and P. Naveau. 2007. "Bayesian Spatial Modeling of Extreme Precipitation Return Levels." *Journal of the American Statistical Association* 102(479): 824-840. https://doi.org/10.1198/016214506000000780

Cooley D., and S. R. Sain. 2010. "Spatial Hierarchical Modeling of Precipitation Extremes from a Regional Climate Model." *Journal of Agricultural, Biological, and Environmental Statistics* 15(3): 381–402. https://doi.org/10.1007/s13253-010-0023-9

Cooley, D., J. Cisewski, R. Erhardt, S. Jeon, E. Mannshardt, B. Omolo, and Y. Sun. 2012. "A Survey of Spatial Extremes: Measuring Spatial Dependence and Modeling Spatial Effects." *RevStat* 10(1): 135-165.

Cowles, M. K., and B. P. Carlin. 1996. "Markov Chain Monte Carlo Convergence Diagnostics: A Comparative Review." *Journal of the American Statistical Association* 91: 833-904.

Dalrymple, T. 1960. *Flood Frequency Analysis*. U.S. Geol. Surv. Water Supply Pap. 1543A. https://doi.org/10.3133/wsp1543A

Daly, C., R. P. Neilson, and D. L. Phillips. 1994. "A Statistical-Topographic Model for Mapping Climatological Precipitation over Mountainous Terrain." *J. Appl. Meteor*. 33: 140-158. https://doi.org/10.1175/1520-0450(1994)033<0140:ASTMFM>2.0.CO;2

Daly, C., M. Halbleib, J. I. Smith, W. P. Gibson, M. K. Doggett, G. H. Taylor, J. Curtis, and P. A. Pasteris. 2008. "Physiographically-Sensitive Mapping of Temperature and Precipitation across the Conterminous United States." *International Journal of Climatology* 28: 2031-2064. https://doi.org/10.1002/joc.1688

Daly, C., J. I. Smith, and K. V. Olson. 2015. "Mapping Atmospheric Moisture Climatologies across the Conterminous United States." *PLoS ONE* 10(10): e0141140. https://doi.org/10.1371/journal.pone.0141140

Das, S., N. Millington, and S. P. Simonovic. 2013. "Distribution Choice for the Assessment of Design Rainfall for the City of London (Ontario, Canada) under Climate Change." *Canadian Journal of Civil Engineering* 40(2): 121-129. https://doi.org/10.1139/cjce-2011-0548

Davison, A. C., and R. L. Smith. 1990. "Model for Exceedances over High Thresholds." *Journal the Royal Statistical Society Series* 52(3): 393-442. https://doi.org/10.1111/j.2517-6161.1990.tb01796.x

Davison, A. C., S. A. Padoan, and M. Ribatet. 2012. “Statistical Modelling of Spatial Extremes.” *Statist. Sci.* 27(2): 161-186. https://projecteuclid.org/download/pdfview_1/euclid.ss/1340110864

Davison, A. C., and M. M. Gholamrezaee. 2012. “Geostatistics of Extremes.” *Proceedings of the Royal Society A: Mathematical, Physical and Engineering Science*. https://doi.org/10.1098/rspa.2011.0412

Dey, D. K., and J. Yan. 2016. *Extreme Value Modeling and Risk Analysis: Methods and Applications*. Boca Raton, FL: CRC Press.

Durrans, S. R., L. T. Julian, and M. Yekta. 2002. “Estimation of Depth-Area Relationships Using Radar-Rainfall Data.” *J Hydrol Eng* 7(5): 356-367.

Dyrrdal, A. V., A. Lenkoski, T. L. Thorarinsdottir, and F. Stordal. 2015. “Bayesian Hierarchical Modeling of Extreme Hourly Precipitation in Norway, Environmetrics.” 26: 89-106. doi:10.1002/env.2301

Eckersten, S. 2016. *Updating Rainfall Intensity-Duration-Frequency Curves in Sweden Accounting for the Observed Increase in Rainfall Extremes*. Department of Earth Sciences, Program for Air, Water and Landscape Sciences, Uppsala University, Villav¨agen 16, SE-751 05 Uppsala.

Economou, T., D. B. Stephenson, and C. A. T. Ferro. 2014. “Spatio-Temporal Modelling of Extreme Storms.” *Annals of Applied Statistics* 8(4): 2223-2246. doi:10.1214/14-AOAS766.

Elsebaie, I. 2012. “Developing Rainfall Intensity–Duration–Frequency Relationship for Two Regions in Saudi Arabia.” *Journal of King Saud University - Engineering Sciences* 24(2): 131-140.

Fawcett, L. 2013. *Case Studies. MAS2317/3317: Introduction to Bayesian Statistics*. Newcastle University. Web. 29 September 2017.

Fisher, R. A., and L. H. C. Tippett. 1928. "Limiting Forms of the Frequency Distribution of the Largest and Smallest Member of a Sample.” *Proc. Cambridge Phil. Soc.* 24(2): 180–190. doi:10.1017/s0305004100015681

Garcia-Aristizabal, A., E. Bucchignani, E. Palazzi, D. D'Onofrio, P. Gasparini, and W. Marzocchi. 2015. “Analysis of Non-Stationary Climate-Related Extreme Events Considering Climate Change Scenarios: An Application for Multi-Hazard Assessment in the Dar es Salaam Region, Tanzania.” *Natural Hazards* 75(1): 289-320. doi: 10.1007/s11069-014-1324-z

Gelman, A., J. B. Carlin, H. S. Stern, and D. B. Rubin. 2004. *Bayesian Data Analysis, Second Edition, Texts in Statistical Science*. Chapman & Hall/CRC.

Gelman, A., and D. B. Rubin. 1992. “Inference from Iterative Simulation Using Multiple Sequences.” *Stat. Sci.* 7(4): 457–472.

Ghosh, S., and B. K. Mallick. 2011. “A Hierarchical Bayesian Spatio-Temporal Model for Extreme Precipitation Events.” *Environmetrics* 22(2): 192-204. doi:10.1002/env.1043

Gilleland E., and R. W. Katz. 2011. “New Software to Analyze How Extremes Change over Time.” *EOS Trans Am Geophys Union* 92: 13-14.

Gilleland, E., M. Ribatet, and A. G. Stephenson. 2013. “A Software Review for Extreme Value Analysis.” *Extremes* 16(1): 103-119.

Gnedenko, B. V. 1943. "Sur la Distribution Limite du Terme Maximum D'une Serie Aleatoire." *Annals of Mathematics* 44(3): 423-453. doi:10.2307/1968974

Gneiting, T., and A. E. Raftery. 2007. “Strictly Proper Scoring Rules, Prediction, and Estimation.” *Journal of the American Statistical Association* 102(477): 359-378. https://doi.org/10.1198/016214506000001437

Granger, C. W. J., and R. Ramanathan. 1984. "Improved Methods of Combining Forecast Accuracy." *Journal of Forecasting* 3(2): 197-204.

Gumbel, E. J. 1958. *Statistics of Extremes*. Columbia University Press.

Guo, Y., and B. J. Adams. 1998. “Hydrologic Analysis of Urban Catchments with Event-Based Probabilistic Models, 1, Runoff Volume.” *Water Resource Research* 34(12): 3421-3431.

Hersbach, H. 2000. “Decomposition of the Continuous Ranked Probability Score for Ensemble Prediction Systems.” *Weather and Forecasting* 15(5): 559-570. https://doi.org/10.1175/1520-0434(2000)015<0559:DOTCRP>2.0.CO;2

Hershfield, D. M. 1962. *Rainfall Frequency Atlas of the United States for Durations from 30 Minutes to 24 Hours and Return Periods from 1 to 100 Years*. U.S. Weather Bureau Technical Paper 40. Washington, DC.

Hoeting, J. A., D. Madigan, A. E. Raftery, and C. T. Volinsky. 1999. “Bayesian Model Averaging: A Tutorial.” *Statistical Science* 14(4): 382-401.

Hosking, J. R. M. 1988. *The Four Parameter KAPPA Distribution*. IBM Research Report RC13412. Yorktown Heights, NY: IBM Research.

Hosking, J. R. M., and J. R. Wallis. 1997. *Regional Frequency Analysis - An Approach based on L-Moments*. New York: Cambridge University Press.

Katz, R. W., M. B. Parlange, and P. Naveau. 2002. "Statistics of Extremes in Hydrology." *Advances in Water Resources* 25(8-12): 1287-1304.

Koutsoyiannis D., D. Kozonis, and A. Manetas. 1998. “A Mathematical Framework for Studying Rainfall Intensity-Duration-Frequency Relationships.” *Journal of Hydrology* 206(1-2): 118-135.

Koutsoyiannis, D. 2004. “Statistics of Extremes and Estimation of Extreme Rainfall: I. Theoretical Investigation.” *Hydrological Sciences Journal* 49(4): 580-590.

Koutsoyiannis, D. 2004. “Statistics of Extremes and Estimation of Extreme Rainfall: II. Empirical Investigation of Long Rainfall Records.” *Hydrological Sciences Journal* 49(4): 600-610.

Koutsoyiannis, D. 2005a. “Uncertainty, Entropy, Scaling and Hydrological Stochastics. 1. Marginal Distributional Properties of Hydrological Processes and State Scaling.” *Hydrological Sciences Journal* 50(3): 381-404.

Koutsoyiannis, D. 2005b. “Uncertainty, Entropy, Scaling and Hydrological Stochastics. 2. Time Dependence of Hydrological Processes and State Scaling.” *Hydrological Sciences Journal* 50(3): pp. 405-426.

Kwon, H.-H., C. Brown, and U. Lall. 2008. “Climate Informed Flood Frequency Analysis and Prediction in Montana Using Hierarchical Bayesian Modeling.” *Geophys. Res. Lett.* 35(5): L05404. doi:10.1029/2007GL032220.

Lee, K. K., and J. C. Risley. 2002. *Estimates of Ground-Water Recharge, Base Flow, and Stream Reach Gains and Losses in the Willamette River Basin, Oregon*. U.S. Geological Survey Water-Resources Investigations Report 01–4215. Reston, VA: U.S. Geological Survey.

Lehmann, E. A., A. Phatak, S. Soltyk, J. Chia, R. Lau, and M. Palmer. 2013. “Bayesian Hierarchical Modeling of Rainfall Extremes.” *MODSIM: 20th International Congress on Modelling and Simulation*, Adelaide, 1-6 December 2013.

Lenkoski, A. 2014. *spatial.gev.bma: Hierarchical Spatial Generalized Extreme Value (GEV) Modeling with Bayesian Model Averaging (BMA) (Version 1.0).* https://cran.r-project.org/web/packages/spatial.gev.bma/index.html

Madigan, D., and A. E. Raftery. 1994. “Model Selection and Accounting for Model Uncertainty in Graphical Models using Occam's Window.” *Journal of the American Statistical Association* 89(428): 1535-1546.

Melack, J. M., J. Dozier, C. R. Goldman, D. Greenland, A. M. Milner, and R. J. Naiman. 1997. “Effects of Climate Change on Inland Waters of the Pacific Coastal Mountains and Western Great Basin of North America.” *Hydrol. Process.* 11(8): 971–992. doi:10.1002/(SICI)1099-1085(19970630)11:8<971::AID-HYP514>3.0.CO;2-Y

Merz, R., and G. Blöschl. 2008a. “Flood Frequency Hydrology: 1. Temporal, Spatial, and Causal Expansion of Information.” *Water Resour. Res.* 44(8): W08432. doi:10.1029/2007WR006744.

Merz, R., and G. Blöschl. 2008b. “Flood Frequency Hydrology: 2. Combining Data Evidence.” *Water Resour. Res.* 44(8): W08433. doi:10.1029/2007WR006745.

Metropolis, N., A. W. Rosenbluth, M. N. Rosenbluth, A. H. Teller, and E. Teller. 1953. “Equation of State Calculations by Fast Computing Machines.” *J Chem Phys* 21(6): 1087-1092.

Miller, J. F., R. H. Frederick, and R. J. Tracey. 1973. *Precipitation Frequency Atlas of the Western United States, Vol. I Montana, Vol. II Wyoming, Vol. III Colorado, Vol. IV New Mexico*. NOAA Atlas 2. Silver Spring, MD: National Weather Service, National Oceanic and Atmospheric Administration, U.S. Department of Commerce. http://www.nws.noaa.gov/ohd/hdsc/currentpf.htm

Mock, C. J. 1996. “Climatic Controls and Spatial Variations of Precipitation in the Western United States. *Journal of Climate* 9(5): 1111-1125.

Morris, D. E., J. E. Oakley, and J. A. Crowe. 2014. “A Web-Based Tool for Eliciting Probability Distributions from Experts.” *Environmental Modelling & Software* 52: 1-4. http://dx.doi.org/10.1016/j.envsoft.2013.10.010.

Najafi, M. R., and H. Moradkhani. 2013. “Analysis of Runoff Extremes Using Spatial Hierarchical Bayesian Modeling.” *Water Resources Research* 49(10): 6656-6670. https://doi.org/10.1002/wrcr.20381

Nicolet, G., N. Eckert, S. Morin, and J. Blanchet. 2015. “Inferring Spatio-Temporal Patterns in Extreme Snowfall in the French Alps Using Max-stable Processes.” *Procedia Environmental Sciences* 27: 75-82, https://doi.org/10.1016/j.proenv.2015.07.102

Olinda, R. A., J. Blanchet, C. A. C. dos Santos, V. A. Ozaki, and P. J. Ribeiro, Jr. 2014. “Spatial Extremes Modeling Applied to Extreme Precipitation Data in the State of Paraná.” *Hydrol. Earth Syst. Sci. Discuss.* https://doi.org/10.5194/hessd-11-12731-2014

Overeem, T. A., and B. I. Holleman. 2008. “Rainfall Depth-Duration-Frequency Curves and Their Uncertainties.” *Journal of Hydrology* 348(1-2): 124-134.

Papalexiou, S. M., and D. Koutsoyiannis. 2013. “Battle of Extreme Value Distributions: A Global Survey on Extreme Daily Rainfall.” *Water Resour. Res.* 49(1). doi:10.1029/2012WR012557.

Parida, B. P. 1999. “Modelling of Indian Summer Monsoon Rainfall Using a Four-Parameter Kappa Distribution.” *International Journal* of *Climatology* 19(12): 1389-1398.

Phien, H. N., and T. Jivajirajan. 1983. “Applications of the Log Pearson Type-3 Distribution in Hydrology.” *Journal of Hydrology* 73(3-4): 359-372.

Plummer, M., N. Best, K. Cowles, and K. Vines. 2006. “CODA: Convergence Diagnosis and Output Analysis for MCMC. *R News* 6: 7-11.

R Core Team. 2013. *R: A Language and Environment for Statistical Computing*. Vienna, Austria: R Foundation for Statistical Computing. http://www.R-project.org/

Raftery, A. E., T. Gneiting, F. Balabdaoui, and M. Polakowski. 2005. "Using Bayesian Model Averaging to Calibrate Forecast Ensembles." *Monthly Weather Review* 133(5): 1155-1174.

Redmond, K. T., and R. W. Koch. 1991. “Surface Climate and Streamflow Variability in the Western United States and Their Relationship to Large-Scale Circulation Indices.” *Water Resources Research* 27(9): 2381-2399.

Reich, B. J., and B. A. Shaby. 2012. “A Hierarchical Max-Stable Spatial Model for Extreme Precipitation.” *Ann. Appl. Stat.* 6(4): 1430-1451. doi:10.1214/12-AOAS591. https://projecteuclid.org/euclid.aoas/1356629046

Renard, B., M. Lang, and P. Bois. 2006. “Statistical Analysis of Extreme Events in a Nonstationary Context via a Bayesian Framework. Case Study with Peak-Over-Threshold Data.” *Stochastic Environmental Research and Risk Assessment* 21(2): 97-112.

Renard, B., X. Sun, and M. Lang. 2015. *Bayesian Methods for Non-stationary Extreme Value Analysis in Extremes in a Changing Climate*. Edited by A. AghaKouchak, D. Easterling, K. Hsu, S. Schubert, and S. Sorooshian. New York: Springer Dordrecht.

Ribatet, M., D. Cooley, and A. C. Davison. 2012. "Bayesian Inference from Composite Likelihoods, with an Application to Spatial Extremes." *Stat. Sin.* 22(2): 813-845.

Ribatet, M. 2013. "Spatial Extremes: Max-Stable Processes at Work." *Journal of Société Française de Statistique* (special edition on extreme value theory) 154(2): 156-177.

Ribatet, M. 2017. *SpatialExtremes: Modelling Spatial Extremes*. R Package Version 2.0-5. http://spatialextremes.r-forge.r-project.org/

Salcedo, D. A. 2000. "Los Flujos Torrenciales Catastróficos de Diciembre de 1999, en el Estado Vargas y en Caracas: Características y Lecciones Apprendidas." *Memorias XVI Seminario Venezolano de Geotecnia, Caracas*, 128-175.

Sancio, R. T., and R. Barrios. 2000. "Disaster in Venezuela: The Floods and Landslides of December 1999." *Natural Hazards Observer* 24(4): 1-2.

Sang, H., and A. E. Gelfand. 2008. "Hierarchical Modeling for Extreme Values Observed over Space and Time." *Environ. Ecol. Stat.* 16(3): 407–426. https://doi.org/10.1007/s10651-007-0078-0

Schaefer, M. G. 1990. "Regional Analysis of Precipitation Annual Maxima in Washington State." *Water Resour. Res.* 26(1): 119-131.

Schaefer, M. G., B. L. Barker, G. H. Taylor, CCM, and J. R. Wallis. 2008. *Regional Precipitation-Frequency Analysis and Spatial Mapping of 24-Hour Precipitation for Oregon*. Final Report SPR 656 for Oregon Department of Transportation Research Unit and Federal Highway Administration, Report No. OR-RD-FHWA-08-05.

Schlather, M. 2002. "Models for Stationary Max-Stable Random Fields." *Extremes* 5(1): 33–44.

Schoof, J. T., S. C. Pryor, and J. Surprenant. 2010. "Development of Daily Precipitation Projections for the United States Based on Probabilistic Downscaling." *Journal of Geophysical Research* 115(D13). https://doi-org.erdclibrary.idm.oclc.org/10.1029/2009JD013030

Sebille, Q., A.-L. Fougeres, and C. Mercadier. 2016. "A Comparison of Spatial Extreme Value Models." *Application to Precipitation Data*. https://hal.archives-ouvertes.fr/hal-01300751/document

Şen, Z., and A. G. Eljadid. 1999. "Rainfall Distribution Function for Libya and Rainfall Prediction." *Hydrological Sciences Journal* 44(5): 665-680.

Shao, J. 1997. "An Asymptotic Theory for Linear Model Selection." *Statistica Sinica* 7(2): 221-242.

Singh, V. P. 2017. *Handbook of Applied Hydrology, Second Edition*. New York: McGraw Hill Education.

Smith, E. 2005. *Bayesian Modelling of Extreme Rainfall Data*. PhD Thesis. University of Newcastle upon Tyne.

Smith, R. L. 1990. "Max-Stable Processes and Spatial Extremes." Unpublished manuscript. https://rls.sites.oasis.unc.edu/faculty/rs/papers/RLS_Papers.html

Smith, R. L., and I. Weissman. 1994. "Estimating the Extremal Index." *Journal of the Royal Statistical Society* 56(3): 515-528.

Smith, R. L., J. A. Tawn, and S. G. Coles. 1997. "Markov Chain Models for Threshold Exceedances." *Biometrika* 84: 249-268.

Soltyk, S., M. Leonard, A. Phatak, and E. Lehmann. 2014. "Statistical Modelling of Rainfall Intensity-Frequency-Duration Curves Using Regional Frequency Analysis and Bayesian Hierarchical Modelling" [online]. *Hydrology and Water Resources Symposium 2014*. Barton, ACT: Engineers Australia, 302-309.

Spiegelhalter, D. J., N. G. Best, B. P. Carlin, and A. Van Der Linde. 2002. "Bayesian Measures of Model Complexity and Fit." *Journal of the Royal Statistical Society: Series B (Statistical Methodology)* 64(4): 583-639. https://doi.org/10.1111/1467-9868.00353

Steinschneider, S., and U. Lall. 2015. "A Hierarchical Bayesian Regional Model for Nonstationary Precipitation Extremes in Northern California Conditioned on Tropical Moisture Exports." *Water Resour. Res.* 51(3): 1472-1492. doi:10.1002/2014WR016664.

Stephenson, A. G. 2002. "evd: Extreme Value Distributions." *R News* 2(2): 31-32. http://CRAN.R-project.org/doc/Rnews/

Stephenson, A., and M. Ribatet. 2014. *evdbayes: Bayesian Analysis in Extreme Value Theory*. R package version 1.1-1. https://CRAN.R-project.org/package=evdbayes

Stephenson, A. G. 2016. Original S functions written by Janet E. Heffernan with R port and R documentation provided by Alec G. Stephenson. ismev: An Introduction to Statistical Modeling of Extreme Values. R package version 1.41. https://CRAN.R-project.org/package=ismev

Stone, M. 1977. "An Asymptotic Equivalence of Choice of Model by Cross-Validation and Akaike's Criterion." *Journal of the Royal Statistical Society*, Series B (Methodological), 39(1): 44-47.

Svensson, C., and D. A. Jones. 2010. "Review of Methods for Deriving Areal Reduction Factors." *Journal of Flood Risk Management* 3(3): 232-245.

Takeuchi, K. 1976. "Distribution of Informational Statistics and a Criterion of Fitting." *Suri-Kagaku* 153: 12-18.

ter Braak, C. J. F., and J. A. Vrugt. 2008. "Differential Evolution Markov Chain with Snooker Updater and Fewer Chains." *Stat. Comput.* 18(4): 435-446. doi: 10.1007/s11222-008-9104-9.

USAID. 2000. *Venezuela Factsheet*. February 2000. USAID-Office of Foreign Disaster Assistance. https://web.archive.org/web/20010305155236/http://www.usaid.gov/hum_response/ofda/venezfl_fs11_fy00.html

Varin, C., and P. Vidoni. 2005. "A Note on Composite Likelihood Inference and Model Selection." *Biometrika* 92(3): 519-528. MR2202643.

Viglione, A., R. Merz, J. L. Salinas, and G. Blöschl. 2013. "Flood Frequency Hydrology: 3. A Bayesian Analysis." *Water Resour. Res.* 92(3): 675-692. doi:10.1029/2011WR010782.

Wieczorek, G. F., M. C. Larsen, L. S. Eaton, B. A. Morgan, and J. L. Blair. 2001. *Debris-Flow and Flooding Hazards Associated with the December 1999 Storm in Coastal Venezuela and Strategies for Mitigation*. U.S. Geological Survey, Open File Report 01-0144. Reston, VA.

Wikle, C. K., L. M. Berliner, and N. Cressie. 1998. "Hierarchical Bayesian Space-Time Models." *Environ. Ecol. Stat.* 5(2): 117-154. doi:10.1023/A:1009662704779.

Wikle, C. K., R. F. Milliff, D. Nychka, and L. M. Berliner. 2001. "Spatiotemporal Hierarchical Bayesian Modeling Tropical Ocean Surface Winds." *J. Am. Stat. Assoc.* 96(454): 382-397. doi:10.1198/016214501753168109.

Winter, H. 2011. *Bayesian Modelling of the Effect of the North Atlantic Oscillation on Extreme Precipitation in the North of England*. University of Exeter.

Yan, H., and H. Moradkhani. 2014. "Bayesian Model Averaging for Flood Frequency Analysis." *American Society of Civil Engineers World Environmental and Water Resources Congress 2014*, Portland, Oregon. Edited by W. C. Huber, 1886-1895. http://dx.doi.org/10.1061/9780784413548.189

Appendix A: Extreme Value Theory

Cooley and Sain (2010) commented on the commonly used phrase "climate is what you expect, weather is what you get," mentioning that it is only partially correct in that climate is the entire distribution of weather events and that it is not only important to characterize the mean of climatological variables but also their extremes. For example, critical infrastructure engineering design specifications must reflect a quantitative understanding of the extremal behavior of environmental processes to ensure a predetermined low-level failure probability. However, estimating the probability of extreme meteorological events is difficult because of the need to extrapolate beyond the available record and to locations where observations are not available. Salient features of EVT are succinctly summarized directly below. The active reader is directed to Katz et al. (2002) and Coles (2001) and references cited therein, for further details.

Block maxima models

EVT provides a framework to model the tail of probability distributions. It focuses on the behavior of

$$M_n = \max\{X_1, \dots, X_n\}$$

where $X_1, \dots, X_n$ is a sequence of independent univariate random variables with a common distribution function F and n is some large number. The extremal types theorem states that if there exists a normalization to stabilize M_n, then it converges to a GEV family with distribution functions of the form

$$G(x) = \exp\left\{-\left[1 + \frac{\xi(x-\mu)}{\sigma}\right]^{-1/\xi}\right\} \quad \text{(A.1)}$$

defined on $\{x: 1 + \xi(x - \mu)/\sigma > 0\}$ and with parameter space $\{(\mu, \sigma, \xi): \mu \in \Re, \sigma > 0, \xi \in \Re\}$. The location ($\mu$), scale ($\sigma$), and shape ($\xi$) parameters of the distribution specify the center of the distribution, the deviation around μ, and the tail behavior of the distribution, respectively. The GEV family in fact combines into one family the three possible extreme value distributions that correspond to $\xi < 0$ (Weilbull), $\xi = 0$, interpreted as the limit as $\xi \to 0$ (Gumbel), and $\xi > 0$ (Fréchet).

For a series of independent observations, X_i, the data can be blocked into m sequences of length n, where n is some large number. By computing the maximum of each block, a series is generated:

$$M_{n,1}, \dots, M_{n,m}.$$

The specified blocks often correspond to a time period of 1 year (i.e., n is the number of observations in a year), which results in a series of annual maxima data. Because of its asymptotic justification, the GEV distribution is used to model maxima of finite-sized blocks such as annual maxima.

In hydrology, the pth quantile, denoted by x_p, is the value with cumulative probability p:

$$G(x_p) = p \tag{A.2}$$

In addition, the return period associated with the pth quantile x_p, denoted and defined by $T = 1/(1-p)$, represents the average frequency of occurrence for an event of magnitude x_p. As previously mentioned, estimates of extreme quantiles of the modeled block maxima are of particular interest in extreme rainfall analysis, as they give an estimate of the level the process is expected to exceed once, on average, in a given number of years. For the GEV family, these extreme quantiles, obtained by inverting Equation A.1, are

$$x_p = \mu + \frac{\sigma}{\xi}\left[1 - \left(-ln(p)\right)^{\xi}\right], \xi \neq 0 \tag{A.3}$$

The simplified Gumbel distribution function, the special limiting case of the GEV distribution, and its extreme quantiles are given by

$$G(x) = \exp\left[-\exp\left\{-\left(\frac{(x-\mu)}{\sigma}\right)\right\}\right] \tag{A.4}$$

$$x_p = \mu - \sigma ln\left(-ln(p)\right), \xi = 0 \tag{A.5}$$

Threshold exceedance models

The block maxima approach has the potential to be wasteful in the sense that by its design it might not include all available information on extremes encapsulated in a given time series dataset. Moreover, every identified maximum may not necessarily be an extreme. An alternative approach is to model all observations exceeding a specified high threshold. If the conditions of the extremal types theorem hold true, then exceedances should approximately follow a GPD as the threshold gets large and the sample size increases. In particular, if X denotes an arbitrary element of the sequence X_i, then for a suitably large threshold u, the distribution of $(X - u)$, conditional on $X > u$, is approximately

$$H(y) = 1 - \left(1 + \frac{\xi y}{\tilde{\sigma}}\right)^{-1/\xi} \tag{A.6}$$

defined on $\{y: y > 0 \; and \; (1 + \xi y/\tilde{\sigma}) > 0\}$, where $\tilde{\sigma} = \sigma + \xi(u - \mu)$. For the case $\xi = 0$, interpreted by taking the limit as $\xi \to 0$, the distribution is exponential with parameter $1/\tilde{\sigma}$:

$$H(y) = 1 - \exp\left(-\frac{y}{\tilde{\sigma}}\right), \, y > 0 \tag{A.7}$$

The GPD shape parameter ξ is equal to the corresponding shape parameter of the GEV distribution. The GPD scale parameter $\tilde{\sigma}$ is equal to $\sigma + \xi(u - \mu)$, where u is the GPD threshold parameter and μ and σ are the location and scale parameters of the GEV distribution. Smith (2005) presented a development for expressions for return level estimates in terms of the GPD parameters. In summary, the N-year return level estimates, z_N, are given by

$$z_N = \begin{cases} u + \frac{\sigma}{\xi}\left[\left(Nn_y\zeta_u\right)^{\xi} - 1\right], \xi \neq 0 \\ u + \sigma ln\left(Nn_y\zeta_u\right), \xi = 0 \end{cases} \tag{A.8}$$

where n_y is the number of observations per year and $\zeta_u = Pr(X > u)$, which has a natural estimator equal in value to the proportion of sample points exceeding u.

Application of the generalized Pareto family involves specification of a threshold wherein all of the observations above that value are defined as extreme (Renard et al. 2006). Threshold selection requires a careful consideration of the tradeoff between bias and variance. A threshold value that is set too low compromises the asymptotic justification of the model, resulting in biased parameter estimates. Conversely, if the threshold value is set too high, then too few observations are defined as extreme and parameter estimation variance is high. The conventional practice is to set the threshold to a value as low as is possible such that the asymptotic limit justification remains, thus resulting in the maximum number of exceedances for the given dataset.

A threshold value can be selected based upon an examination of the mean residual life plot (Davison and Smith 1990), which consists of the set of points $\left(u_i, e(u_i)\right)$ for a range of possible threshold values u_i and where $e(u_i)$ is the empirical mean of the set $\{x_i - u : x_i > u\}$. Because of an identity for the generalized Pareto model for the expected value for exceedances above a given threshold, the mean residual life plot should be linear above a given value for u (Coles et al. 2003). Another approach to threshold selection involves plots of a rescaled scale parameter and also the shape parameter for a range of threshold values and identifying the lowest threshold value where both of these parameter's estimates stabilize.

A disadvantage of the GPD, which models the distribution of exceedances above a given high threshold, is that extreme events can occur in clusters, which violates the independence assumption. The typical means by which to address this problem is to decluster the dependent data by empirically defining clusters of exceedances and selecting the maxima within each cluster (Coles 2001). It is assumed that this filtering process yields a near independent dataset that has no effect on the limit laws for extremes. A common empirical rule approach to defining clusters is to consider a cluster to be active until r consecutive values fall below the threshold for some pre-specified value of r. Conventional guidance associated with declustering is to evaluate sensitivity by examining return level results rather than parameter estimates given that the GPD scale parameter is expected to change with threshold. As indicated in Equation A.9 below, computation of a return level requires estimation of the extremal index, θ, a parameter defined on the interval [0,1] which measures the degree of clustering of extremes in a stationary process and whose inverse can be interpreted as an approximation to the mean cluster size.

$$z_N = \begin{cases} u + \frac{\sigma}{\xi}\left[\left(N n_y \zeta_u \theta\right)^{\xi} - 1\right], \xi \neq 0 \\ u + \sigma ln\left(N n_y \zeta_u \theta\right), \xi = 0 \end{cases} \tag{A.9}$$

Coles (2001) and Smith and Weissman (1994) present methods for estimating the extremal index. An alternative to declustering, which can be somewhat arbitrary and reduce information about extremes such as within-cluster behavior, is to model extremes of a stationary first-order Markov chain (Coles 2001; Smith et al. 1997).

Another disadvantage of the GPD model is that its parameters depend on the threshold choice. An alternative threshold modeling approach is the PP characterization of extremes. The timing, t, and magnitude, X, of extreme events, viz., $\{(t_1, X_1), \dots, (t_n, X_n)\}$, can be viewed as points in a two-dimensional PP space. For large threshold values u, the sequence $\{(t_i, X_i), i = 1 \dots, n\}$ on the interval $(0,1) \times [u, \infty)$, wherein the time axis has been rescaled to the unit interval, converges in distribution to a non-homogeneous Poisson process with intensity measure given by

$$\Lambda(A) = (t_2 - t_1)\left[1 + \frac{\xi(x-\mu)}{\sigma}\right]^{-1/\xi} \quad \text{(A.10)}$$

where A is any region of the form $A = [t_1, t_2] \times (u, \infty)$ with $[t_1, t_2] \subset [0,1]$. Coles (2001) demonstrated the GEV and GPD models to be special cases of the PP representation for the analysis of extremes. For example, reformulating the intensity measure as

$$\Lambda(A) = n_y(t_2 - t_1)\left[1 + \frac{\xi(x-\mu)}{\sigma}\right]^{-1/\xi} \quad \text{(A.11)}$$

where n_y is the number of years of observations results in the estimated parameters (μ, σ, ξ) to correspond directly to the GEV parameters of the annual maxima distribution of the observed process. The PP modeling approach can be seen as an indirect way of fitting data to the GEV distribution that makes use of more information about the upper tail of the distribution than does the block maxima approach (Coles 2001). Coles (2001) further underscored that the likelihood formulation associated with the PP threshold exceedance modeling framework supports a more natural treatment of non-stationarity when compared with the Generalized Pareto model.

Appendix B: Other Distributions for Extreme Rainfall Analysis

As previously mentioned, there are many different distributions beyond those briefly profiled from EVT that have been documented to model extreme rainfall, including among others the Kappa, exponential, Weibull, Gamma, Gumbel, generalized extreme value, log-Pearson type III, Fréchet (EV2), Halphen IB, Inverse Gamma, Halphen type A, Halphen type B, and Pearson type III distributions. For example, rainfall probabilities for durations of days, weeks, months, and years have been estimated by the Gamma distribution (Şen and Eljadid 1999). For many years, the most common approach to summarizing precipitation frequency analyses in the United States was the work of Hershfield (1962), which is commonly referred to as TP-40. Hershfield (1962) recommended the simplified Gumbel distribution, the special limiting case of the GEV distribution, to model the annual maxima series of 24 hr rainfall. The Gumbel distribution remains as a widely used distribution for rainfall frequency analysis owing to its suitability for modeling maxima (Elsebaie 2012; Das et al. 2013). While the empirical data might support this in some cases, it is also often argued that the Gumbel is more appropriate than the full GEV family since there are many distributions of the X_i that lead to a limiting Gumbel distribution for the M_n, including, for example, the normal, lognormal, exponential, Weibull, and Gamma distributions. However, Koutsoyiannis (2004 a,b) concluded that the Gumbel distribution is quite unlikely to apply to hydrological extremes, and its application may misjudge the risk as it seriously underestimates the largest extreme rainfall amounts. Coles et al. (2003) came to a similar conclusion while considering mode of inference and also model choice to compare parameter and return level estimates using the rainfall annual maxima dataset at the Maiquetia International Airport located on the North Central coast of Venezuela, both with and without consideration of the 1999 event. The Maiquetia International Airport station's rainfall annual maxima, available for the period 1951-1999, is notable because the 1999 maximum is almost three times larger than the second largest maximum, and it resulted in significant loss of life and property damage. Model choice involved selection of either the three-parameter GEV distribution or the often used two-parameter Gumbel distribution. For the pre-1999 series of rainfall annual maxima, regardless of inference methodology, the two-parameter Gumbel model return level point estimates were three orders of magnitude larger than their respective values obtained using the GEV distribution. Koutsoyiannis (2004 a,b) recommended using the extreme value type 2 (EV2) distribution instead of the Gumbel distribution and further indicated that the shape parameter κ of the EV2 distribution is constant for all examined geographical zones (Europe and North America), with a value of $\kappa = 0.15$ (Koutsoyiannis, 2004 a,b). Using both at-site and regional L-moment goodness-of-fit results, climatic considerations, and sensitivity testing, the GEV distribution was selected to best represent the underlying distributions of all daily and hourly annual maxima series rainfall data. The more recent work by Papalexiou and Koutsoyiannis (2013) contains additional guidance to follow regarding selection among the GEV family of distributions.

Appendix C: Generalization of Model Selection

Clearly, model choice is confounded by the existence of multiple models from which to select to analyze extreme rainfall. Analysis results will differ depending upon the model selected. A means by which to accommodate this observed source of epistemic uncertainty in the modeling of extreme rainfall is to generalize the problem of model selection. In particular, rather than rely upon a single selected model, instead model average the various available competing models in such a way that the weighted linear model estimate is a predictor of the observations at least as good as any one of the individual models. There are different ways in which one can combine multiple models, including, for example, equal weights averaging, Bates-Granger averaging (Bates and Granger 1969), Information criterion averaging (Buckland et al. 1997; Burnham and Anderson 2002), Granger-Ramanathan averaging (Granger and Ramanathan 1984), Bayesian model averaging (Raftery et al. 2005; Yan and Moradkhani 2014), and averaging based on expert elicitation.

With equal weights averaging, one simply assigns an equal weight to each of the models of the ensemble. The Bates-Granger model averaging technique assigns a weight to each model based on its error variance, normalized across all of the models which constitute the ensemble. Information criterion averaging calculates individual model weights, β_k, in the following manner:

$$\beta_k = \frac{\exp\left(-\frac{1}{2}I_k\right)}{\sum_{k=1}^{K}\exp\left(-\frac{1}{2}I_k\right)} \tag{C.1}$$

where K and I_k denote the total number of models and the information criterion for model k, respectively. The information criterion I_k is a function of data fit and model complexity. Two commonly used information criterion include the AIC and the BIC. Granger-Ramanathan averaging uses ordinary least squares to estimate the weight value to assign to each individual model. In contrast with the three previous methods, this model averaging technique accounts for any correlation that may exist.

BMA is a means by which to include the model selection process into the assessment of uncertainty. BMA is a scheme to infer a combined probabilistic prediction whose average possesses more reliability and skill than that which can be obtained from any one of the individual models that constitute the model combination (Madigan and Raftery 1994). The combined model predictive density computed using BMA is a weighted average of the probability density functions for each of the individual models (Hoeting et al. 1999). Hoeting et al. (1999) list and discuss several other BMA-related implementation matters, one key nontrivial issue being inclusion/exclusion into the set of models that constitute the model combination.

Appendix D: Bayesian Inference Methodology and Markov Chain Monte Carlo Simulation

Bayes formula is a consequence of the axioms of probability and the definition of conditional probability, and the required posterior density $p(\theta|y)$ of the unknowns is given by

$$p(\theta|y) = \frac{p(y|\theta)p(\theta)}{p(y)} = \frac{p(y|\theta)p(\theta)}{\int_{\Theta} p(y|\theta)p(\theta)\,d\theta} \tag{D.1}$$

where $p(y|\theta)$ and $p(y)$ are the data likelihood and marginal likelihood, respectively. Suppose the data y are realizations of a random variable with a density from the parametric family $\mathcal{F} = \{f(y;\theta): \theta \in \Theta\}$. If the y_i are independent, then the data likelihood is given by

$$p(y|\theta) = \prod_{i=1}^{n} f(y_i;\theta) \tag{D.2}$$

The marginal likelihood $p(y)$ may be obtained by computing the integral in Equation D.1, and it acts as a normalizing constant to ensure that $p(\theta|y)$ integrates to 1. As a result, one may write

$$p(\theta|y) \propto\ p(y|\theta)p(\theta) \tag{D.3}$$

viz., that the posterior density of the unknowns (updated evidence) is proportional to the likelihood (data evidence) times the prior (historic evidence or elicited model assumptions) (see Congdon 2010 and references cited therein).

Applied model optimization and inference is most often performed with the intent to subsequently predict, and an additional attractive feature of the Bayesian inference methodology is its capacity to compute a predictive density for a future observation that accounts not only for uncertainty in the model but also variability in future observations. In particular, if z denotes a future observation having probability density $f(z|\theta)$ and $p(\theta|y)$ denotes the posterior distribution of θ on the basis of observed data y, then

$$f(z|y) = \int_{\Theta} f(z|\theta)p(\theta|y)\,d\theta \tag{D.4}$$

is the posterior predictive density of z given y (Coles 2001). If Z is the annual maximum, suppose, for example, $Z \sim GEV(\mu, \sigma, \xi)$, and Z_L is the maximum rainfall over a future period of L years, then the posterior predictive distribution for Z_L is given by

$$\Pr(Z_L \leq z|y) = \int_{\Theta} \Pr(Z \leq z|\theta)^L p(\theta|y)\, d\theta \qquad \text{(D.5)}$$

where $\Pr(Z \leq z|\theta)$ is the distribution function (i.e., Equation D.1, evaluated at z [Smith 2005]). A design level that will be exceeded with probability p in an L-year period is the level z_p such that

$$\Pr\left(Z_L \leq z_p\middle|y\right) = 1 - p \qquad \text{(D.6)}$$

With application of Bayesian MCMC, the previously mentioned posterior predictive distribution can be approximated using the post burn-in random draws from $p(\theta|y)$. In particular, the right-hand side of Equation D.5 can be estimated by

$$\frac{1}{n-b+1}\sum_{i=b}^{n} \Pr(Z \leq z|\theta_i)^L \qquad \text{(D.7)}$$

where b and n indicate the beginning and ending indices of the post burn-in monitoring period for the MCMC simulation. To obtain predictive return levels, the equation

$$\frac{1}{n-b+1}\sum_{i=b}^{n} \Pr\left(Z \leq z_p\middle|\theta_i\right)^L = 1 - p \qquad \text{(D.8)}$$

can be solved for z_p.

For example, if $Z \sim GEV(\mu, \sigma, \xi)$ and $L = 1$, then Equation D.8 becomes

$$\frac{1}{n-b+1}\sum_{i=b}^{n} \exp\left\{-\left[1 + \frac{\xi(z_p - \mu)}{\sigma}\right]^{-1/\xi}\right\} = 1 - p \qquad \text{(D.9)}$$

The R software (R Core Team 2013) packages extRemes (Gilleland and Katz 2011) and evdbayes (Stephenson and Ribatet 2014) both support the application of Bayesian optimization and inference using models from EVT (Gilleland et al. 2013) for station-specific extremes analysis.

Appendix E: Spatial Bayesian Hierarchical Modeling

The mathematical exposition of the BHM framework for extreme rainfall analysis that is presented directly below closely follows the presentation provided in Dyrrdal et al. (2015) wherein the application context was block annual maxima data and use of the GEV model. Let $\mathcal{S}$ denote the spatial region of interest and $s \in \mathcal{S}$ a specific site within this region. In addition, let y_{ts} denote the maximum annual rainfall of a given duration at location s for a year t. As was previously mentioned, it is assumed the y_{ts} follow a GEV distribution with spatially dependent parameters, viz.,

$$y_{ts} \sim GEV(\mu_s, \sigma_s, \xi_s) \tag{E.1}$$

where:

$$\begin{aligned} \mu_s &= \boldsymbol{x}_s^{\mathrm{T}} \boldsymbol{\theta}^{\mu} + \tau_s^{\mu} \\ \kappa_s &= \boldsymbol{x}_s^{\mathrm{T}} \boldsymbol{\theta}^{\kappa} + \tau_s^{\kappa} \\ \xi_s &= \boldsymbol{x}_s^{\mathrm{T}} \boldsymbol{\theta}^{\xi} + \tau_s^{\xi} \end{aligned} \tag{E.2}$$

with $\kappa_s = 1/\sigma_s$, and $\boldsymbol{x}_s$, $\boldsymbol{\theta}^{\nu}$, $\nu \in \{\mu, \kappa, \xi\}$, and τ_s^{ν} denoting the covariates, the linear model parameters, and spatial random effects terms, respectively. In particular, each GEV model parameter is defined by a linear model of the covariates plus a spatial random effects term that accounts for residual spatial association not captured by the covariates. One or more of the extremal model parameters may also be indexed in time to support the development of a spatio-temporal BHM (Economou et al. 2014). The spatial random effects term is assumed to be a zero-centered Gaussian spatial process (Banjeree et al. 2015). Dyrrdal et al. (2015) specified an isotropic exponential covariance function with a sill and range, viz., $\tau_s^{\nu} \sim GP(\alpha^{\nu}, \lambda^{\nu})$, $\nu \in \{\mu, \kappa, \xi\}$. In particular,

$$E\left(\tau_{s_t}^{\nu}\right) = 0 \tag{E.3}$$

$$cov\left(\tau_{s_t}^{\nu}, \tau_{s_r}^{\nu}\right) = \mathcal{K}_{\alpha^{\nu},\lambda^{\nu}}(s_t, s_r) = \frac{1}{\alpha^{\nu}} exp\left(-\frac{d_{s_t s_r}}{\lambda^{\nu}}\right),\ s_t, s_r \in \mathcal{S} \tag{E.4}$$

where $d_{s_t s_r}$ is the Euclidean distance between locations s_t and s_r. Several of the few previously published BHM studies of extreme rainfall have used an isotropic exponential covariance function to characterize the spatial random effects (Dyrrdal et al. 2015; Cooley et al. 2007; Lehmann et al. 2013; Soltyk et al. 2014). Banjeree et al. (2015) and Davison et al. (2012) summarize common covariance functions and also technical considerations associated with covariance model selection. The likelihood is given by

$$p(\boldsymbol{y}|\{\mu_s, \kappa_s, \xi_s\}_{s\in\mathcal{S}}) = \prod_{s\in\mathcal{S}_o} \prod_{t=1}^{T_s} p(y_{ts}|\mu_s, \kappa_s, \xi_s) \tag{E.5}$$

where $\boldsymbol{y}$ and $\mathcal{S}_o \subset \mathcal{S}$ denote the entire set of block maxima observations and the set of observation locations, respectively. The likelihood definition does imply that y_{ts} and $y_{t\acute{s}}$ are conditionally independent for any $s \neq \acute{s}$ where $s, \acute{s} \in \mathcal{S}$. Model inference is performed using MCMC.

Prediction at locations $q \in \mathcal{S} \setminus \mathcal{S}_o$ using the post burn-in MCMC draws requires specification of the spatial random effects terms. Dyrrdal et al. (2015) note that if $\tau_s^\nu \sim GP(\alpha^\nu, \lambda^\nu)$, then

$$\tau_q^\nu \big| \{\tau_s^\nu\}_{s\in\mathcal{S}_o} \sim N\left(\hat{\tau}_q^\nu, \hat{\kappa}_q^\nu\right) \tag{E.6}$$

where:

$$\hat{\tau}_q^\nu = \mathcal{K}_{\alpha^\nu,\lambda^\nu}(q, \mathcal{S}_o)\mathcal{K}_{\alpha^\nu,\lambda^\nu}(\mathcal{S}_o, \mathcal{S}_o)^{-1}\boldsymbol{\tau}_{\mathcal{S}_o}^\nu \tag{E.7}$$

$$\hat{\kappa}_q^\nu = \alpha^\nu - \mathcal{K}_{\alpha^\nu,\lambda^\nu}(q, \mathcal{S}_o)\mathcal{K}_{\alpha^\nu,\lambda^\nu}(\mathcal{S}_o, \mathcal{S}_o)^{-1}\mathcal{K}_{\alpha^\nu,\lambda^\nu}(\mathcal{S}_o, q) \tag{E.8}$$

with $\boldsymbol{\tau}_{\mathcal{S}_o}^\nu$ the vector of current τ_s^ν for $s \in \mathcal{S}_o$ and $\mathcal{K}_{\alpha^\nu,\lambda^\nu}(a, b) = \left[\mathcal{K}_{\alpha^\nu,\lambda^\nu}(\mathcal{A}, \mathcal{B})\right]_{ab}$ is a matrix of size $\mathcal{A} \times \mathcal{B}$ where $a \in \mathcal{A}$, $b \in \mathcal{B}$ and $\mathcal{A}$ and $\mathcal{B}$ are subsets of $\mathcal{S}$.

Appendix F: Modeling Results and Related Observations for 3.1.5.1 Case Study Demonstration - White Sands National Monument Rainfall Station IDF Curve Development

Table F-1. Tabular summary by duration of the PM estimate for the GEV distribution parameters, its related computed quantiles, and also the 2.5, 50, and 97.5 percentile values from each respective predictive posterior distribution for five return periods computed under stationary conditions.

Stationary Treatment								
Duration	PM			Quantiles (mm/h) for Return Periods, T in years; PM estimate, and Percentiles (2.5, 50, 97.5) of Predictive Distribution				
(hours)	μ	σ	ξ	2	10	25	50	100
1	13.235	5.946	-0.025	15.425	27.008	33.051	37.630	42.256
				(13.546, 15.564, 17.828)	(24.061, 27.853, 34.630)	(28.803, 34.219, 47.047)	(31.981, 39.061, 58.616)	(34.833, 43.964, 72.428)
2	15.670	6.453	-0.068	9.033	15.678	19.357	22.244	25.248
				(7.979, 9.108, 10.384)	(13.930, 16.204, 20.468)	(16.708, 20.106, 28.722)	(18.607, 23.183, 36.865)	(20.335, 26.412, 47.094)
3	17.004	6.753	-0.082	6.506	11.231	13.900	16.018	18.245
				(5.749, 6.556, 7.473)	(9.988, 11.621, 15.039)	(11.952, 14.479, 21.982)	(13.246, 16.776, 29.234)	(14.409, 19.216, 38.929)
6	20.200	7.874	0.081	3.841	6.065	7.062	7.754	8.403
				(3.407, 3.855, 4.338)	(5.549, 6.234, 7.490)	(6.391, 7.293, 9.733)	(6.900, 8.037, 11.755)	(7.315, 8.744, 14.096)
12	22.163	8.534	0.128	2.102	3.238	3.714	4.032	4.321
				(1.863, 2.103, 2.360)	(2.974, 3.311, 3.892)	(3.389, 3.811, 4.884)	(3.628, 4.146, 5.736)	(3.818, 4.455, 6.690)
24	25.446	9.454	0.183	1.200	1.787	2.014	2.159	2.285
				(1.074, 1.203, 1.341)	(1.659, 1.826, 2.098)	(1.866, 2.063, 2.543)	(1.981, 2.215, 2.901)	(2.071, 2.350, 3.285)
48	28.541	11.790	0.055	0.684	1.114	1.315	1.457	1.592
				(0.604, 0.687, 0.776)	(1.011, 1.145, 1.375)	(1.180, 1.358, 1.773)	(1.287, 1.509, 2.124)	(1.381, 1.654, 2.525)
96	36.215	14.399	0.104	0.431	0.678	0.786	0.859	0.926
				(0.383, 0.432, 0.485)	(0.622, 0.695, 0.815)	(0.716, 0.810, 1.017)	(0.775, 0.888, 1.186)	(0.825, 0.961, 1.370)

Table F-2. Tabular summary by duration of the PM estimate for the time varying GEV distribution parameters, its related computed quantiles, and also the 2.5, 50, and 97.5 percentile values from each respective predictive posterior distribution for five return periods computed under nonstationary conditions. The reported GEV location parameter is computed using the PM derived estimates for μ_1 and μ_0, and Equation 4 for the 95th percentile.

Nonstationary Treatment								
Duration	PM			Quantiles (mm/h) for Return Periods, T in years; PM estimate, and Percentiles (2.5, 50, 97.5) of Predictive Distribution				
(hours)	μ	σ	ξ	2	10	25	50	100
1	22.244	5.623	-0.009	24.308	35.028	40.494	44.580	48.661
				(17.487, 24.917, 34.818)	(28.700, 36.610, 46.513)	(33.841, 42.546, 54.510)	(37.298, 46.821, 63.478)	(40.335, 50.909, 75.449)
2	27.095	6.022	-0.039	14.659	20.629	23.803	26.235	28.716
				(10.869, 14.876, 20.181)	(17.195, 21.434, 26.889)	(20.208, 24.946, 31.946)	(22.238, 27.543, 37.941)	(24.043, 30.082, 45.955)
3	31.282	6.273	-0.030	11.198	15.295	17.447	19.083	20.741
				(8.224, 11.285, 15.352)	(12.670, 15.779, 19.735)	(14.790, 18.165, 23.222)	(16.176, 19.882, 27.786)	(17.381, 21.528, 34.271)
6	41.110	6.598	0.090	7.248	9.092	9.909	10.471	10.995
				(5.671, 7.239, 8.966)	(7.708, 9.275, 11.072)	(8.560, 10.213, 12.376)	(9.093, 10.853, 13.752)	(9.539, 11.436, 15.524)
12	45.233	7.133	0.149	3.981	4.906	5.282	5.529	5.749
				(3.128, 3.994, 4.924)	(4.161, 5.002, 5.952)	(4.575, 5.426, 6.448)	(4.823, 5.704, 6.883)	(5.027, 5.950, 7.416)
24	49.271	7.434	0.108	2.164	2.671	2.890	3.038	3.175
				(1.758, 2.180, 2.641)	(2.301, 2.725, 3.209)	(2.508, 2.959, 3.528)	(2.630, 3.115, 3.827)	(2.725, 3.254, 4.197)
48	53.067	9.410	-0.070	1.178	1.583	1.808	1.985	2.169
				(0.952, 1.191, 1.461)	(1.356, 1.630, 1.971)	(1.544, 1.869, 2.413)	(1.669, 2.050, 2.903)	(1.779, 2.235, 3.540)
96	59.863	12.945	0.052	0.673	0.910	1.021	1.100	1.176
				(0.495, 0.672, 0.859)	(0.742, 0.932, 1.147)	(0.846, 1.054, 1.351)	(0.912, 1.139, 1.556)	(0.968, 1.218, 1.807)

Table F-3. Computed percent increase obtained when the nonstationary PM-based quantile estimates are compared with their counterparts that were computed assuming a stationary climate.

Duration	Percent Increase in Quantiles (mm/hr) for Return Periods, T in years				
(hours)	2	10	25	50	100
1	57.6	29.7	22.5	18.5	15.2
2	62.3	31.6	23.0	17.9	13.7
3	72.1	36.2	25.5	19.1	13.7
6	88.7	49.9	40.3	35.0	30.9
12	89.5	51.5	42.2	37.1	33.1
24	80.4	49.5	43.5	40.7	38.9
48	72.3	42.1	37.5	36.2	36.2
96	56.0	34.2	30.0	28.1	27.0

Figure F-1. Bayesian MCMC simulation-derived, 2 hr IDF curves for the White Sands National Monument rainfall station computed under stationary and nonstationary conditions. The 2.5, 50, and 97.5 percentile values from each respective predictive posterior distribution are shown at each quantile level. Plots of the posterior predictive distributions for the 2-year and 100-year return period level quantiles are also shown.

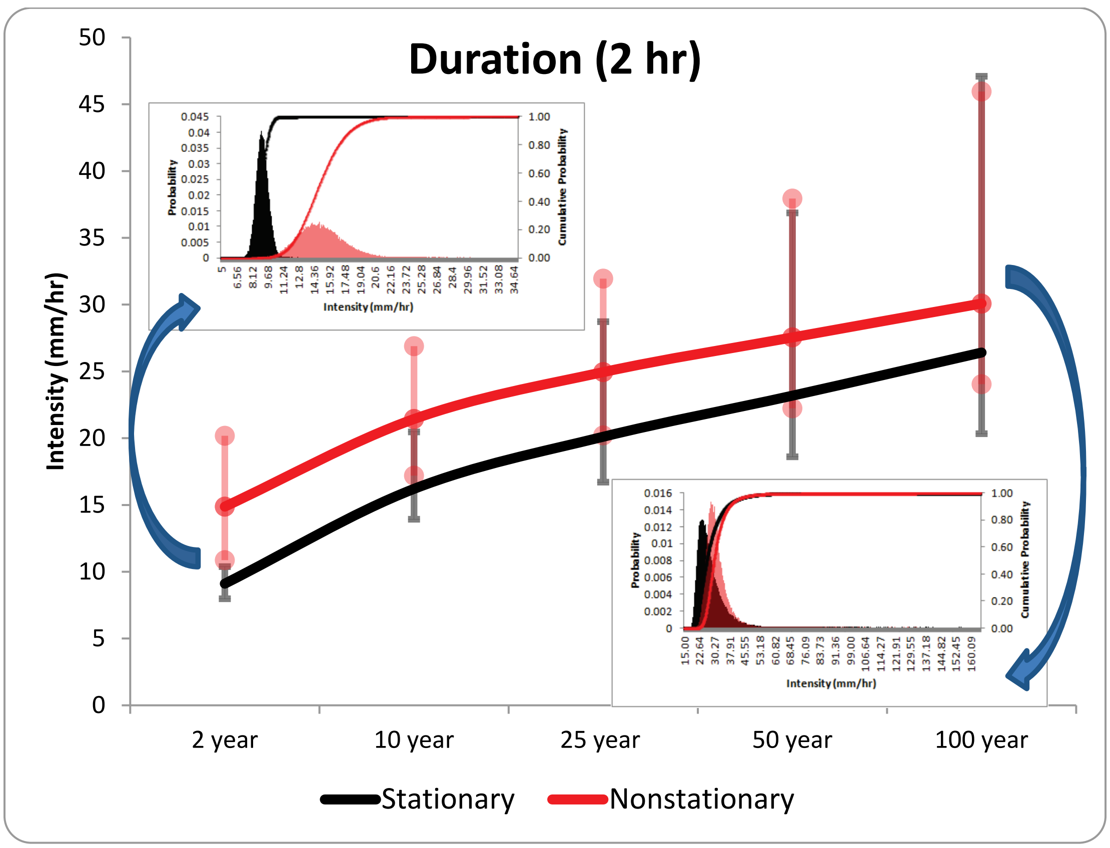

Figure F-2. Bayesian MCMC simulation-derived, 3 hr IDF curves for the White Sands National Monument rainfall station computed under stationary and nonstationary conditions. The 2.5, 50, and 97.5 percentile values from each respective predictive posterior distribution are shown at each quantile level. Plots of the posterior predictive distributions for the 2-year and 100-year return period level quantiles are also shown.

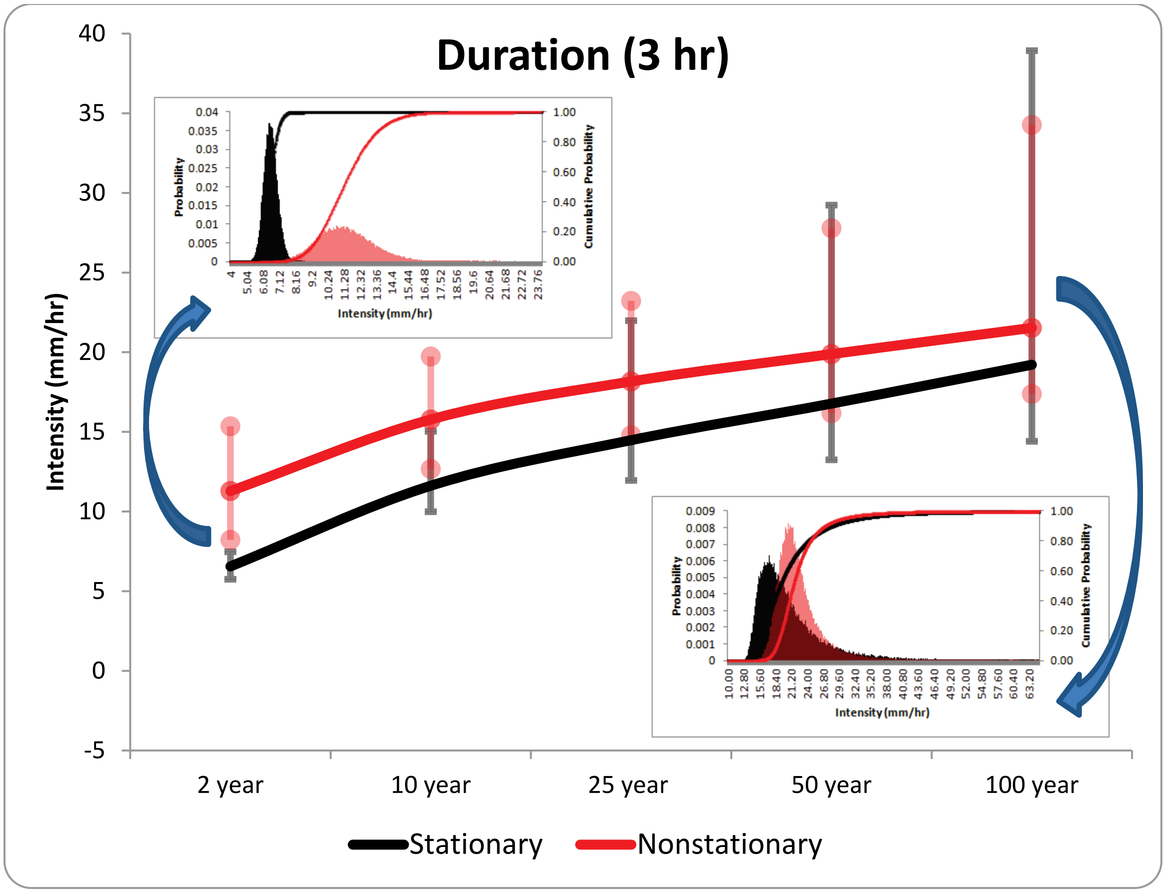

Figure F-3. Bayesian MCMC simulation-derived, 6 hr IDF curves for the White Sands National Monument rainfall station computed under stationary and nonstationary conditions. The 2.5, 50, and 97.5 percentile values from each respective predictive posterior distribution are shown at each quantile level. Plots of the posterior predictive distributions for the 2-year and 100-year return period level quantiles are also shown.

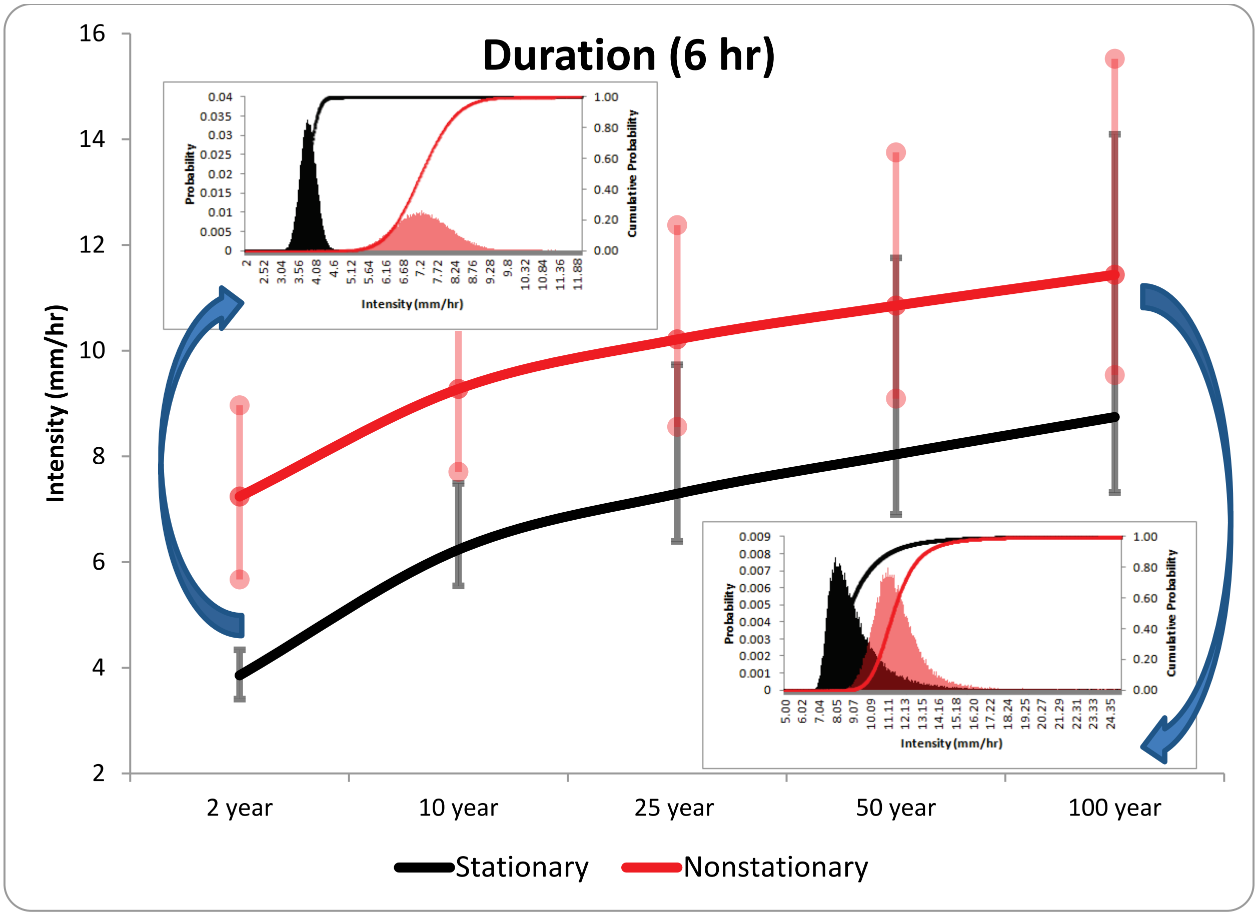

Figure F-4. Bayesian MCMC simulation-derived, 12 hr IDF curves for the White Sands National Monument rainfall station computed under stationary and nonstationary conditions. The 2.5, 50, and 97.5 percentile values from each respective predictive posterior distribution are shown at each quantile level. Plots of the posterior predictive distributions for the 2-year and 100-year return period level quantiles are also shown.

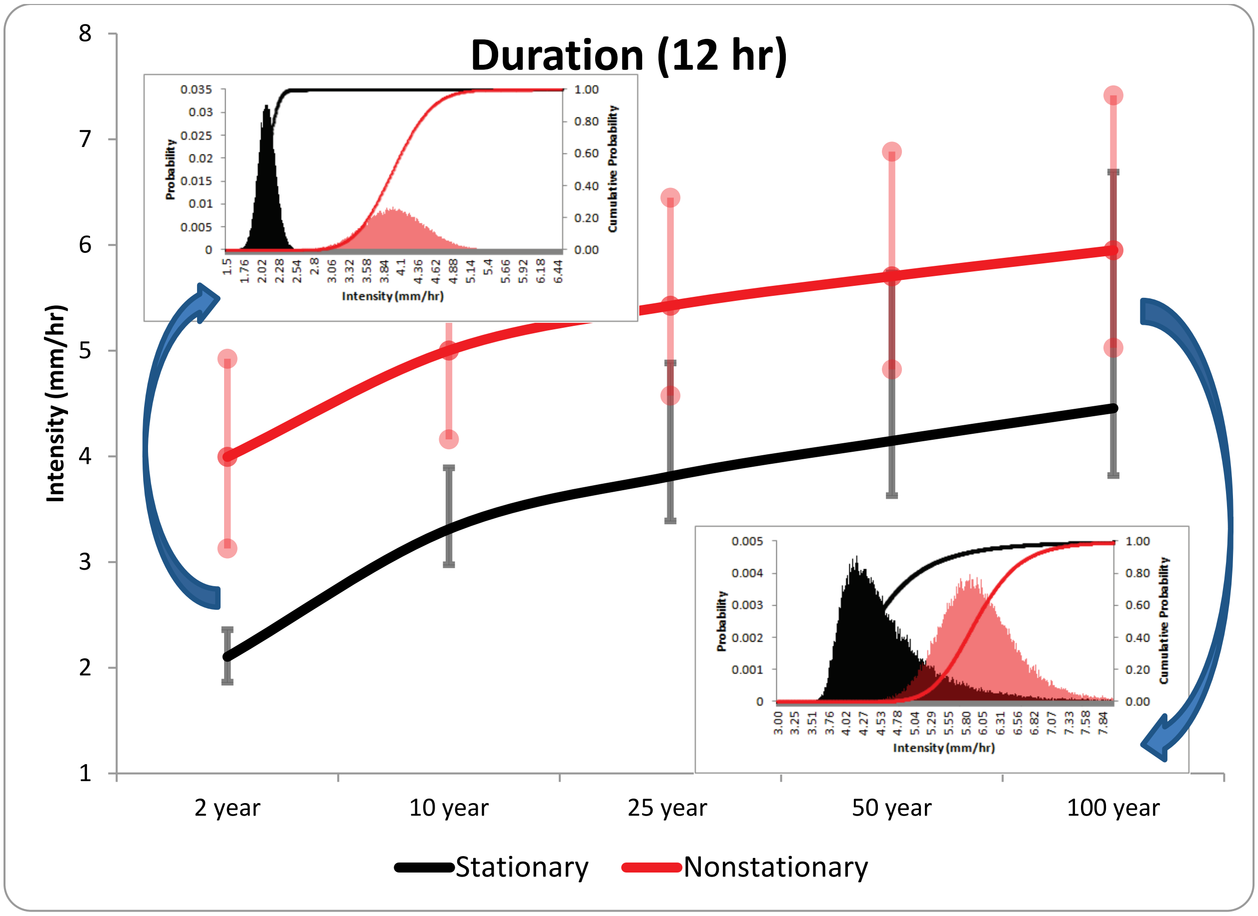

Figure F-5. Bayesian MCMC simulation derived, 24 hr IDF curves for the White Sands National Monument rainfall station computed under stationary and nonstationary conditions. The 2.5, 50, and 97.5 percentile values from each respective predictive posterior distribution are shown at each quantile level. Plots of the posterior predictive distributions for the 2-year and 100-year return period level quantiles are also shown.

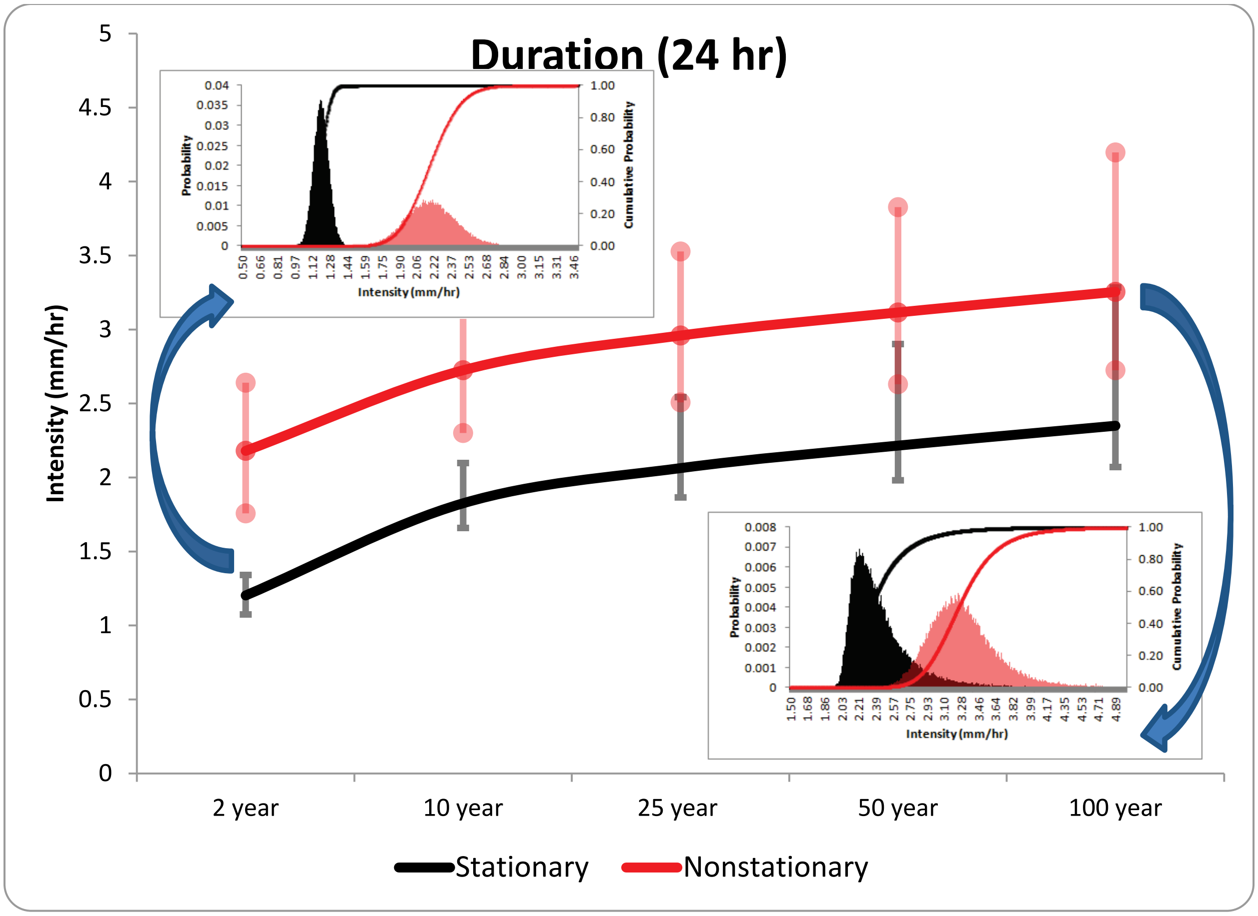

Figure F-6. Bayesian MCMC simulation-derived, 48 hr IDF curves for the White Sands National Monument rainfall station computed under stationary and nonstationary conditions. The 2.5, 50, and 97.5 percentile values from each respective predictive posterior distribution are shown at each quantile level. Plots of the posterior predictive distributions for the 2-year and 100-year return period level quantiles are also shown.

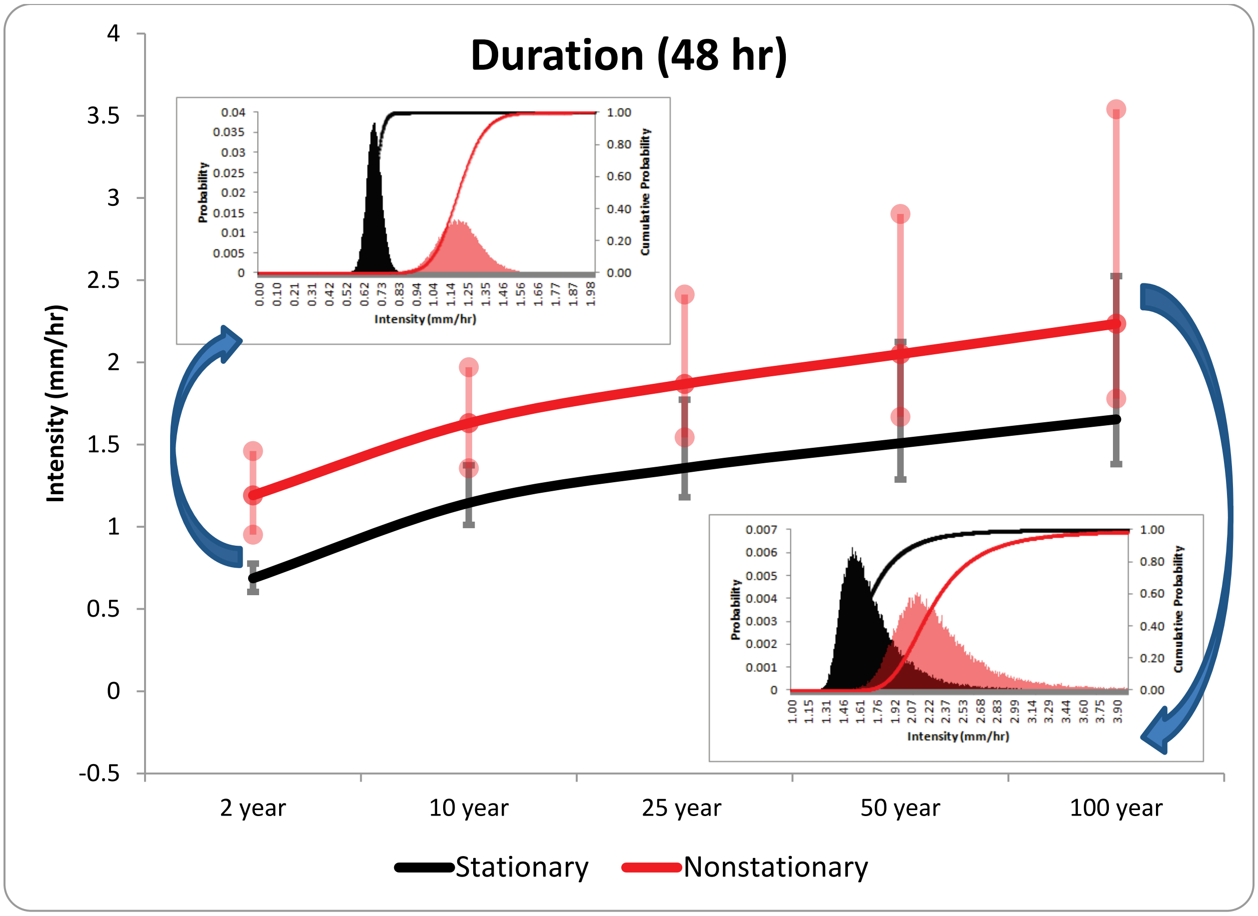

Figure F-7. Bayesian MCMC simulation-derived, 96 hr IDF curves for the White Sands National Monument rainfall station computed under stationary and nonstationary conditions. The 2.5, 50, and 97.5 percentile values from each respective predictive posterior distribution are shown at each quantile level. Plots of the posterior predictive distributions for the 2-year and 100-year return period level quantiles are also shown.

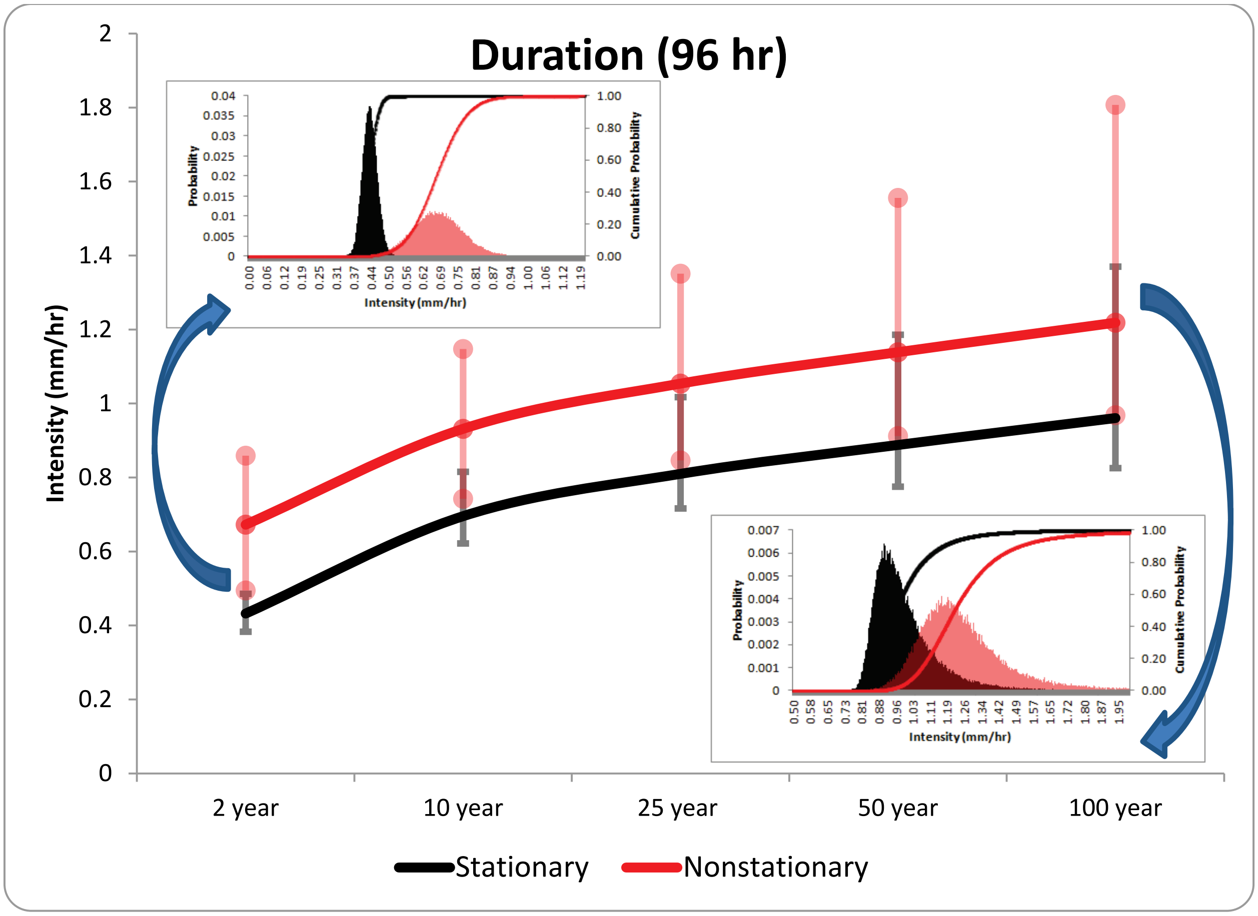

Figure F-8. Computed percent increase for five distinct return periods, T, obtained when the nonstationary PM-based quantile estimates are compared with their counterparts that were computed assuming a stationary climate.

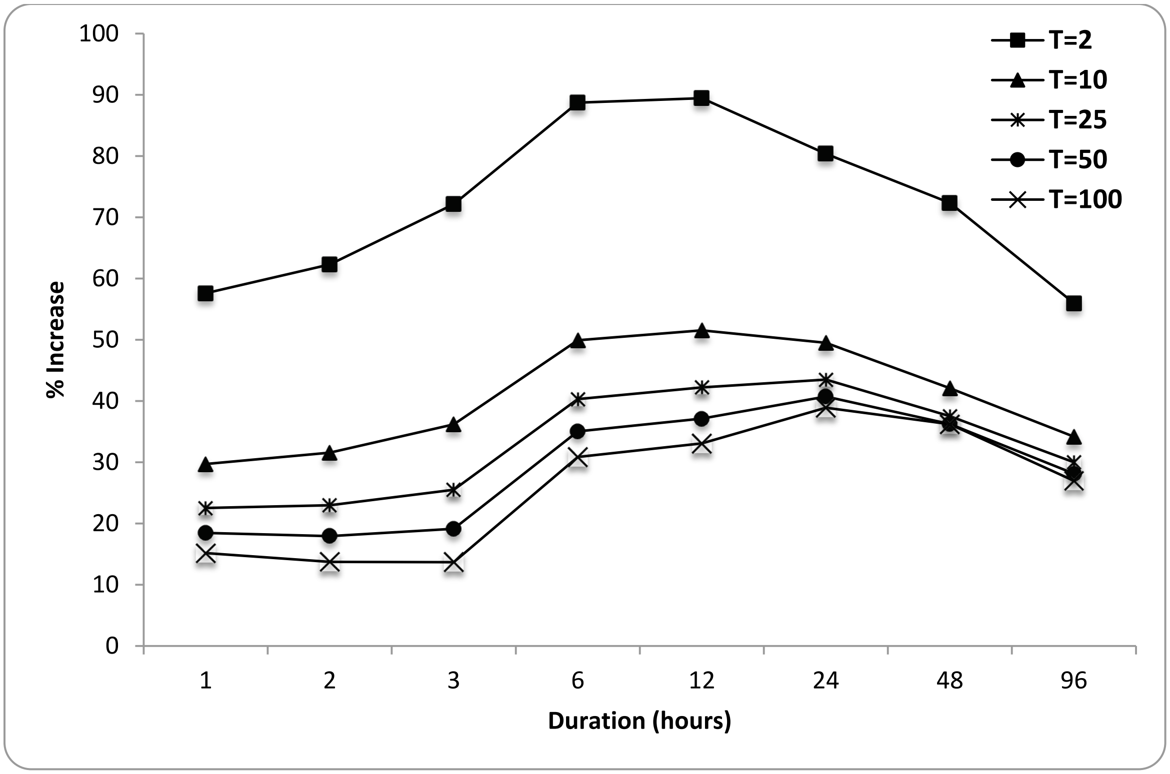

While not the main focus of the simple example that profiled a capacity of Bayesian inference to readily support treatments of non-stationarity, several observations can nevertheless be made upon examination of the results encapsulated in Tables F-1 through F-3 and Figure 23 and also Figures F-1 through F-8 for the White Sands National Monument rainfall station:

1. The stationary assumption delivers IDF curves that underestimate extreme events across all durations and return periods when the comparisons are based on the computed and reported 50th percentile values for each quantile, viz., the red lines are always above the black lines in Figure 23 and also Figures F-1 through F-7.
2. In particular, for example, for a 2-year, 2 hr storm, the difference between the nonstationary (14.66 mm/hr) and stationary (9.03 mm/hr) PM extreme precipitation estimates is approximately 5.63 mm/hr (+62.3%) while for a 10-year, 1 hr event, the difference between the nonstationary (35.03 mm/hr) and stationary (27.01 mm/hr) PM extreme precipitation estimates is 8.02 mm/hr

(+29.7%). These values are both in close agreement with previously reported comparisons (Cheng and AghaKouchak 2014).

3. The most substantial underestimation of extremes that result from ignoring the nonstationary condition occur at the 12 hr duration for the 2-year and 10-year return periods while for the remaining return periods it occurs at the 24 hr duration.
4. The percent increase between the PM nonstationary and stationary extreme precipitation estimates decreases as the return period increases, viz., in Figure F-8, the curve for T=2/T=10/T=25/T=50 is always above the curve for T=10/T=25/T=50/T=100, across all durations.
5. The largest percent increase between the PM nonstationary and stationary extreme precipitation estimates occurs at the 2-year return period level, which is significantly higher than for the remaining return periods.
6. While the differences between the PM nonstationary and stationary estimates decrease as the duration increases, as Cheng and AghaKouchak (2014) observed, the computed percent increases nevertheless indicate notable change occurring across all durations and return periods. In fact, the percent increases are greater for the longer duration events than for the shorter events for all but the 2-year return period.
7. The 95% credible intervals shown at each quantile level suggest that for a given duration, the uncertainty in the computed quantiles for the nonstationary and stationary estimates grow with increasing return period and that this occurrence is more dramatic for the stationary estimates than for the nonstationary estimates. Moreover, for the nonstationary estimates, this phenomenon is less active at the 6 hr, 12 hr, and 24 hr durations wherein the 95% credible intervals are observed to be more uniform across the five return periods relative to the remaining durations.
8. At the 2 hr duration, the 95% credible interval of the stationary 100-year quantile covers its nonstationary counterpart. For the 3 hr duration, the stationary 50-year and 100-year quantile 95% credible intervals cover their nonstationary counterparts.
9. For many durations and return periods, the 50th percentile of stationary simulations are below the lower bounds of the credible intervals of their nonstationary counterparts.

10. Across all durations, the nonstationary 95% credible intervals for the 2-year and 10-year quantile levels are greater than their stationary counterparts.
11. In general, for any given duration, the nonstationary and stationary 95% credible intervals intersect more as the return period increases.
12. For the 2-year return period quantile level, across all durations, the nonstationary and stationary 95% credible intervals intersect minimally, if at all.
13. For a given duration, across all return periods, the degree of intersection of the nonstationary and stationary 95% credible intervals is the least at the 24 hr duration.
14. The posterior distributions presented for the 2-year and 100-year quantiles for each duration, which are also available for other quantile levels using the available draws from each respective duration-based MCMC simulation, are a means by which to make probabilistic statements regarding extreme precipitation at the White Sands National Monument rainfall station. For example, the approximate cumulative probability that the 3-hr, 2-year rainfall intensity, assuming stationarity, is less than or equal to 8 mm/hr is effectively 1 (0.9986) whereas the approximate complement cumulative probability for the same intensity, duration, and frequency computed under a nonstationary climate condition is 0.983. The approximate cumulative probability that the 24 hr, 100-year rainfall intensity, assuming stationarity, is less than or equal to 2.75 mm/hr is 0.873 whereas the approximate complement cumulative probability for the same intensity, duration, and frequency computed under a nonstationary climate condition is 0.968.

Appendix G: The Willamette River Basin (WRB), Including Hydrography, Projects, and Cities Located in the Basin and Its Relative Location in the State of Oregon

Figure G-1. The Willamette River Basin, including hydrography, projects, and cities located in the basin, and also its relative location in the state of Oregon.

REPORT DOCUMENTATION PAGE

Form Approved
OMB No. 0704-0188

1. REPORT DATE
August 2019

2. REPORT TYPE
Final Report

3. DATES COVERED *(From - To)*

4. TITLE AND SUBTITLE
Probabilistic Flood Hazard Assessment Framework Development: Extreme Rainfall Analysis

5a. CONTRACT NUMBER

5b. GRANT NUMBER

5c. PROGRAM ELEMENT NUMBER

6. AUTHOR(S)
Brian E. Skahill and Joseph Kanney

5d. PROJECT NUMBER

5e. TASK NUMBER

5f. WORK UNIT NUMBER

7. PERFORMING ORGANIZATION NAME(S) AND ADDRESS(ES)
Coastal and Hydraulics Laboratory
U.S. Army Engineer Research and Development Center
3909 Halls Ferry Road
Vicksburg, MS 39180-6199

U.S. Nuclear Regulatory Commission
Office of Nuclear Regulatory Research
11555 Rockville Pike, Rockville, MD 20852-2738, Mail Stop TWFN-10A12

8. PERFORMING ORGANIZATION REPORT NUMBER
ERDC/CHL TR-19-14

9. SPONSORING/MONITORING AGENCY NAME(S) AND ADDRESS(ES)
U.S. Nuclear Regulatory Commission
11555 Rockville Pike
Rockville, MD 20852-2738

10. SPONSOR/MONITOR'S ACRONYM(S)
USNRC

11. SPONSOR/MONITOR'S REPORT NUMBER(S)

12. DISTRIBUTION/AVAILABILITY STATEMENT
Approved for public release; distribution is unlimited.

13. SUPPLEMENTARY NOTES
U.S. Nuclear Regulatory Commission NRC Agreement Number NRC-HQ-60-14-I-0022, “Probabilistic Flood Hazard Assessment Framework Development”

14. ABSTRACT
This report introduces a framework for probabilistic flood hazard assessment (PFHA) whose basis leverages recent advances in the science of spatial extremes. The framework basis includes a latent variable model (LVM) or a max-stable process application wherein for either case model inference is likelihood based. The framework is flexible in that it can leverage robust approaches to quantify model uncertainty while also supporting the capacity to readily combine additional relevant data types; for example, historical and/or paleoflood data for flood frequency analyses. This report profiles applications of Bayesian inference for flood hazard curve development for at-site and spatial LVM analyses. Pointwise spatial model development using an LVM or a max-stable process requires the parameters of the model characterizing the pointwise extremes to vary spatially as a function of gridded covariate data relevant to the hydrometeorological extreme under consideration. Recent advances in mathematical regularization facilitate spatial pointwise model reduction. The PFHA framework accommodates the multiple model parameterizations encapsulated within a given LVM or max-stable process deployment by generalizing model choice using information criteria.

15. SUBJECT TERMS
Flood control, Flood damage prevention, Floods, Nuclear facilities, Rain and rainfall, Rainfall probabilities

16. SECURITY CLASSIFICATION OF: a. REPORT	b. ABSTRACT	c. THIS PAGE	17. LIMITATION OF ABSTRACT	18. NUMBER OF PAGES	19a. NAME OF RESPONSIBLE PERSON / 19b. TELEPHONE NUMBER *(Include area code)*
Unclassified	Unclassified	Unclassified	SAR	124	971-804-0373

Standard Form 298 (Rev. 8/98)
Prescribed by ANSI Std. Z39.18